Dynamic Finite Element Modelling of Pile Tip Deformation

Delft University of Technology
Faculty of Civil Engineering

Ioannis Kourtis

Dynamic Finite Element Modelling of Pile Tip Deformation

MSc thesis
by

Ioannis Kourtis

January 31, 2022

TU Delft supervisors: Dr. ir. Apostolos Tsouvalas
Dr. Alessandro Cabboi
Athanasios Tsetas

Van Oord supervisors: Menno Jorna
Ralph Luiken

To my parents

Abstract

As offshore wind industry grows, challenges are presented by future sites located further from shore, in harsher conditions and deeper waters. Monopiles are the most common foundation type for offshore wind turbines and they are likely to remain the most preferred option in the future. To ensure cost competitiveness, optimization of the standard solutions became a necessity, leading to more slender monopiles. As the ratio of pile diameter to plate thickness (D/t) increases, plate buckling during driving becomes even more critical. A possible failure mechanism during driving and a largely unknown phenomenon, is local buckling of the pile tip during the impact with a boulder.

Damage at the pile tip has been documented in some cases (Goodwyn A, Valhall) with significant structural and economic consequences. At the same time, in the relative guidelines, local buckling at the tip level due to impact with an object is not taken into account and there is no available recommendation on the initiation or avoidance of tip damage.

Finite Element Analysis was conducted to investigate the initiation and extent of pile tip damage during impact with an object as the driving takes place. The study was focused on the steel monopile response so the contribution of soil was not taken into account. The model consisted of the monopile and the boulder at its tip. A real pulse was applied at the top of the pile and the tip response was investigated after the impact took place. Through a parametric investigation, the influence of the impact orientation (central or eccentric) and the D/t ratio to the tip response was studied and monitored.

It was concluded that the induced stress at the tip exceeds the general driving stress limits set by the standards (API) or the international literature. In case of central impact the stress intensity is higher and the plasticity more extended but for eccentric impacts the radial deformations of the tip are larger and they were selected as a more appropriate measure of the distortion of the pile tip. The vertical reaction force is higher for the central impact and the lateral reaction force was much lower and not influenced by the impact orientation confirming the inability of the pile to sustain lateral loads in absence of soil.

It was concluded that local pile tip damage due to impact with an object is a critical aspect of the driving process and further investigation is necessary to realistically capture the tip response and for the development of relative guidelines.

Preface

The thesis presented herein was submitted to obtain the MSc in Civil Engineering at the Technical University of Delft (TU Delft), in the track of Structural Engineering and the specialization in Steel, Timber and Composite Structures. The research was conducted in collaboration with TU Delft and the Engineering & Estimating department at Van Oord.

During the research I had the chance to collaborate with a number of acknowledged professionals and I consider myself privileged for that. I would like to thank Van Oord and specifically Ferdy Hengeveld and Ralph Luiken for giving me the chance to work on monopile tip deformations and be involved in a real case application. I would like to express my thankfulness to Menno Jorna who as my supervisor, on behalf of Van Oord, was constantly helping me with his experience on how to deal with Ansys and how to overcome the modelling obstacles. I would like to thank Dr. ir. Apostolos Tsouvalas for accepting to be the chairman of the thesis committee and for his useful criticism during the meetings. I also want to thank Dr. Alessandro Cabboi for accepting to be a member of the committee and for his helpful advices. Last but not least, I would like to thank Athanasios Tsetas for being a member of the committee and my daily supervisor on behalf of TU Delft and for being there and giving me his advice whenever I needed him.

Finally, I would like to express my deepest gratitude to my parents for their constant support. Without them nothing would have been achieved.

Ioannis Kourtis
January 31, 2022
Delft

Contents

1. Introduction

1.1 Monopiles and offshore wind industry trend

Offshore wind industry has grown rapidly during the last decade and this trend seems to continue in the years to come. In Europe, 2020 was a record year for the financing of new offshore wind farms (WindEurope, 2021). As offshore industry grows, challenges are presented by future sites located further from shore, in harsher conditions and deeper waters. For these reasons, optimization of the standard solutions, in the design of offshore wind turbines used so far, is necessary to achieve cost reductions and ensure the cost competitiveness of offshore wind in the energy sector.

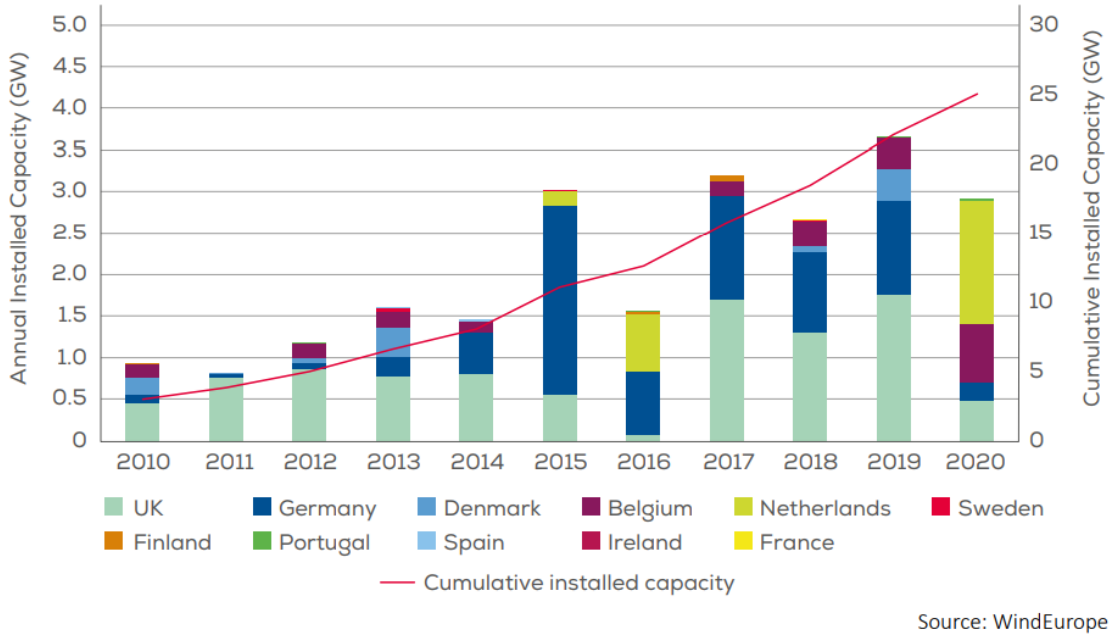

Figure 1.1 *Annual offshore wind installations by country (left axis) and cumulative capacity (right axis) (WindEurope, 2021)*

The harsher conditions in which future wind farms are expected to be built in combination with the continuously increased size of wind turbines, require advances in turbine foundation technology. The development of optimized foundations will play a crucial role in the cost reduction of offshore wind projects.

Monopiles are the most common foundation type in the offshore industry and they are likely to remain the most preferred option in the future (Leanwind Project, 2017). In 2020, 80.5% of all installations were founded on monopiles (WindEurope, 2021). The fact that monopile foundations are much cheaper makes them a popular choice among other offshore foundation types like jacket structures. Although, monopiles are mainly used for foundations in shallow waters so far, the new generation of monopiles, with increased diameters of up to 10 m, have the potential of being deployed in much deeper waters with a depth of more than 50 m.

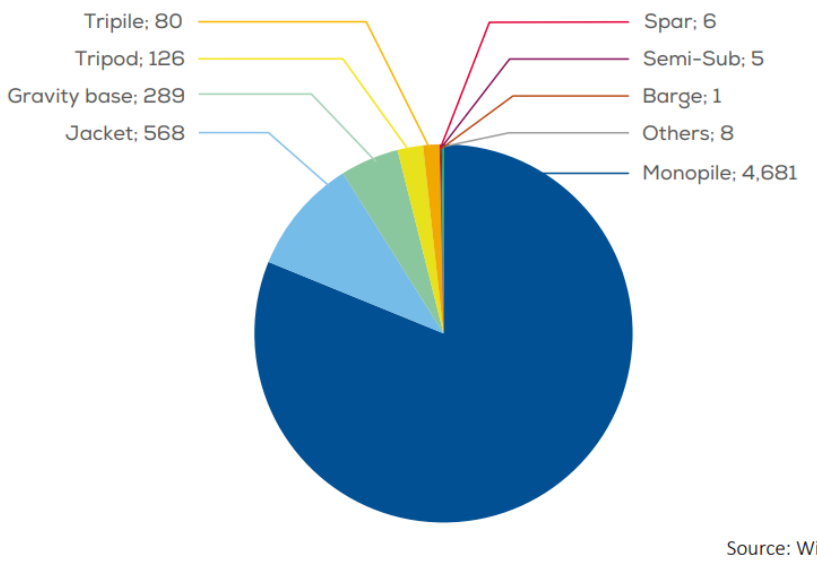

Figure 1.2 *Cumulative number of foundations installed by substructure type (WindEurope, 2021)*

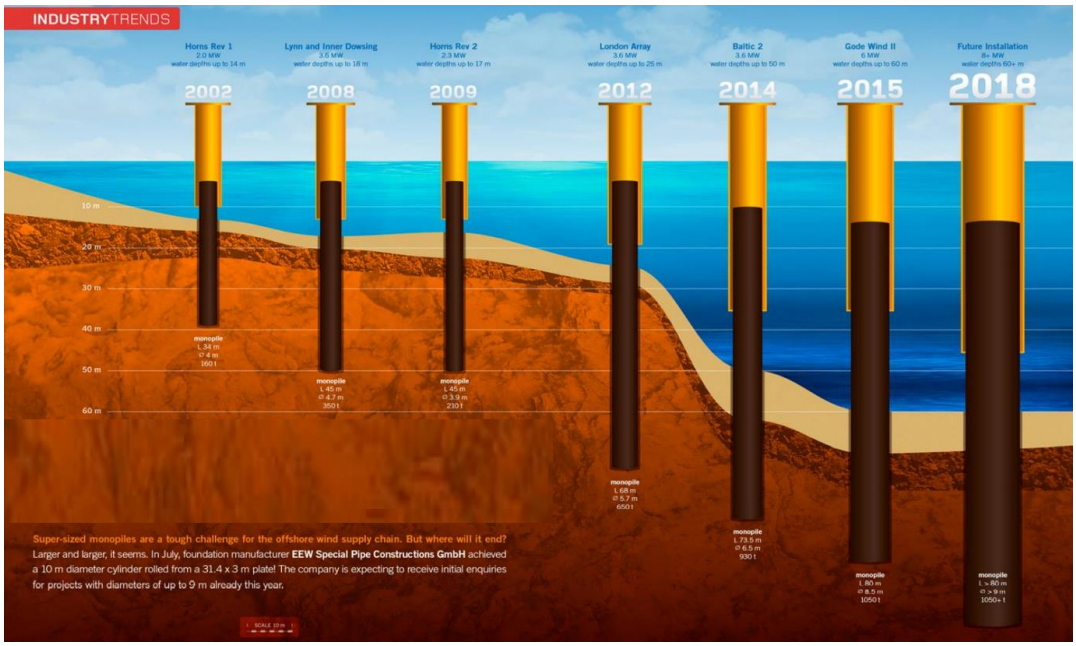

Figure 1.3 *Monopiles size growth over the years (Elkadi, 2019)*

For the above reasons, monopiles tend to be more and more slender. As the ratio of pile diameter to plate thickness increases, plate buckling during driving becomes even more critical. A possible failure mechanism during driving and a largely unknown phenomenon, is local buckling of the pile tip during the impact with a boulder.

1.2 Problem Statement

Large diameter, thin-walled monopiles are susceptible to damage at the pile tip, during driving, when a boulder or a hard soil stratum is encountered. Depending on the pile, boulder and soil parameters this impact could result either in failure of the pile tip, failure of the boulder, displacement of the boulder into the soil or in a more realistic scenario a combination of them with propagation of the pile damage as the driving continues (extrusion buckling). This could lead to premature refusal of the driving process or may even go undetected with the only indication being a driving resistance that deviates from the expected profile. In both cases, the axial or lateral capacity or stiffness of the monopile would not be the expected which would have structural consequences and depending on the magnitude of these consequences there could also be economic consequences with the worst case scenario being the need for a new foundation.

Collapse of the pile at tip level has been documented at some cases but may have gone undetected on a number of others. Widespread damage in the vicinity of the pile tip was noticed after the extraction of piles during widening a harbour basin at Rotterdam (Bros et al., 2017). Although, the piles were not monopiles, the case is worth mentioning. The diameter to wall thickness ratio (D/t) of the piles was equal to 84 and the damage went completely unnoticed during the original installation. For the Goodwyn A gas platform in the North-West Shelf of Australia thin walled (D/t=59) primary piles were driven to a depth of 120 m, in the late 1980s (Barbour and Erbrich, 1994). However, it was found that 16 out of 20 piles had undergone progressive distortion over the lower 20 to 40 m to the extent that the pile types had become almost closed into a peanut shape. At the Valhall water injection platform in the North Sea in 2002, 5 out of 8 piles (D/t=40) reached premature refusal with significant distortion of the piles near their tips (Alm. et al., 2004). For both of the two latter examples, very costly remedial actions were taken.

Figure 1.4 *Damaged pile toes in Port of Rotterdam (left), Pile distortion in Goodwyn A platform (right)*

In spite of significant advances in current offshore monopile design guidelines (DNVGL, API, ISO, HSE) there is still lack of knowledge for fully understanding the dynamic behaviour of

the monopile through the driving process and predicting its axial capacity. Moreover, design methods used for the determination of shaft friction and end-bearing capacity still rely heavily on empirical correlations. In many cases, the current design guidelines were unable to provide safe guidance on the avoidance of pile tip deformation.

The main reason that could lead to initiation of pile tip deformation is the impact with a boulder during the driving process. API recommendations for the pile thickness is based on rough estimations where the impact with a hard object or soil stratum is not taken into account. Very few analytical models exist (HSE, Aldrige et al., Holeyman et al.) for the boulder-pile-soil interaction which they are based on simplifications. Even less numerical attempts are available (Barbour and Erbrich, Erbrich et al., Jorna).

For all the above reasons, the development of tools and design methods, tailored to the needs of the offshore wind sector and able to accurately predict the performance of monopiles, is necessary for an optimized design. In the absence of full-scale test results, Finite Element Modelling of the monopiles is believed to be the most accurate indicator of their behaviour (LEANWIND Project, 2017) [2].

Therefore, the problem statement is defined as follows.

Pile tip damage, due to the impact with an object (boulder), during the driving process of monopiles is of main concern in the offshore wind sector. Current guidelines do not cover this problem, making further study of the phenomenon even more necessary. Numerical modelling could accurately describe this failure mechanism and used as a tool in practice but also for the development of appropriate guidelines.

1.3 Research goal

The main goal of the research project is the investigation of the pile tip damage when an object (boulder) is encountered, during the driving process of a monopile into the soil. For this purpose, dynamic Finite Element Analysis will be conducted in order to achieve modelling the driving and impact process and properly capture the response of the monopile toe. Eventually, insight will be provided on ***what are the potential pile tip deformation mechanisms as a result of collision with an obstacle.***

To achieve this goal, focus will be given on the influence of two aspects to the pile tip deformation after contact with a boulder during driving:

- The boulder position with respect to the pile.
- The pile slenderness, expressed through the D/t ratio.

The thesis is focused on the initiation stage of the tip damage. In the relative literature, the importance of the initial distortion is highlighted as once a dent is formed it will probably propagate as the driving continues, resulting in extensive tip damage.

This research will be done under Van Oord and will be a continuance of the thesis 'Pile tip deformation caused by obstacles' done by M.M. Jorna in 2018, where the focus was on the statics of the impact of a pile with a boulder.

1.4 Methodology

Modelling the impact of a monopile with a boulder requires an extensive study due to the complexity of the phenomenon. This is also evident from previous studies where in most of the cases analytical modelling is done based on simplifications and no numerical model exists able to completely describe the dynamic behaviour of the pile-boulder-soil interaction. Consequently, this research will include a lot of intermediate steps during which the influencing parameters and the way to model them should be identified while trying to achieve a balance between the computational cost and the accuracy of the result.

First, a literature study will be realized in order to comprehend as much as possible the nature of the phenomenon and gather information regarding the influencing parameters. Gathering this knowledge is fundamental for accomplishing a solid research since it will not only set the basis for building the numerical model but it will also give an insight on the way different parameters could be incorporated.

The most important part of this project is the numerical modelling of the pile-boulder-soil interaction. The greatest amount of time was dedicated to this part. Through this period of time, all the knowledge gained from the literature study and from the meetings with the supervisors was implemented to try to achieve the goal of this thesis, namely the dynamic Finite Element Modelling of the impact of the pile with a boulder during the driving process. The modelling was done in parts and in each part the goal was to investigate the chosen parameter. Such parameters were the mesh size, the impact orientation and the slenderness of the pile expressed through the diameter over thickness (D/t) ratio of the pile. The outcome of the modelling process is expected to be a dynamic Finite Element Model capable of describing, as much accurate and realistic as possible, the monopile-boulder interaction.

2. Theoretical background

2.1 Introduction

When loads acting on a structure, stresses are generated and displacements occur. If the load varies in time, also the stresses and the movement of the structure will vary in time. The rate of these variations is usually small in many civil engineering structures, like buildings, for which a quasi (static) analysis might be sufficient. However, fast varying transient loads may also occur in civil engineering structures causing disturbing or damaging vibrations. In such cases, dynamic analysis is needed to capture the actual behaviour of the structure.

2.2 Wave mechanics

When a pile is driven into the ground by a series of impacts, longitudinal waves are excited in the pile which are propagating up and down making the pile move into the ground. The basic assumption in wave mechanics in piles is that the pile responds to impact according to the one-dimensional wave equation. This equation of motion can directly be obtained by implementing the second Newton law in a small part of a straight, prismatic rod. But it could also be obtained for the easiest example of wave motion which is the transverse waves propagation in long taut strings. Physically, longitudinal wave motion in a thin rod and the transverse wave motion of a taut string are different. However, mathematically are quite similar and it turns out that the same wave equation, which governs the motion of the string, also governs the longitudinal motion of the rod, at least within a range of circumstances.

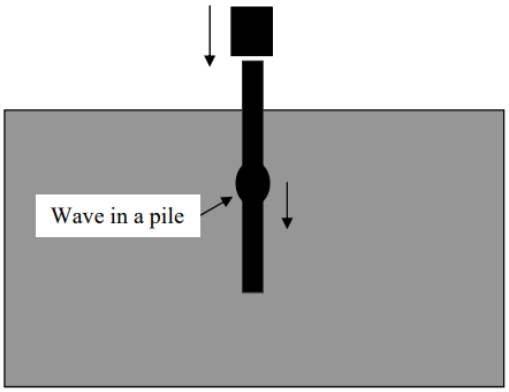

Figure 2.1 *Longitudinal wave in a pile*

The one-dimensional wave equation, which can describe the propagation of longitudinal waves along a thin, long rod, it is formulated as shown below.

$$\frac{\partial^2 u(x,t)}{\partial x^2} = \frac{1}{c^2}\frac{\partial^2 u(x,t)}{\partial t^2}$$

The coordinate x refers to a cross section of the rod, while the longitudinal displacement of this section is given by $u(x,t)$ and c is the speed of the longitudinal waves which depends on the Young's modulus E and the mass density ρ of the rod material and equals to

$$c = \sqrt{\frac{E}{\rho}}$$

By substituting typical properties of steel we can compute the speed of waves propagating in steel, which is approximately 5000 m/s.

$$c = \sqrt{\frac{210\ GPa}{7850\ m/kg^3}} = 5172\ m/s$$

There are several assumptions implicit in the development of the above wave equation. It is assumed that the rod is homogenous with a prismatic shape and that plane, parallel cross sections remain plane and parallel. A uniform distribution of stress over the rod cross section is assumed and there are no body forces acting on the rod. Finally, a very important aspect is the fact that the lateral inertia effects associated with lateral expansions and contractions arising from the axial stress (the Poisson's effect) are neglected.

D'Alembert (1747) proved that any motion described by the wave equation can be represented in the form of a superposition of two counter propagating waves. The classical D'Alembert solution to the wave equation is represented below.

$$u = f^+(x - ct) + f^-(x + ct)$$

According to this formula, functions f^+ and f^- represent counter propagating waves which both propagate with the same wave speed c. The shape of these functions is defined by the initial conditions or the forcing function of a given problem and that shape is maintained during the propagation. Thus, the waves propagate without distortion.

The wave speed with which disturbances travel in the rod is not equivalent to the velocity of the particles in the rod. This can be shown by implementing the D'Alembert solution in a linear elasticity context. If done so, the relation between the particle velocity and the stress reads

$$v(x,t) = -\frac{c}{E}\sigma(x,t)$$

Under elastic conditions, the stress is always much smaller than the elastic modulus, resulting in a much smaller particle velocity compared to the wave propagation velocity.

Problems involving wave transmission and reflection are often studied in terms of the impedance. Impedance express the ratio of a driving force to the resulting velocity at a given point of the structure. For an elastic rod, the impedance is given by

$$Z = \frac{F(t)}{v(t)} = \frac{\sigma(t)A}{v(t)} = \frac{EA}{c}$$

The pile impedance is an important quantity in pile driving analysis since it is a measure of the way in which piles transmits force. A pile with high impedance can transfer force with relatively low strains, stresses and velocities, while in case of a low impedance the pile would require higher strains, stresses and velocities for the same force. This aspect can affect the drivability of a pile in terms of the driving stresses and the pile penetration.

Impedance is also a useful pile attribute when the wave transmission and reflection at a junction of two rods is studied or when in general a discontinuity exists in the cross section, the material or both. Although the phenomenon can be fully explained by the D'Alembert solution and the right boundary and interface conditions, if impedance is implemented makes the outcome interpretation easier. In the general, when the wave reaches the interface, there will be a transmitted and reflected stress field and the transmitted stress pulse always keeps the sign of the incident stress pulse. The sign of the reflected stress pulse depends on the ratio of the impedances of the two parts. When the impedance of the second part is larger, the reflected stress pulse keeps the sign of the incident one while in the opposite case the signs of the reflected and the incident pulses are opposite. If the impedance of both rods is equal, no reflected wave occurs at the junction.

Finally, the impedance could be useful when modelling the hammer system since the entire pile can be modelled as a velocity-based dashpot according to following rule

$$F(t) = Zv(t)$$

This allows the generation of force-time curves for various hammer configurations.

2.3 Reflection of waves at boundaries

If a wave falls on a boundary, it reflects in a certain manner, which is defined by the type of the boundary. The type of the boundary, in a mathematical concept, is expressed by the boundary conditions. In general, the more sophisticated the boundary is considered, the more complex the reflection process becomes. Nevertheless, by using appropriate expressions for the boundary conditions in combination with the D'Alembert solution, almost any case can be defined within the scope of one-dimensional wave propagation.

In general, when an incident pulse meets a boundary, like in the case of an elastic boundary, it will undergo distortion unless the boundary is fixed, free or attached to a dashpot. In case of a dashpot, the reflected wave keeps the shape of the incident wave but with a different amplitude. Depending on the reflection factor, which is a function of the boundary damping, the reflected pulse could have the same sign as the incident pulse, similar to the free end reflection, opposite sign similar to the fix end reflection or there could be no reflected pulse and the incident pulse would be fully absorbed.

For the more simple, but yet fundamental, cases of the free and fixed boundaries a more intuitive approach is also possible, which is called the method of images. This method allows to study reflection from the free and fixed end and some other boundaries by making no use of laborious mathematical elaborations. According to this method, the boundary is removed and

an “image” pulse is introduced so that its superposition with the incident pulse would satisfy the boundary condition.

In case of the fixed boundary, the “image” pulse should be introduced symmetrically (with respect to the boundary) to the incident pulse, be opposite in sign and propagate in the opposite direction with the wave speed c. Thus, having been reflected by a fixed end, the pulse reverses, keeping its original shape. By computing the resulting stress from the displacement of the incident pulse, it can be seen that the stresses of the reflected pulse have the same sign as the incident stresses. This causes the stress doubling during reflection of a pulse from a fixed end. This phenomenon is called “stress multiplication”.

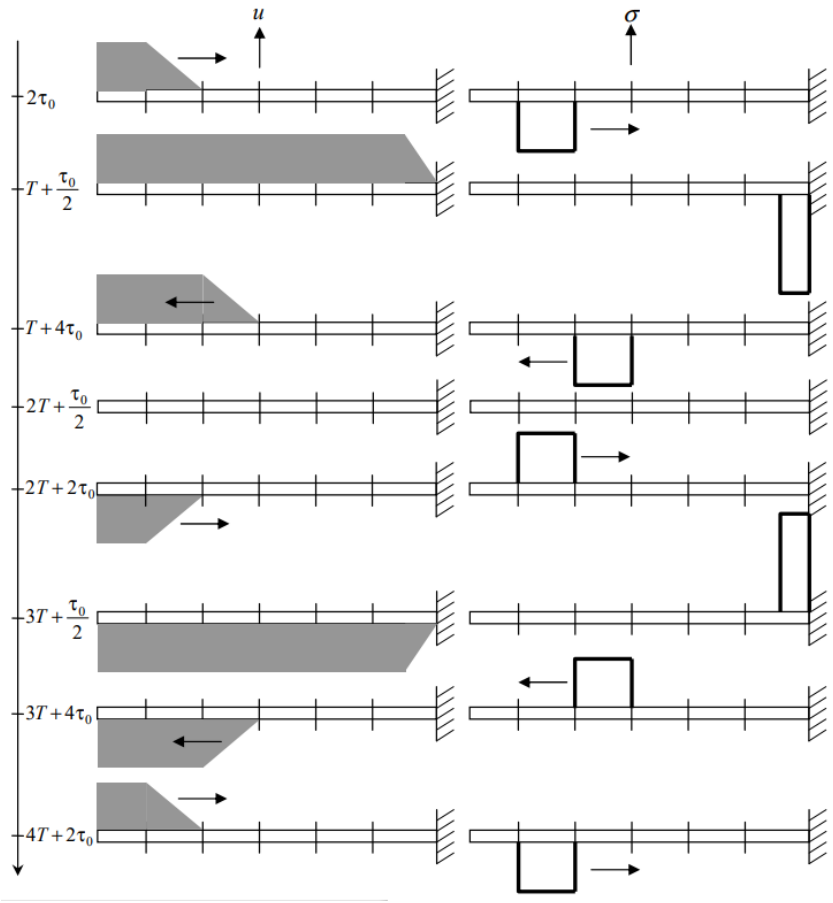

Figure 2.2 *Displacement (left) and corresponding stress (right) for a pulse propagating in a free-fixed pile*

In case of the free end, the “image” pulse should be symmetrical with respect to the boundary, propagating in the opposite direction but have the same sign as the incident pulse in order to satisfy the boundary condition. Thus, at a free end, the displacement in the reflected pulse is identical to that in the incident pulse, while the stress is opposite. So, in contrast to the fixed end, reflection from a free end doubles the displacement and not the stress.

2.4 Longitudinal and transverse wave motion

Mechanical waves propagate through a material medium at a wave speed that depends on the elastic and inertia properties of the medium. There are two main types of mechanical wave motion. The longitudinal and the transverse motion.

So far, the discussion was restrained under the one-dimensional longitudinal wave propagation. This is usually the primary wave motion of concern. In longitudinal waves the vibration of the medium is parallel to the direction of wave propagation and the same holds for the displacement of the medium. These waves are also called compression or pressure waves. Longitudinal waves travel with the largest speed among the wave modes which is approximately 5200 m/s in steel, as shown earlier. In the transverse wave motion, the particle motion is perpendicular to the wave direction. These waves are also called shear waves. Shear waves propagate with a smaller velocity and they have a shorter wavelength than longitudinal waves of the same frequency. Typical shear wave velocity in steel is 3250 m/s.

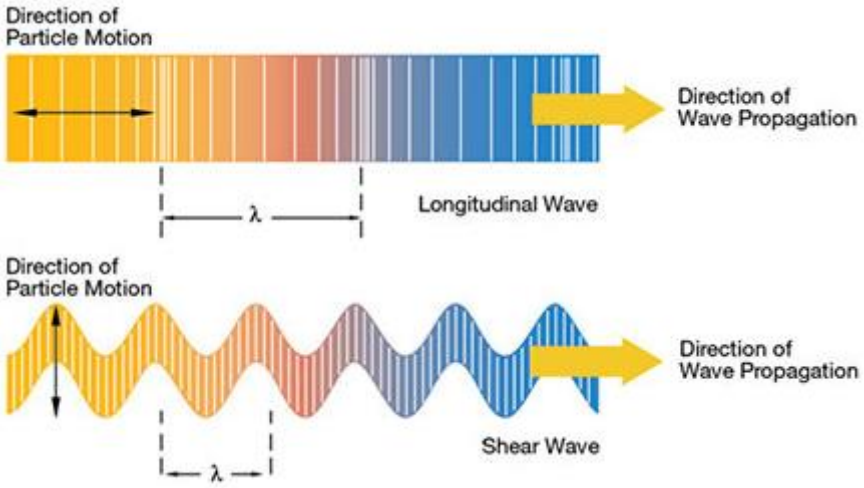

Figure 2.3 *Longitudinal and shear waves*

In order to accurately capture the whole wave propagation, both wave motions should be taken into account. However, depending on the problem studied different assumptions can be made and may only one of the wave motions be considered.

2.5 Pile driving

A blow of a pile hammer is considered a transient load, which means short-term or passing load. In some cases, the blow could be considered as a pulse shaped load, which is an idealisation of the real transient load. In such a case, an infinitely large force occurs during an infinitely short interval of time. However, the time integral of this function is finite and it is called the impulse of this force.

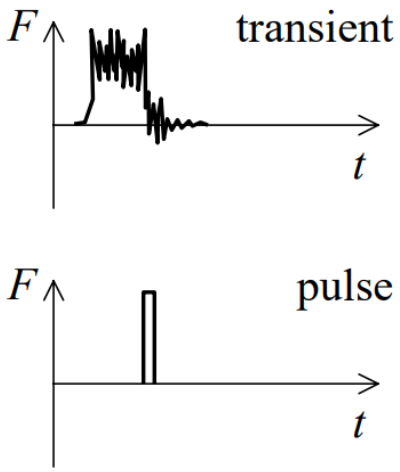

Figure 2.4 *Transient (above) and pulse (below) load*

When a hammer strikes the pile head, the suddenly applied compression force travels along the pile in a wave form that propagates at a constant speed c, which is a function of the material elastic modulus and density. The compressive wave reaches the pile toe at a time L/c after impact (where L is the length of the pile) and reflects as an upwards travelling wave. For a uniform pile with no soil resistance and no constraints at the bottom the compressive wave will reflect back as an upwards travelling tensile force. If shaft friction is included or an end bearing force is generated by the pile motion, then a compressive wave will also travel upwards and reduce the effect of the tension wave.

If at any point the compressive stresses induced by impact exceed the material strength, then pile crushing would occur. For purely end bearing piles with high resistance, the compressive force at the pile toe could double in magnitude compared to the applied force. For local impacts between the pile and a hard object the locally induced stresses could reach much higher values. This can cause pile toe damage although the initial compressive stress was not sufficiently high to cause the more obvious pile top damage

Another cause of wave reflections is change in pile impedance Z. As the wave propagates along the pile, an increase in impedance would cause a compressive reflection while a decreases causes a tension reflection. For severe and abrupt impedance changes, these reflections may contribute significantly to the generated stresses leading to pile damage.

2.6 Pile-soil interaction

In this chapter, the effect of soil reaction on waves in a pile will be discussed inside the frame of one dimensional wave mechanics. Two approaches will be discussed. A local model for the pile-soil interaction, where only the tip of the pile is subjected to the soil reaction and a distributed model, where the soil reaction is modelled by continuously distributed springs and dashpots along the pile.

In the case of the local model, the soil reaction along the length of the pile is neglected and the longitudinal motion of the pile can be described by the wave equation as mentioned in previous

chapter. In addition to the wave equation, the right boundary condition at the pile tip should be formulated, taking into account the applied stiffness and damping and considering force equilibrium in the following way.

$$-AE\frac{\partial u(0,t)}{\partial x} - ku(0,t) - c_{dp}\frac{\partial u(0,t)}{\partial t} = 0$$

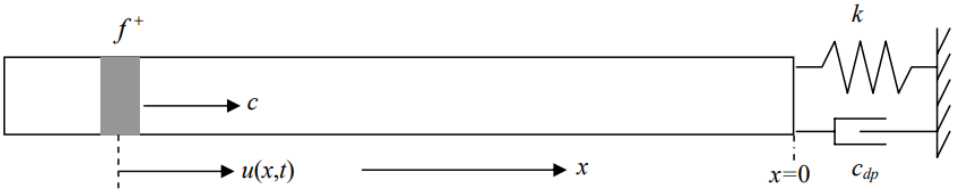

Figure 2.5 *Local model for pile - soil interaction*

Then, by considering the D'Alembert solution, the propagation and reflection of the wave along the pile can be described. By studying the solution, it can be shown that no reflected wave occurs in the pile if the visco-elastic boundary element has zero stiffness and its damping coefficient is equal to the pile impedance.

$$c_{nr} = Z = \frac{EA}{c} = A\sqrt{\rho E}$$

It is much more realistic if the soil reaction is not implemented only at the pile tip but all over the pile surface which is inside the soil. To take this into account a distributed model for the soil reaction can be considered by applying springs and dashpots continuously distributed along the pile. The springs represent the elastic part of the soil reaction while the dashpots represent the energy dissipation due to the soil.

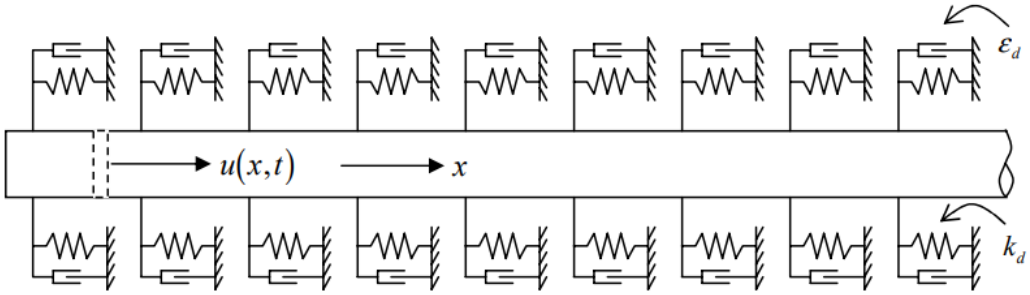

Figure 2.6 *Distributed model for pile – soil interaction*

In such a case the equation of motion can be formulated as follows

$$c^2\frac{\partial^2 u(x,t)}{\partial x^2} = \frac{\partial^2 u(x,t)}{\partial t^2} + \frac{k_d}{\rho A}u(x,t) + \frac{\varepsilon_d}{\rho A}\frac{\partial u(x,t)}{\partial t}$$

Where k_d (force/length) is the stiffness and ε_d (force x time/length) the viscosity of the soil.

It is clear that in case the elastic foundation is implemented the equation of motion in no longer the wave equation which means that the D'Alembert solution I no longer valid. Since the D'Alembert solution is characterized by an undistorted pulse propagation, it is expected that the pulse will be distorted during its propagation along the pile on elastic foundation.

2.7 Fourier Transform

Frequency domain analysis is very important when dealing with signal analysis and the Fourier Transform is a powerful tool that can be implemented. Fourier transform converts a signal in the time domain to a frequency domain signal. The concept behind this transformation is that every non-linear function can be represented as the summation of (infinite) sine waves. A Fourier Transform will break apart a time signal and will return information about the frequency of all the sine waves needed to form this time signal.

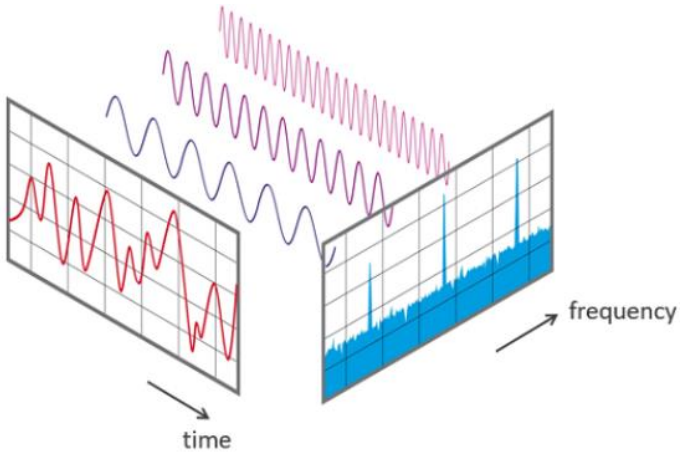

Figure 2.7 *View of a signal in the time and frequency domain [1]*

The implementation of the above method is done through the Discrete Fourier Transformation (DFT) which mathematically is defined as

$$X_k = \sum_{n=0}^{N-1} x_n e^{-i2\pi kn/N}$$

Where

N	is the number of samples
n	is the current sample
x_n	is the value of the signal at time n
k	is the current frequency
X_k	is the result of the DFT

Because of the complex exponential, X_k will take complex values. For this reason it must be scaled and converted to its polar representation to obtain its magnitude and phase. These quantities determine the magnitude and phase of the underlying complex exponential. $X(\omega)$ tells how much content the original signal has at frequency ω.

Fast Fourier Transformation (FFT), is an optimized algorithm for the implementation of the Discrete Fourier Transformation (DFT). The FFT returns the complex valued spectrum and then the amplitude and the phase can be computed for each frequency value, by using the following equations

$$Amplitude\ spectrum = \frac{\sqrt{(real[FFT(x)])^2 + (imag[FFT(x)])^2}}{N}$$

$$Phase\ spectrum = arctangent\left(\frac{imag[FFT(x)]}{real[FFT(x)]}\right)$$

Two of the basic parameters used in FFT are the sampling frequency f_s, which is the average number of samples obtained in one second and the selected number of samples, which always has to be an integer power to the base 2. The theoretical maximum frequency f_n that can be determined by the FFT is half the sampling frequency $(f_s/2)$. If the maximum frequency is exceeded, the signal is reflected at this imaginary limit. The FFT returns a complex spectrum that is conjugate symmetrical, which means symmetric in the real part and antisymmetric in the imaginary part. In other words, for real number inputs, n is the complex conjugate of N-n. For this reason, the second half of the FFT sequence is ignored.

2.8 Finite Element Approach

2.8.1 Introduction

As mentioned before, the analysis of the dynamics of structures leads to the formulation of partial differential equations. These equations contain all the information about the behaviour of the structure under the examined circumstances and by solving them one could have a full view of the structural response. This means that having an analytical solution for these differential equations would be very beneficial. However, this is only possible for very simple structures while a slight increase in complexity could make it an unrealistic task.

Finite Element Analysis (FEA) is a way to tackle the complexity of deriving analytical solution by applying a numerical approach in the analysis of more complex structures. This numerical approach is based on the discretization of a continuous structure and on the approximation of the response of each of the parts (elements) that constitute the whole structure. In this way, obtaining a solution for the structural response becomes much easier and the main issue is then the quality of the solution obtained.

All in all, the steps in a Finite Element Analysis (FEA) consist of the discretization of the structure, the formation of the element stiffness and mass matrices, the assembly of the element matrices into the global matrices and the introduction of the boundary conditions. Detailed explanation of the FEA is not in the scope of this thesis and for any additional information the reader can refer to the literature (Bathe, 2014). Instead, specific crucial aspects of the numerical analysis of wave propagation in structures will be explained.

2.8.2 Discretization requirements

2.8.2.1 Element size

Choosing the right size and type of elements in modern finite element tools is a challenging task which requires a broad knowledge about the background theory of the problem under investigation and experience of the user. The main issue is to find the balance between the chosen accuracy and efficiency in terms of computational time. Mesh sensitivity analyses are a common method to prove the element performance against analytical solutions or experimental results. However, when investigating the complete mesh of an arbitrary structure, the comparison of the mesh performance is quite challenging due to the lack of closed form solutions or available experimental data.

As a general rule, compact meshes with smooth transitions between elements are desired in order to produce more accurate results. Also, in cases of rapid changes of displacements, small element sizes must be used in the respective regions, while in areas with little or no change, the element size can be larger without influencing the accuracy of the overall solution.

It is widely accepted that the element size in wave propagation computations should be related to the wavelength. The waves are characterized by a wavelength λ in space, whose value depends on the frequency f and the speed c of the wave in the medium according to

$$\lambda = \frac{c}{f}$$

This wavelength has to be resolved by the mesh. To accurately represent a wave, the mesh elements must be smaller than the wavelength. This means, that several degrees of freedom are needed per wavelength in the direction of propagation. The smallest element length that can be used is determined by the shortest wavelength, which is referring to the highest frequency to be analysed. Often, a fixed number of elements along the wavelength is chosen based on the desired accuracy. This number, in general varies between six and ten elements.

The idea of using a fixed number of elements per wavelength is a consequence of Shannon's sampling theorem which states the dependency between the frequency content of the signal and the minimum sampling frequency (Jerry, 1977). This is a fundamental theorem in vibration and acoustics for experimental measurements and frequency detection. According to this theorem, at least two points per wavelength are necessary to capture the corresponding frequency. Schmiechen (1997), in his investigation of discretization of axisymmetric structures for modal analysis, states that two points are strictly sufficient, but will still not lead to accurate modeshapes in the eigensolution and a factor of three to five is advised. This is equivalent to the number of six to ten nodes per wavelength. Thompson and Pinsky (1994), suggested at least 10 elements should be considered per smallest wavelength in order to capture the wave propagation with reasonable accuracy. Marburg (2002) found that six elements per wavelength can provide acceptable accuracy. Across the literature no standard recommendation exists about the discretization. Depending on the problem under investigation and the influencing parameters different requirements apply which makes the mesh size a varying parameter. However, it is clear that the rule of thumb of six to ten elements along the wavelength, for an accurate representation of the wave propagation, it is generally confirmed and accepted.

2.8.2.2 Time increment

If the critical wavelength to be represented is L_w, the total time for this wave to travel past a point is

$$t_w = \frac{L_w}{c}$$

where c is the wave speed. Assuming that n time steps are necessary to represent the travel of the wave, the time step equals to

$$\Delta t = \frac{t_w}{n}$$

and the effective length of a finite element should be

$$L_e = c\Delta t$$

This effective length and the corresponding time step must be able to represent the complete wave travel accurately and are chosen differently depending on the kind of element idealization and time integration scheme used.

If low-order finite elements are used, the mesh should be constructed as uniform as possible and L_e is equal to the smallest distance between any two of the nodes of the mesh employed. This length determines the time increment Δt by applying the above expressions. If higher order elements are used, again the mesh should be as uniform as possible with the same measure of effective length L_e, but the time step has to be further reduced because the interior nodes are having a stiffer response than the corner nodes.

In general the time increment should follow the condition

$$\Delta t \leq \frac{element\ length}{wave\ speed}$$

which is referred to as the CFL condition after R. Courant, K. Friedrichs and H. Lewy.

The above considerations are well established for linear dynamic analysis but are largely also applicable in nonlinear analysis. An important aspect in nonlinear analysis is that the periods and wave velocities represented in the finite element system change during its response. Therefore, the selection of the time step size must take into account that in structural dynamics problems the significantly excited frequencies change magnitudes and that in wave propagation problems the wave speed c is not constant.

2.9 Saint-Venant's principle in shell structures

In both static and dynamic problems, difficulties are encountered when trying to obtain analytical solutions in cases where the forces are applied on small portions of the body. As an example, a cylindrical rod could be considered, inserted in tensile test machine. If a numerical simulation of the problem was performed, by using the finite element method, one could obtain useful results. Near the loaded parts of the body, the displacement and stress field would found to vary significantly in all directions reaching very high values. Such fields characterize the local response of the system. Sufficiently far from the loaded regions, the stress field would found to reduce to basically one component, namely the uniform axial stress. At this point, the stress and the displacement field would become independent of the distribution of the loading by the grips to the rod and they would define the global response of the system.

From the above considered example, it becomes clear that sufficiently far from the loaded regions the analytical solution of the problem becomes straightforward. In continuous systems the distinction between the local and the global response is fundamental and it has been stated as a principle by A. J. C. B. de Saint-Venant (1885) as follows:

The elastic response induced by a local force system, whose resultant force and torque are both zero, becoming negligible far enough from the small loaded portion of the body. In other words, if sufficiently far from the loaded domain, the response depends solely upon the resultant force and torque of the actual loading system.

Saint-Venant principle, basically states that the exact distribution of a load is not important far away from the loaded region. In the above statement, *local* means a small part compared to the size of the whole body, or of the boundary in case of contact forces and *far* means significantly greater distance compared to the length scales of the loaded part.

The Saint-Venant principle is fundamental in modelling solids as structural elements. Nevertheless, care has to be taken when using it since its validity is not universal. In the book series of "Modelling of Mechanical Systems", in Volume 2 "Structural Elements" this is illustrated through the finite element modelling of thick and thin cylindrical shells. For modelling the thick shell, higher order solid elements were used while for the thin shell, shell elements were used. The shells were fixed at one edge and along the other edge an axial harmonic load was applied. For the thick shell, where solid elements were used, a stress concentration was obtained close to the vicinity of the loaded contour, in agreement with the Saint-Venant principle. In case of the thin shell and the shell elements, the stress concentration was extended in a larger axial distance, contradicting the Saint-Venant principle.

According to the authors, the fairly large length scales necessary to attenuate the local responses, in case of the shell elements, was attributed to the shell curvature, since the same problem when investigated to a plate led to a much smaller length scale. However, an additional consideration that should probably be taken into account is the limited stress distribution capacity of thin structures, especially when modelling them using shell elements. The application of the Saint-Venant principle requires that the stresses are free to redistribute. Disturbances will travel longer distances, when using shell elements, since the available load paths are limited. So, for shell elements, the Saint-Venant principle cannot be applied in the same way as it does when using solid elements where the stress distribution capacity is larger.

For the above reasons, when modelling cylindrical shell structures loaded by concentrated axial loads, it would be more appropriate to use solid elements in order to capture more accurately the local response of the system. Shell elements, would be sufficient when the interest lies more in the global response of the structure.

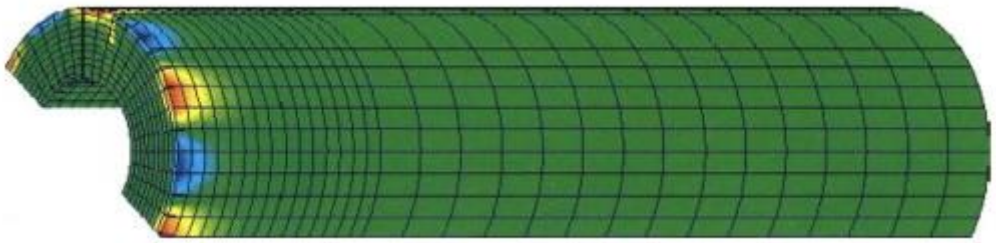

Figure 2.8 *Axial stress field of a thick cylindrical shell – solid elements*

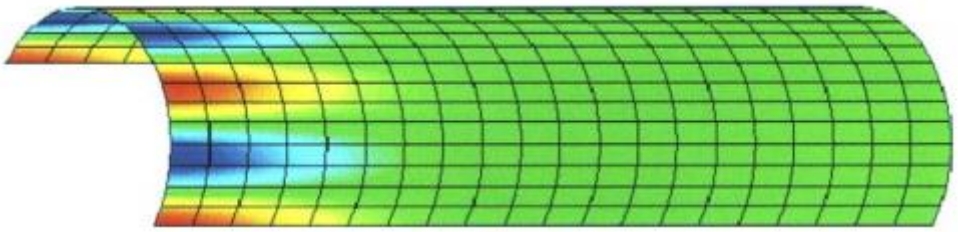

Figure 2.9 *Axial stress field of a thin cylindrical shell – shell elements*

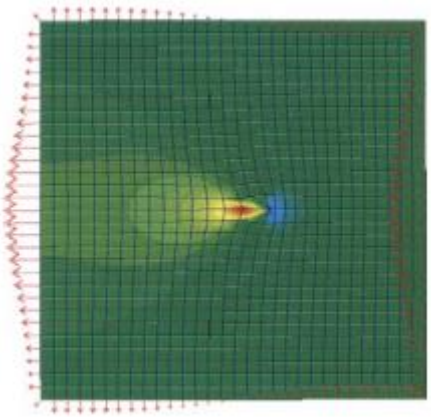

Figure 2.10 *Longitudinal normal stress field of a square plate*

3. Pile integrity during driving

3.1 Introduction

Pile driving is an intense procedure of foundation construction. During installation the piles are subjected to high stress levels, perhaps the highest the piles will ever experience during their service life. Hence, the installation process itself may be the cause of pile structural failure. Causes of driving induced pile damage include the use of inappropriate hammer, insufficient cushioning, tight pile cap, misalignment between pile and driving system, very easy or very hard driving conditions, obstructions in the ground, uneven contact between hammer and pile head and concentrated soil resistance (Hussein and Rausche, 1991).

Observations like driving resistance, made during installation, have long been used to evaluate the structural integrity of driven piles. However, they can be misleading. Dynamic monitoring has been used for decades to evaluate not only the installation stresses, but also to check for potential pile damage. Although, the technology around the monitoring has significantly advanced over the decades to produce accurate results in many cases, there are still a lot of limitations, especially when it comes to damage near the pile tip.

Large diameter, thin-walled, open-ended piles are susceptible to distortion at the tip, particularly when installed into stratified sediments where the soil conditions may vary spatially, both with depth and within planes normal to the pile axis (Randolph, 2018). There is limited data around this phenomenon. However, in a few cases, particular pile damage was detected with structural and economic consequences.

3.2 Limit states

3.2.1 Pile limit states

The term “damage” usually is associated with failure, yielding or buckling but in case of pile driving it should include any pile tip deformation, denting or ovalisation. Axial pile buckling implies yielding of the pile material due to axial stresses while shell buckling is yielding induced by radial stresses. In reality, both of these two buckling modes will take place with combination of axial and radial stresses acting on the pile. Pile tip local buckling refers to the situation where the pile fails or yields at the tip due to an axial force such as the one generated when a hard stratum or an object is encountered. Pile deformations include any out of roundness deformations. While deformation of the pile wall does not necessarily implies material or structural failure, it can eventually lead to axial or shell buckling.

Another pile failure mode is that of damage propagation or extrusion buckling. Damage propagation is the progressive yielding and distortion of the pile during driving, stemming from an initial imperfection or an induced distortion and developing into full pile failure. Full pile failure will usually be a combination of axial and shell buckling and is typically evident by crushed pile ends with axial crimping and/or closed pile ends resulting in peanut shape cross section.

3.2.2 Boulder and soil limit states

As far as the boulder concerns, two are the possible failure modes. Either local failure of the boulder due to the pile penetration into it or splitting. These failure modes could be implemented to a model by characterizing the boulder strength under triaxial loading. Hoek-Brown criterion could be adopted for this purpose. This criterion uses several parameters to describe rock weathering on top of a reference intact rock strength. Implementing rock failure criteria in the impact process of piles during driving is a complicated process which is out of the scope of this research.

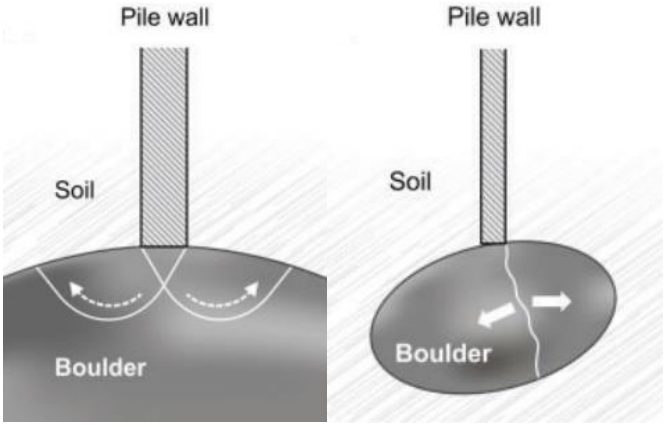

Figure 3.1 Boulder failure mechanisms (Holeyman et al., 2015)

An additional failure mechanism would include soil failure and the boulder penetrating and going through the soil. Zone failure of the soil could be used based on Prandtl and Terzaghi's theory. Soil modelling was out of the scope of this thesis so there will be no further consideration of it.

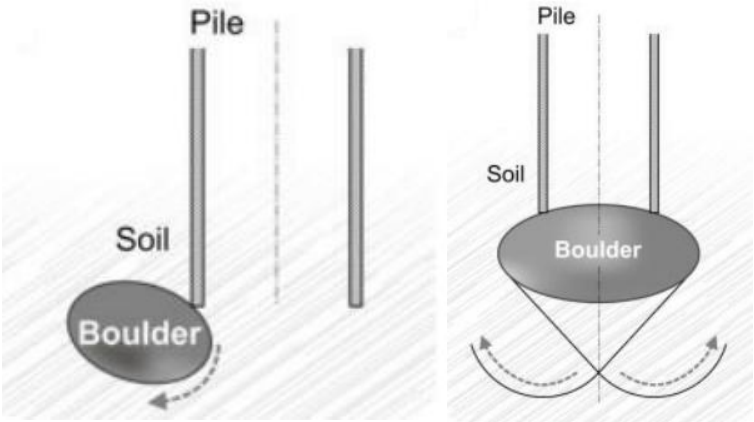

Figure 3.2 *Soil failure mechanisms (Holeyman et al., 2015)*

3.3 Dynamic monitoring

3.3.1 Case Method

Dynamic monitoring of driven piles has its origin as a research project at Case Western Reserve University aimed at the development of methods to compute static pile capacity given field dynamic measurements of pile force and velocity under a hammer blow. The method was later expanded to evaluate hammer performance, pile driving stresses and pile structural integrity assessment from the same dynamic pile top force and velocity records (Hussein and Rausche, 1991).

A Pile Driving Analyzer (PDA) is used to measure the pile top force and velocity caused by the impact of a hammer blow. The signals are obtained in terms of acceleration and strain from piezoelectric accelerometers and strain transducers. The PDA conditions and calibrates these signals and computes average pile force and velocity and then applies the closed form solution of the Case Method.

Strain measurements are converted to force F by multiplication with the Young's modulus E and the pile area A while velocity is obtained by integrating the measured acceleration. Until reflections occur, the force and velocity are proportional by the pile impedance Z. Stress waves due to hammer impact can be separated from reflections by separating the measurements into downward and upward travelling wave components. Considering that superposition of the forces in these stress waves will give the total force at any point, the soil resistance, the stress and other results of interest can be derived.

The total soil resistance is computed from the downward wave at time t and the upward wave at time t+2L/c, where L is the pile length and c is the material wave speed. The reduction of the wave during the period 2L/c, in which the wave travels through the pile, activates the soil resistance and turns back, is called dynamic resistance. The dynamic resistance is calculated as the sum of the downward travelling force at time t and the upward travelling force at time t+2L/c.

$$R_{tot} = F\downarrow(t) + F\uparrow(t + 2L/c)$$

Where

$$F\downarrow = (F + Zv)/2$$

$$F\uparrow = (F - Zv)/2$$

The above dynamic resistance is the total soil resistance activated by a specific impact force and assumed to be the sum of static resistance R_s and damping resistance R_d.

$$R_{tot} = R_s + R_d$$

The total soil resistance is assumed to be concentrated at the pile toe and the damping resistance is assumed to be proportional to the maximum velocity of the pile toe.

$$v_{toe} = \frac{2v(t)Z - R_{tot}}{Z}$$

$$R_d = J_c Z v_{toe}$$

$$R_{tot} = R_s + J_c Z v_{toe}$$

The Case damping constant J_c is a nondimensional empirical and soil type dependent factor. Finally, the static capacity can then be calculated from the following formula

$$R_s = R_{tot} - J_c(2v(t)Z - R_{tot})$$

3.3.2 The Beta method (β-method)

The β-method was first introduced for evaluation of the extent of damage in driven piles since rejecting piles with indications of minor damage was considered unreasonable. An equation was derived from the wave propagation theory which related the stress magnitude of the reflected wave from the potential damage to the magnitude of the impact force, taking into consideration the effects of soil resistance above the damage. This approach resulted in an integrity factor β indicating the theoretical remaining cross section where 100% represents an undamaged cross section and 0% a fully damaged cross section.

The β-method looks for an early tension reflection caused by a reduced cross section along the pile shaft. The maximum reduction in the upward wave from this early reflection is related to the extent of damage. The local reflection caused by damage along the pile shaft can be computed as

$$\Delta = Zv(t) - F(t) + R$$

where t is a time, between the initial impact and reflection from the toe, of the local minimum in the upward wave that corresponds to the damage and R is the total shaft resistance, above the damage location. According to Rausche and Goble (1979), the percentage of the remaining cross section, compared to the original pile cross section, can be computed from the following formula

$$\beta = \frac{1 - a}{1 + a}$$

where

$$a = \frac{0.5\Delta}{F(t1) - R}$$

where $t1$ is the time of the initial impact.

3.4 Pile damage cases

Piles are vulnerable to damage during driving into strong soils. Below two examples from onshore pile driving are presented. In one case tip buckling of an H-pile has occurred due to encountering basalt at a shallower depth than anticipated and in the other case a thin-walled tubular pile become distorted during driving, possibly due to encountering an object within the ground (Randolph, 2018).

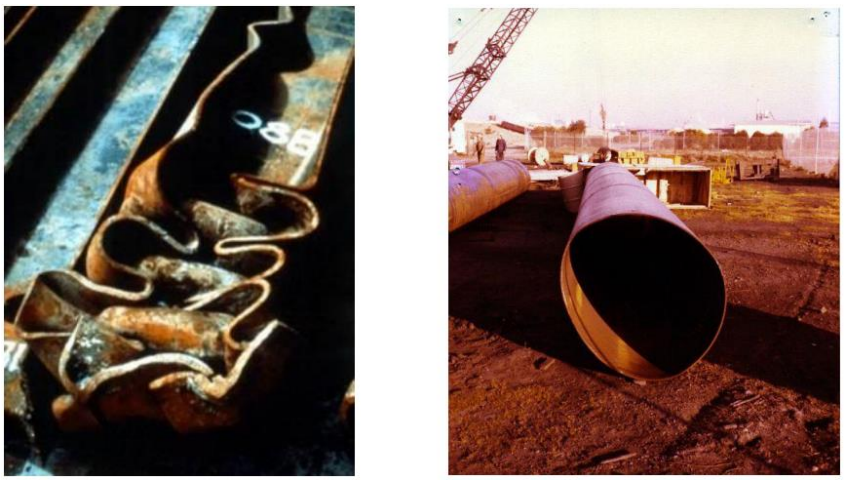

Figure 3.3 *Tip buckling of H-pile (left), Distortion of thin-walled tubular pile (right) (Randolph, 2018)*

Pile tip damage during driving is hard to be monitored and may often go undetected with the only indication being a driving resistance that deviates from the expected profile. For this reason limited cases of damaged piles in real case projects are known. However, still, in some cases damage in piles during driving was documented, either due to successful monitoring or due to later extraction, with structural and economic consequences.

During widening a harbor basin in the Port of Rotterdam, the piles comprising the old quay wall were extracted. Bros et al. (2017) investigated the construction process and widespread damage in the vicinity of the pile tip was discovered, which went completely unnoticed during the original installation. The quay wall was never dredged to its final depth. Over 20% of the pile toes appeared to be damaged. These piles were supposed to provide horizontal stability and hence, the design safety was never achieved. The extracted piles had a diameter of 1420 mm and a thickness of 17 mm resulting in a D/t ratio equal to 83.5 and the soil was medium to dense sand with cone resistance of 25 to 40 MPa. The inclination of the piles was also considered as a possible contribution to the distortion, since the pile tip would have encountered any stronger stratum at one edge of the tip resulting in a dent. Although, the piles in this example were not monopiles, their slenderness could be considered as conservative in today's monopile design. Nevertheless, the damaged piles can work as a reference and indicate how critical the driving process could be in the design phase.

Figure 3.4 *Port of Rotterdam – Damaged pile toes (Bros et al., 2017)*

The Goodwyn A gas platform was installed on the North-West Shelf of Australia in the late 1980s (Barbour and Erbrich, 1994). Driven primary piles were used, below which grouted piles were to be installed to provide the main axial support. 20 primary thin walled piles were used with diameter 2.65 m and wall thickness 45 mm leading to a D/t ratio of 59. However, it was found that 16 out of 20 piles had undergone progressive distortion, over the lower 20 to 40 m, to the extent that pile tips had become almost closed into a peanut shape. The distortion started at about the depth of a layer of cemented material (cone resistance of 60 MPa) embedded within the calcareous silt and sand layers. Although the driving through the variable soil sediments was relatively easy, collapse was attributed to the relatively large D/t ratio at that time, the presence of the hard layer and to the possibility of some initial damage at the pile tips. It was shown that any slight imperfection in the roundness of the pile, particularly due to a localised distortion, can propagate as the pile is driven.

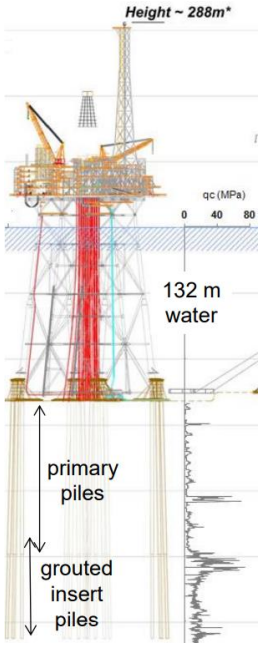

Figure 3.5 *Goodwyn A platform – Overview (Randolph, 2018)*

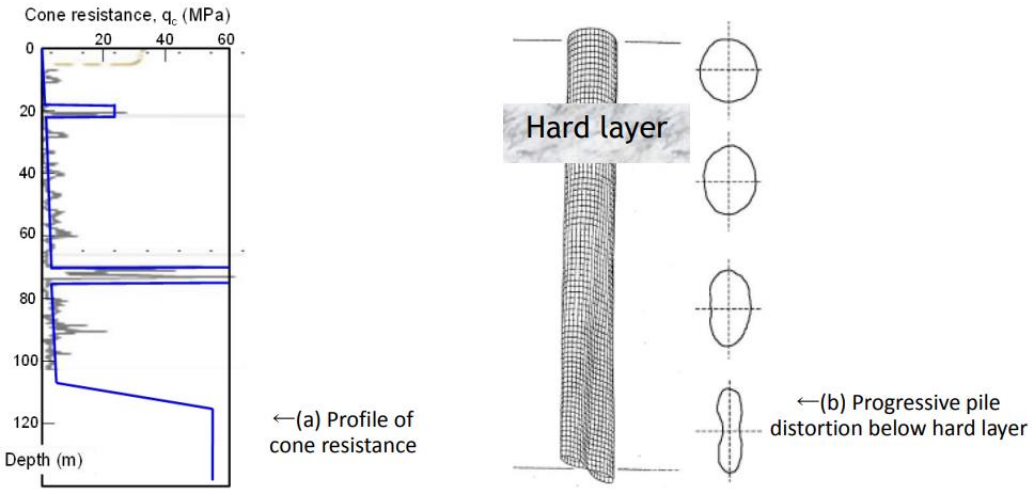

Figure 3.6 *Goodwyn A platform – Soil strength profile (left) and measured growth in pile distortion (right) (Randolph, 2018)*

A more recent collapse occurred at the Valhall water injection platform in the North Sea in 2002 (Alm et al., 2004). The driven piles had a diameter of 2.44 m and wall thickness of 60 mm resulting in D/t ratio equal to 40. 5 out of the 8 piles met premature refusal at depths between 45 and 55 m while target penetration was around 70 m. Investigation revealed that the pile had undergone significant distortion near their tips to the extent that tips were almost closed. The soil comprised very dense sands with cone resistances estimated to about 80 MPa. The investigation showed that the factors which contributed to the damage were the very dense and slopping sand layer and the tapered pile tip.

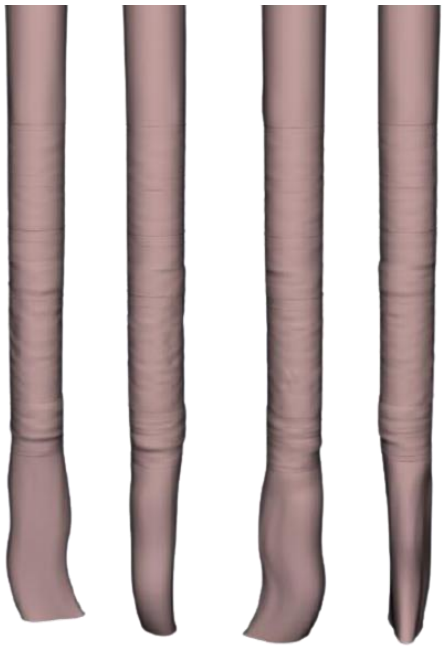

Figure 3.7 *Valhall platform – Typical distortion of lower part of piles (Randolph, 2018)*

Both for Goodwyn A and Valhall platforms, very costly remedial actions were implemented. In case of the Goodwyn A platform, the collapsed piles were reformed (expanded) and in case of the Valhall platform, additional "piggyback" piles were attached (Randolph et al., 2005).

3.5 D/t ratio & Hammer energy

Mostafa (2011) reviews the existing research on the relation between the D/t ratio, the hammer energy and the pile damage during driving into hard soils. According to Mostafa, Tsinker (1997) reported that, for offshore piles, bending stress is not critical when D/t is less than 60, otherwise the piles should be checked for buckling stability. However, Tsinker did not consider the soil type or the hammer energy. Gerwick (2000) reported that in case of Goodwyn offshore platform on the Northwest Shelf of Australia, the pile damage occurred due to the relatively thin walled piles at that time which were driven into dense sand. The pile D/t ratio was equal to 58. Mostafa provides the following figure with the relationship between the D/t ratio and the hammer energy divided by the steel cross sectional area, for a number of cases where steel pipe piles were used. The figure also includes information regarding the pile damage after driving as well as the recommended limits based on the American Petroleum Institute (API, 2007) and the Canadian Foundation Engineering Manual (CFEM, 2006).

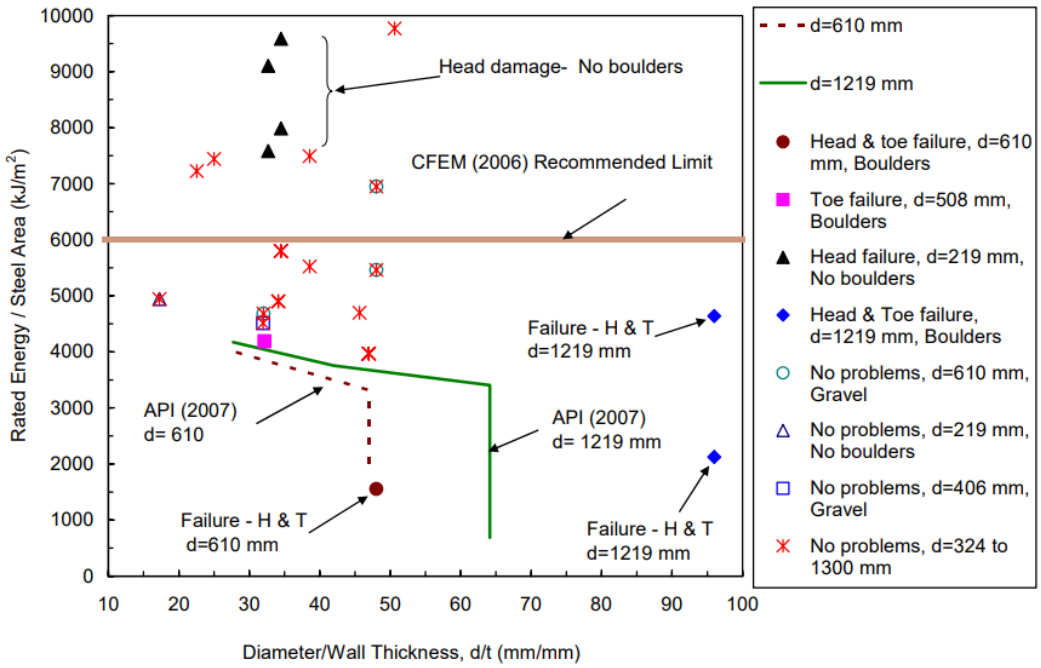

Figure 3.8 *Case studies for D/t ratio versus hammer energy showing API and CFEM recommended limits (Mostafa, 2011)*

It is shown that pile damage during driving in soils where boulders are contained may occur even with relatively low D/t ratios and E/A ratios. It is also noted that CFEM sets a standard limit in hammer energy regardless the soil condition or the D/t ratio. API (2007) guidelines do take into account the D/t ratio but there is no consideration of how hard the soil is or whether cobbles or boulders will be encountered during driving. The above data indicate that steel pipe

piles driven into soils that contain boulders are susceptible to head and/or toe damage even with D/t ratios of less than 32.

3.6 Minimum wall thickness (API, 2007)

Recommended Practice for Planning, Designing and Constructing Fixed Offshore Platforms – Working Stress Design (API, RP 2A-WSD, 2007) are the API guidelines for the design of offshore structures and the main document used in practise for the determination of pile thickness, when it comes to pile foundations. This document states that the D/t ratio of the pile should be small enough to preclude local buckling at stresses up to the yield strength of the pile material. Additionally, it states that in cases when hard driving (820 blows per meter) is expected, the minimum pile wall thickness should not be less than

$$t = 6.34 + \frac{D}{100}$$

where

t is the wall thickness (mm)
D is the diameter (mm)

Based on the above equation, D/t ratio for typical offshore steel pipe piles ranges from 47 to 82 (Mostafa, 2011). However, API (2007) recommends decreasing D/t ratio for increased hammer energy. Nevertheless, the pile slenderness used in offshore wind industry nowadays, is exceeding by far the D/t ratios that are under consideration in the API guidelines, as it can be up to 160. In addition, there is no consideration of the soil type or the amount of boulders which could be encountered during driving. The generation of excessive axial stresses, during installation by driving, are considered in a global frame, ignoring the possibility of local tip buckling caused by impact with an object.

Randolph (2018) is dealing with extrusion buckling of piles and provides the following figure where a number of projects are represented with respect to the D/t pile ratio and they are compared with the API thickness recommendation. In Figure 3.9, the red circles are referring to projects where tip damage followed by extrusion buckling is confirmed while the purple circle indicates suspected damage. It is evident that API does not provide safe guidance for gradual distortion that occurs in extrusion buckling.

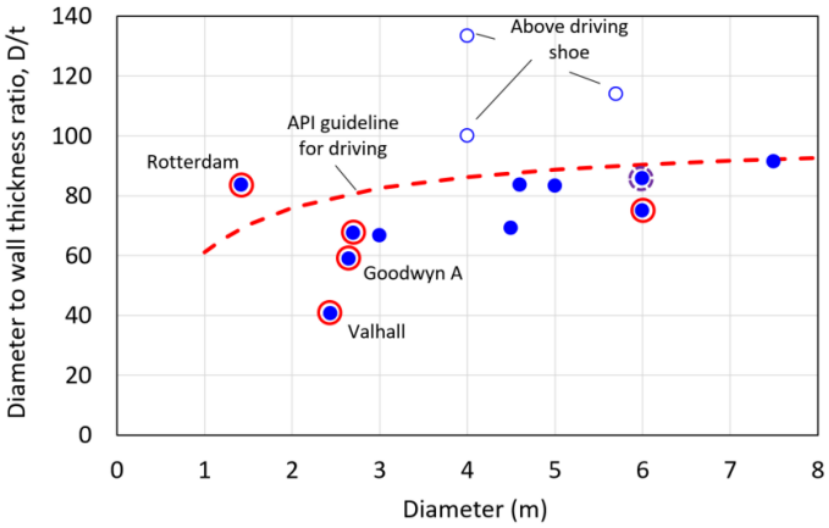

Figure 3.9 *Confirmed (red circle) and suspected (purple circle) extrusion buckling damage in open-ended pile geometries (Randolph, 2018)*

3.7 Stress limitation

In Mostafa's (2011) research a review on the recommendations about the maximum driving stresses can be found. This review is discussed next. Dismuke (1979) recommended a limiting driving stress of 1.4 to 1.7 times the specified yield stress (F_y). Davisson (1979) recommended a maximum dynamic stress of $1.1F_y$. According to Mostafa, it is believed that the allowable driving stress recommended by Dismuke and Davisson is too high. Thompson and Thompson (1979) compiled data from nine sites and reported that steel piles with yield strengths of 240 to 350 MPa were driven to impact stresses of more than $0.8F_y$ without damage. Most of their reported cases included steel piles driven in sandy silt or dense to very dense sand while in a few cases, gravel or shale bedrock was encountered at pile toes. Lee et al. (1995) recommended limiting the driving stress of steel pipe piles to $1.0F_y$ at pile head and $0.5F_y$ at pile toe, based on field test results.

The American Association of State Highway and Transportation (AASHTO, 2010) indicated that the maximum allowable driving stress for driven piles should be limited to $0.9F_y$. US Army Corps of Engineers (2004) recommended $0.85F_y$ as a limit to the maximum allowable driving stress for steel piles.

Schneider et al. (2003) stated that due to different hammer performance and soil conditions, significant variation in transferred energy may induce high compressive stresses near the end of driving. They concluded that allowable driving stresses close to the pile yield stress may cause pile damage during driving in dense soils.

Mostafa (2011) provides the following figure where the D/t ratio and the impact driving stresses are represented for some case studies. The driving stresses shown represent the maximum stresses at the pile heads as they were measured from PDA tests or calculated using the wave equation analysis. In all the cases the yield stress was reported as 300 MPa. It can be

noted that several piles installed in dense soils were damaged at pile head and/or toe even when the driving stress was below $0.6F_y$.

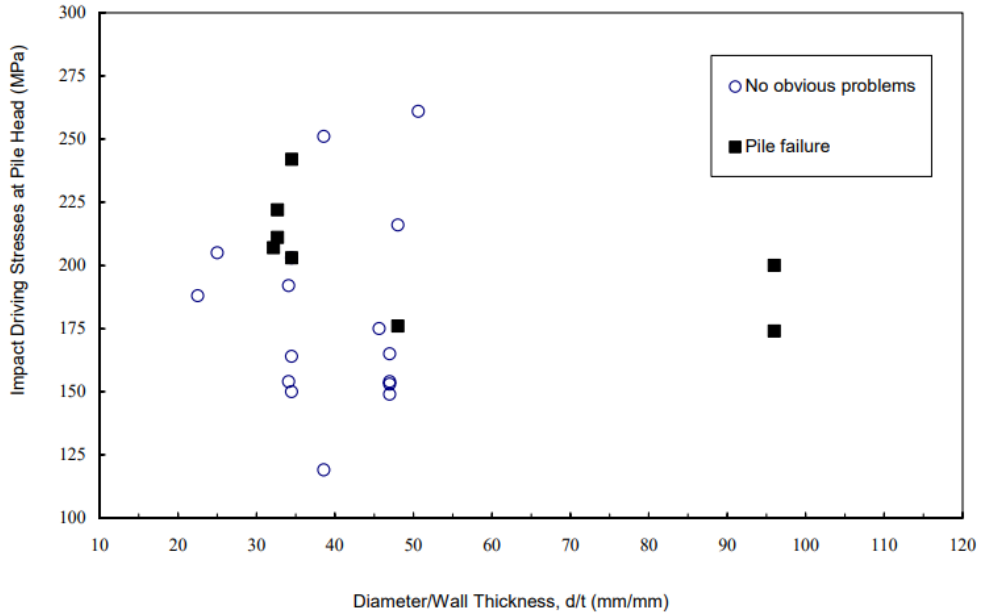

Figure 3.10 *Data presentation of case studies for D/t ratio versus impact driving stresses at pile head ($F_y = 300\ MPa$) (Mostafa, 2011)*

Mostafa (2011) recommended, based on field observations and data analyses for several case studies, that the driving stress should be limited to about $0.5F_y$ if piles are driven in very dense sands, especially if cobbles and/or boulders are present.

In API (2007) the allowable stresses for cylindrical members are discussed in the structural steel design section. In case of axial compression, local buckling of the member is defined in terms of the elastic and the inelastic local buckling stress. The elastic local buckling stress is determined from

$$F_{xe} = 2CEt/D$$

where

C is the critical elastic buckling coefficient
D is the outside diameter (m)
t is the wall thickness (m)

The theoretical value of C is 0.6. However a reduced value of 0.3 is recommended to account for the effect of initial geometric imperfections.

The inelastic local buckling stress is considered more critical and for D/t>60 it is determined from

$$F_{xc} = F_y \left[1.64 - 0.23 \left(\frac{D}{t} \right)^{\frac{1}{4}} \right] \leq F_{xe}$$

For a monopile with a D/t ratio of 100, the inelastic local buckling stress equals to approximately $0.9F_y$. In addition, in the API (2007) pile foundation design section, it is stated that the dynamic stresses during driving should not exceed the values of $0.8F_y$ to $0.9F_y$.

It should be noted that most recommendations reported in literature for maximum driving stresses are somewhat general and do not provide limits for piles driven into very dense soils comprising cobbles and/or boulders. The API stress recommendations are referring in general to the driving process but no consideration is taken about impact of the pile tip with boulders. Hence, although these limits can constitute an initial assumption of the allowable driving stress, they would not suffice when tip damage is at stake due to the intensity of impact.

3.8 Pile tip integrity

3.8.1 Analytical models

Limiting the stress magnitude from solutions of classical elastic mechanics for tubular systems may be used to assess pure axial or shell buckling of the pile. Over the years, a few analytical models were created to describe the pile tip response during driving. Classical mechanics were applied for their derivation and a number of assumptions and simplifications were implemented.

HSE (2001) revealed a study with the objective to determine the sensitivity of piles to fatigue with respect to both foundation soils and welding details and to review the propensity of pile tips, built to usual fabrication tolerances or with initial dents, to further damage. In this study, solutions, based on classical mechanics, are provided for pure axial and shell buckling of the pile. The methods of Ellinas and Walker, for calculating the dent damaged, were used and the maximum pile tip force to cause a local dent was expressed as

$$Q_{tip} = 4.65 f_y t^2 \sqrt{\delta / D}$$

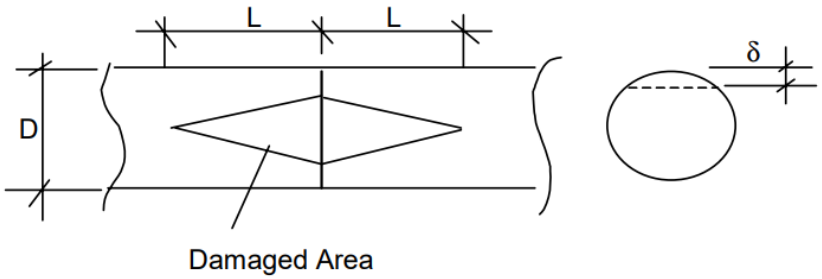

Figure 3.11 *Plan and section on damaged tubular, HSE (2001)*

By substituting the typical value of $\sqrt{\delta/D}$ equal to 0.1 used in the Ellinas and Walker work, then the pile tip force was expressed as

$$Q_{tip} = 1.2 f_y t^2$$

Aldridge et al. (2005) investigated the lateral and axial forces at the pile tip to initiate a local dent by applying upper bound theory for an assumed plastic hinge mechanism and proposed the following, similar expressions.

$$F_{lateral} = 1.4 f_y t^2$$

$$F_{axial} = 2.8 f_y t^2$$

Based on solutions for inward deflection of a ring, they also proposed expressions to compare the pile D/t ratio with the pile and soil stiffness and yield strengths that would likely lead to pile damage propagation.

Holeyman et al. (2015) investigated the premise that encountering a boulder during driving will cause a contact force at the pile tip that may be large enough to initiate a local imperfection or even local pile tip buckling. The magnitude of the contact force was considered to depend on the hammer settings, the pile and boulder properties and the embedding soil. The boulder-pile interaction was modelled based on the 1-D wave theory and the following figure illustrates the assumed 1-D mechanical model.

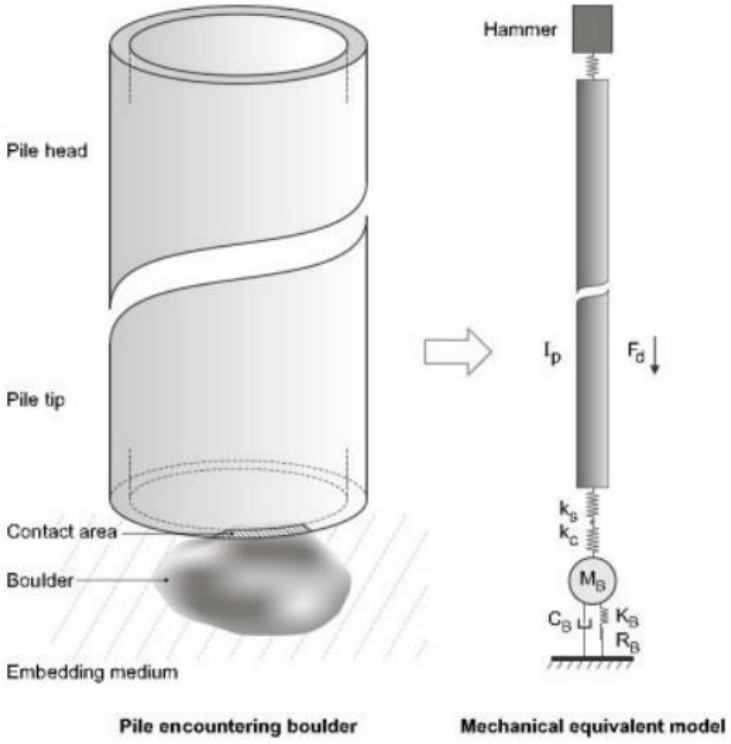

Figure 3.12 *Pile-boulder-soil model (Holeyman et al, 2015)*

The model was developed within the lumped parameter software GRLWEAP through user-defined elements representing the interacting boulder. The model rests on two major assumptions which are linear material behaviour and interaction laws and only the axial behaviour is modelled. The numerical analysis can output the load exerted by the obstructing boulder as a result of the hammer generated incoming wave force. Then, the peak contact force can be compared to the minimum axial force required to initiate local pile tip buckling as it can be computed by analytical expressions. The boulder was considered as rigid body embedded in an elastic medium and the embedment stiffness and damping were computed accordingly. The impact was assumed to be done at the very top of the pile to remain under the 1-D axial framework. Different boulder failure modes were considered such as splitting or local failure. A parametric analysis of the boulder size was conducted using the proposed model and the results are represented in the following figure.

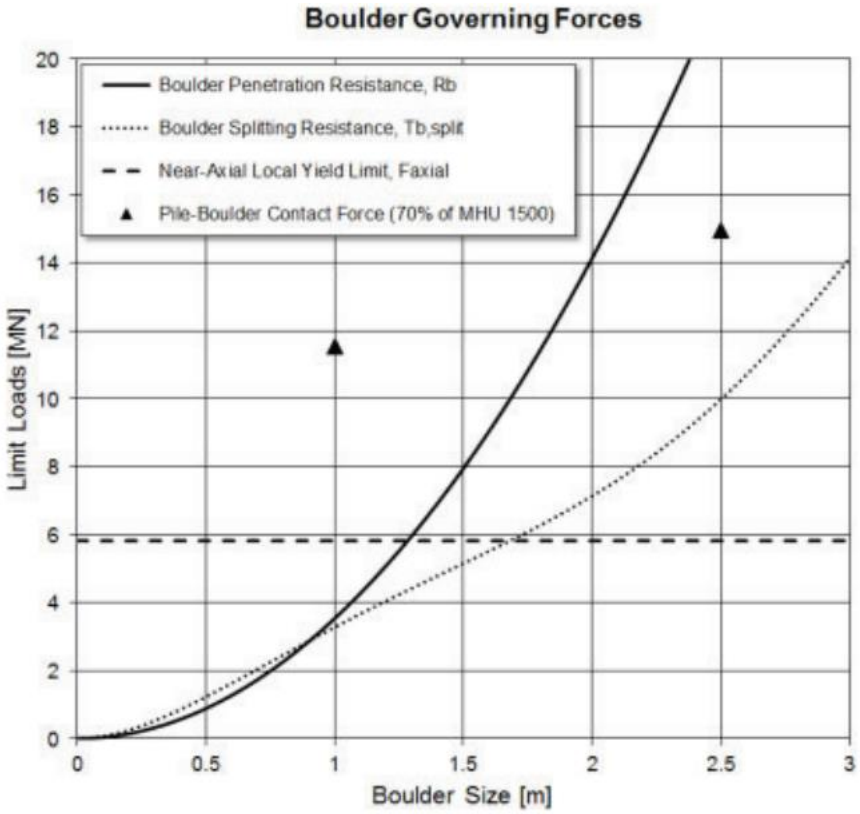

Figure 3.13 *Limit loads of pile, boulder and soil as functions of boulder diameter (Holeyman at al., 2015)*

The yield limit of the pile tip was taken equal to the axial load F_{axial} necessary to initiate a local dent at the tip as was defined by Aldridge et al. (2005). It was concluded that the peak driving force transmitted to the boulder exceeds the pile yield load, the boulder splitting resistance and to some extent the soil limit load (boulder penetration resistance). The mode of failure depends on the boulder size and the need to define boulder size and fully characterize boulder strength with respect to breaking and splitting was highlighted.

3.8.2 Numerical models

In order to investigate the process of extrusion buckling, which was noticed in the distorted piles of the Goodwyn A platform, Balbour and Erbrich (1994) developed a numerical technique (BASIL) within Abaqus. The pile-soil interaction was represented by layers of springs distributed around the embedded section of the pile and each spring had an appropriate non-linear load-displacement curve. As the pile advances, any forced radial displacement at the spring will produce a force acting on the pile wall. The analysis starts with pile already embedded to some depth and with a pile tip distortion according to the shape of a radial buckle mode. The out of roundness was ranging between 0.5% and 2% of the pile radius.

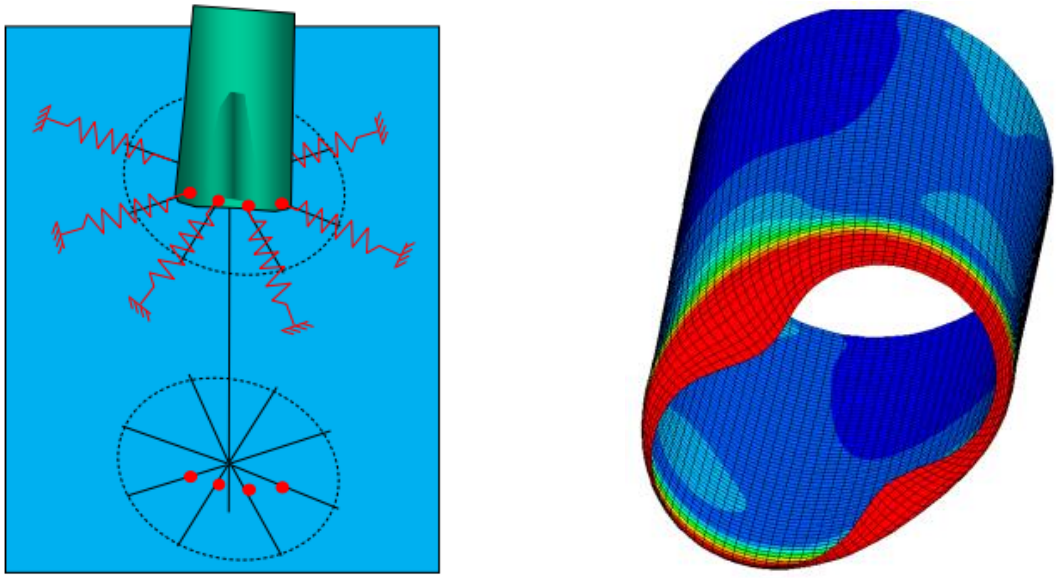

Figure 3.14 *BASIL - Soil represented as springs (left) and initial tip imperfection (right) (Randolph, 2018)*

An example outcome from a BASIL simulation of the a Goodwyn A pile is shown below. To achieve progressive distortion, an initial imperfection of 25 mm (1.9% of the pile radius) was necessary. The need to apply a more significant initial distortion indicated that some external factor might have contributed to initial damage of the pile tip prior to installation, either a collision or lateral heterogeneity of the cemented sediment layer (Randolph, 2018).

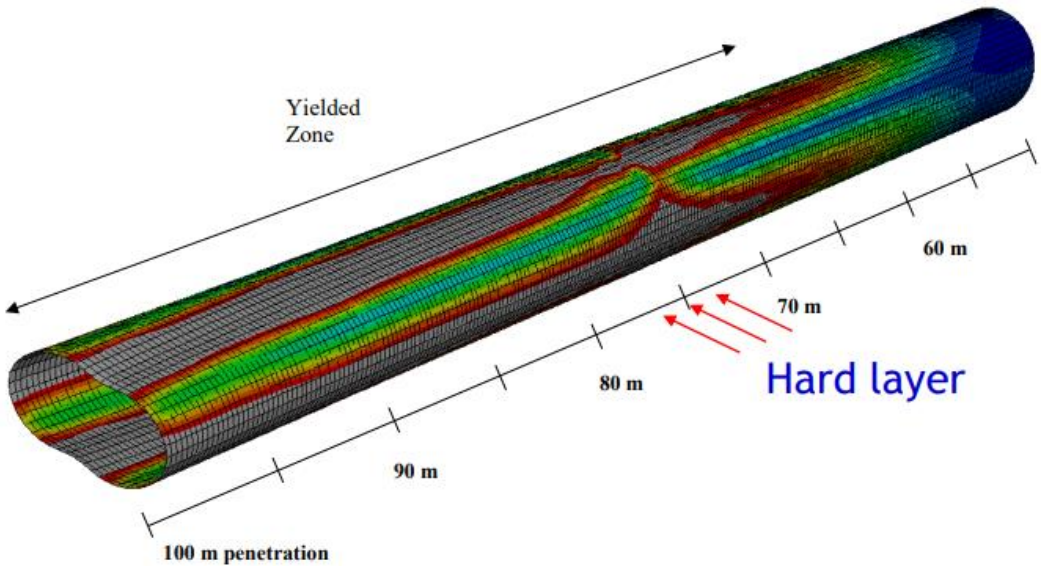

Figure 3.15 *BASIL – Plastic strains of a pile pushed 25 m beyond the hard layer (Randolph, 2018)*

Jorna (2018) investigated the potential deformations that could occur to the pile tip due to impact with a boulder during the driving process. A finite element model was built using Ansys and the impact process was simulated through a number of static analysis. The boulder was considered to be fixed and to have a spherical shape. A friction coefficient of 0.3 was used. The soil around the pile was also included through the use of non-linear Winkler springs. The study was focused on the contact angle and the pile thickness. Among the conclusions, it was found that large contact angles might lead to local ovalisation, sliding and propagation of damage. The thickness influence fount to dominate over the diameter and hence, D/t is insufficient as a single design parameter.

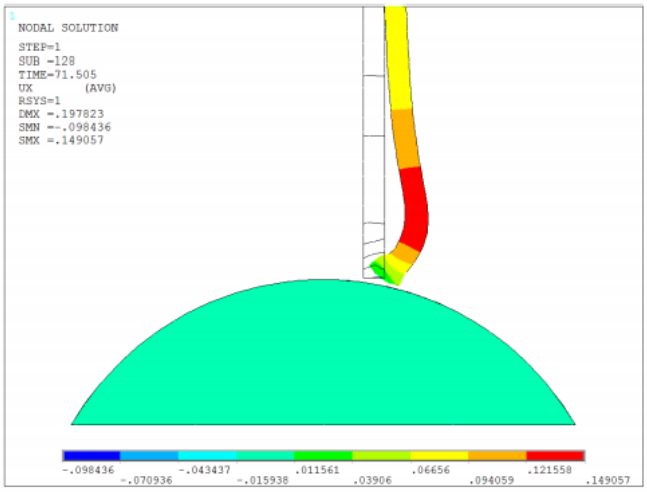

Figure 3.16 *Example of the resulting radial deformations at the pile tip (Jorna, 2018)*

4. Introduction to the model

4.1 Introduction

The goal of this research was the representation of the impact process between a monopile and an object which would be encountered during driving, through Finite Element Modelling (FEM). For this reason, a model was created in the finite element software Ansys. Modelling of such a complex phenomenon for which limited research is available, required a number of simplifications and assumptions in order to limit the research scope and focus on specific selected aspects. Due to the number of parameters involved, the model should be constructed in a parametric way so that different aspects could be inspected and compared with each other. A parametric Ansys APDL script was built which automated the extraction of results for different scenarios. The intention was to build a model capable of representing the impact process to a specific extent and also be used in future research when additional parameters would be studied.

4.2 Monopile and boulder characteristics

The monopile geometry was selected such to be representative of the piles used by Van Oord for the foundation of a regular size wind turbine. As a reference, in Borssele 3 and 4 wind farms the global characteristics of the pile used by Van Oord, for the foundation of a 9.5 MW turbine, were a diameter of 7.4 m and a D/t ratio equal to 100. In this research the pile geometry was close to that. A D/t ratio of 100 was used with an outer diameter of 9 m, resulting in a pile wall thickness of 9 cm. The length of the monopile was set to 80 m. The whole monopile was selected to be modelled due to the fact that the mesh size was found to be the main parameter influencing the total analysis time. Limiting the size of the model would have an insignificant influence on the computational time compared to the influence of an efficient mesh topology. The analysis time is represented later in the chapter about the mesh sensitivity investigation.

The steel grade applied to the pile was S355, a common choice in practice for offshore monopile foundations. Material non-linearity was considered according to the stress-strain curve that is defined in DNVGL-RP-C208 (2016). The guideline defines different curves with respect to the member thickness and as the thickness increases the yield stress decreases. In this case, the curve for thickness values between 63 and 100 mm was considered. More information on the DNVGL stress-strain curve and the steel S355 properties can be found in Appendix B.

Table 4.1 *Pile geometric properties*

Parameter	Value
Outer diameter – D (m)	9
Wall thickness – t (m)	0.09
Length – L (m)	80

Table 4.2 *Steel S355 material properties, DNVGL-RP-C208 (2016)*

Parameter	Value
Density – ρ (kg/m^3)	7850
Young's modulus - E (GPa)	210
Yield strength - $\boldsymbol{\sigma_y}$ (MPa)	316.7
Shear modulus – G (GPa)	80.8
Poisson ratio – ν	0.3

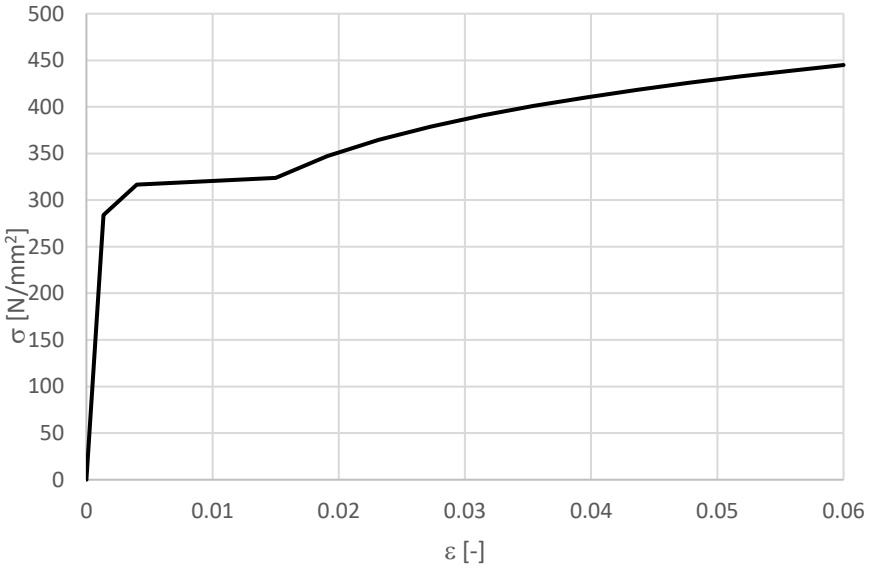

Figure 4.1 *S355 steel stress-strain curve (DNVGL-RP-C208, 2016)*

A boulder with a diameter of 2 m was used in the analysis. This represents a relatively large boulder which is likely to be found in offshore driving operations. Properties of granite were applied to the boulder. This is a conservative approach since granite is a much stiffer rock than the ones which are likely to be encountered during driving. The use of stiffer rock types will result in less energy absorption and larger induced tip deformations. The focus of this thesis was on the structural integrity of the pile so besides the definition of the rock stiffness, the Poisson ratio and the steel-rock friction coefficient no additional investigation was done regarding the rock properties. The rock material was defined as linear elastic.

Table 4.3 *Boulder properties*

Parameter	Value
Boulder diameter (m)	2
Young's modulus (GPa)	50
Poisson ratio	0.3
Stell-rock friction coefficient	0.3

4.3 Boundary conditions

In the considered model, the only thing constraining the vertical movement of the pile was the boulder at the bottom of the pile. The surrounding soil was not taken into account. This approach can be considered as conservative since, in reality, the soil will take some part of the loading, reducing the force magnitude which would reach the pile tip. Moreover, the soil is expected to limit to some extent the pile tip deformations. However, the focus of this study was purely on the effect the impact with an object could have on the pile tip. Hence, it was decided to neglect the soil contribution at this point of the research.

The boulder was fixed on all directions at its bottom. This is an additional conservative criterium since the movement of the boulder through the soil would limit the generated stress at the contact region and hence, the deformations would also be limited to some extent. Fixing the boulder represents a scenario where the pile impacts to solid immovable rock, resulting in higher stress values and increased deformations at the pile tip. Although, this scenario does not seem as a realistic one, it could be close to some real case examples of very dense soils or relatively large boulder sizes. In such cases, indeed, the generated force at the tip could be less than the boulder penetration resistance. This is also illustrated by Holeyman et al. (2015).

In general, the considered boundary conditions reflect to an upper bound model where the worst case damage scenario at the pile tip is investigated.

4.4 Element type

In Finite Element Modelling, a usual dilemma is whether shell or solid elements should be used. Both of them have advantages and disadvantages. Concisely, shell elements are suitable for representing thin structures where the through thickness behavior is not important while solid elements are more suitable to describe complex non-linear behavior and represent the through thickness behavior. Due to their solid structure, solid elements usually provide more accurate results but with a cost in computational time.

For modelling the axial behavior of a pile, shell elements are expected to sufficiently describe the global response. However, when impact between the pile and an object is studied, the problem includes large stress concentrations, local out of plane deformations and non-linear behavior. Hence, solid elements were selected as more appropriate to capture the distortion at the pile tip due to contact with an object.

The SOLID186 element was used from the Ansys element library. SOLID186 is a high-order 3-D 20-node solid element that exhibits quadratic displacement behavior. The element is defined by 20 nodes, having three degrees of freedom per node namely translation in the nodal x, y and z directions. The different forms of the element are represented in the Figure 4.2.

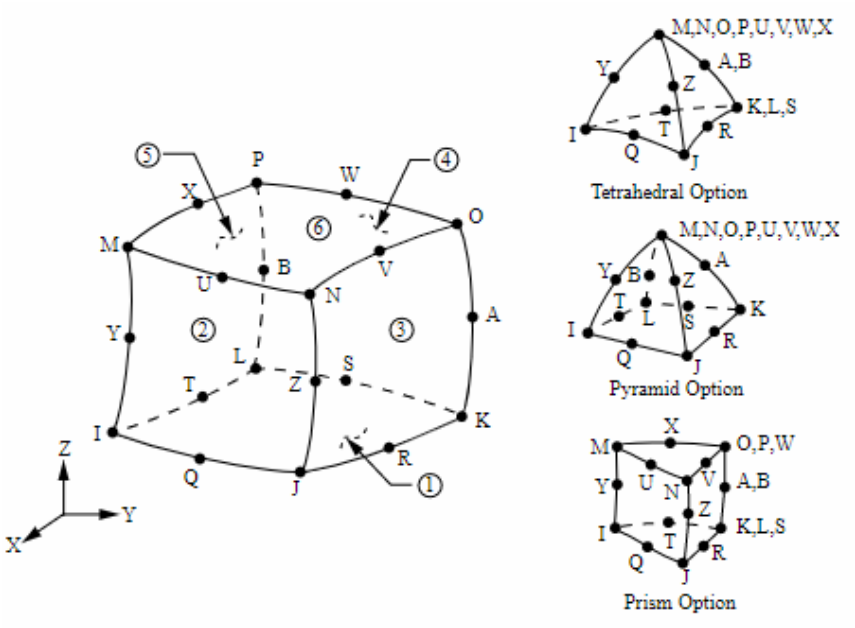

Figure 4.2 *Higher order (SOLID186) element in Ansys*

4.5 Loading & Analysis time

A real pulse was applied to the top of the pile as it was measured by Van Oord. The impact force versus time is represented below. The duration of the pulse was 0.0104 s. The loading process was modelled in three stages. First, a stage of 0.001 s was defined where no load was applied to the pile. In the second stage, the pulse was applied between 0.001 and 0.0114 s. Finally, in the third stage no external load existed and the wave was propagating through the pile.

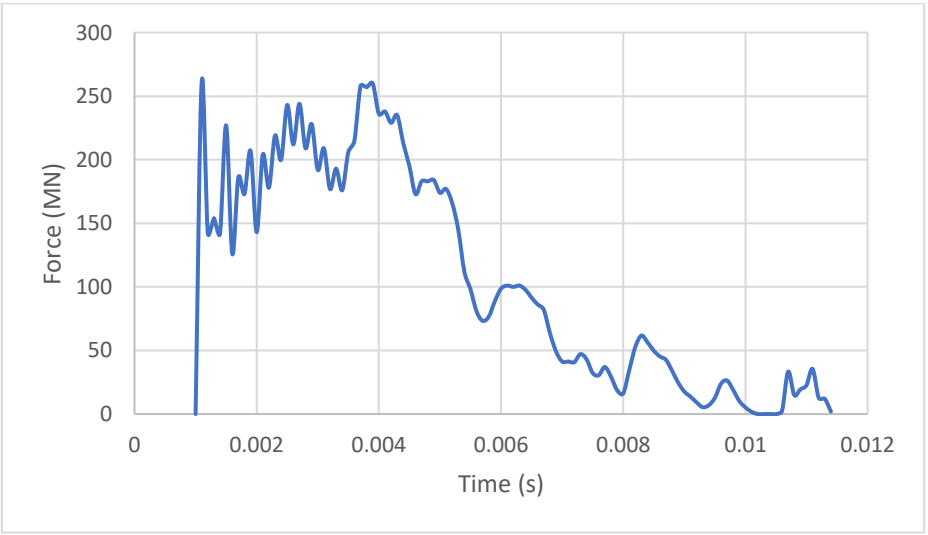

Figure 4.3 *Impact force (Van Oord)*

The goal of the thesis was to retrieve information regarding the initiation of damage at the pile tip due to impact with a boulder. For this reason the FEA was focused on capturing the pile

response after the first applied pulse reached the bottom of the pile and reflected back. The time needed for one pulse to travel from the top to the bottom of the pile can be computed by dividing the pile length with the wave speed. Hence, in approximately (80 m/5172 m/s) 0.016 s the wave will reach the pile tip. The total analysis time was set to 0.0314 s, so that the wave can reflect sufficiently back and during the final time step, the residual tip deformation is represented.

4.6 Contact modelling

4.6.1 General

When studying the contact between two bodies in Ansys, the surface of one body is taken as a contact surface and the surface of the other body as a target surface and together they constitute a “Contact Pair”.

To model the physical interaction between contact and target surfaces in a transient dynamic analysis, the contact forces must maintain force and energy balance and proper transfer of linear momentum. This requires imposing additional constraints on relative velocities between the contact and target surfaces (Laursen and Chawla , Armero and Petocz).

An automatic time stepping scheme is used to predict the time of impact and adjust the size of the time increment to minimize penetration. The allowable penetration is decided such that energy and momentum are conserved. When contact is detected, the relative velocity constraints are imposed using a contact algorithm and based on the velocity constraint the contact pressure, the slip increment and the frictional stress are computed.

Imposition of the impact constraints at Gauss points of contact elements ensures satisfaction of momentum and energy balance in a finite element sense. Total energy at the contact-target interface is conserved for frictionless contact when relative velocity constraints are satisfied exactly. If the relative velocity constraints are not satisfied to a tight tolerance there may be some loss of kinetic energy.

When friction is included, energy is conserved when the contact and target surfaces are not slipping with respect to each other. During slipping, energy equal to the work done by frictional forces is dissipated.

4.6.2 Contact elements

As mentioned earlier, when modelling contact problems in Ansys, a contact and target surface should be defined and proper elements should be assigned to them. Contact elements are constrained against penetrating the target surface. However target elements can penetrate through the contact surface.

The contact element used in the pile surface, was the CONTA174. This is a 3-D, 8-node, higher order quadrilateral element that is used to represent contact and sliding. The contact detection points are the integration points of the element which can be located either at nodal points or Gauss points. CONTA174 uses Gauss integration points by default, which generally provides more accurate results than when using the nodes themselves as the integration points.

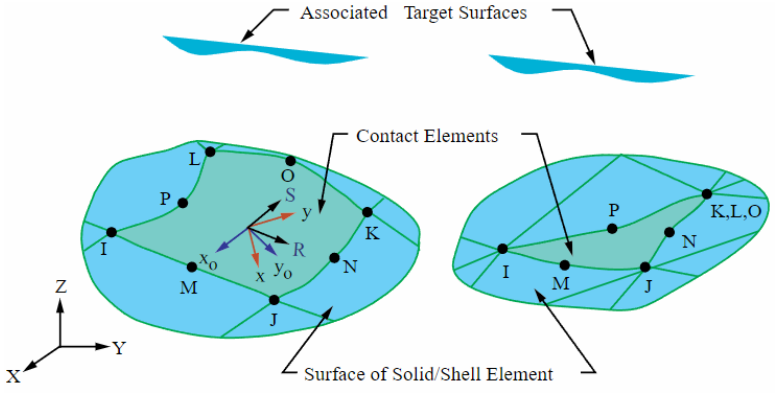

Figure 4.4 *CONTA174 geometry*

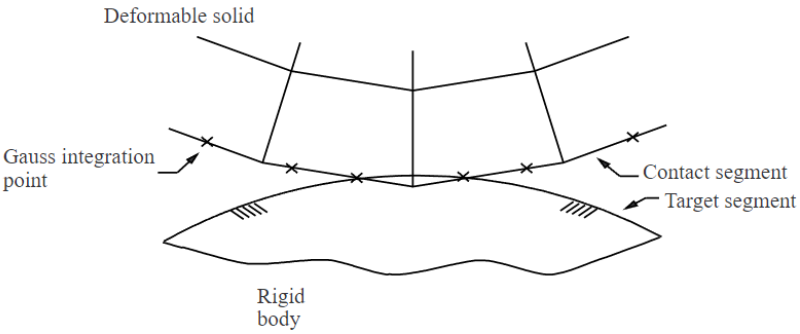

Figure 4.5 *Contact detection point at Gauss points*

For the target surface the TARGE170 element was used, which depending on the underlying elements can be a 3-D triangular or quadrilateral element.

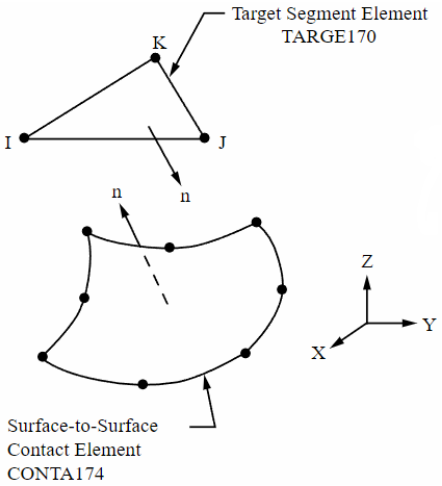

Figure 4.6 *TARGE170 geometry*

4.6.3 Contact algorithm

The contact algorithm used for modelling the contact behaviour between the pile and the boulder is the augmented Lagrangian method. According to this method the contact tractions (pressure and frictional stresses) are augmented during the equilibrium iterations so that the final penetration is smaller than the allowable tolerance. The augmented Lagrangian method usually leads to better conditioning and is less sensitive to the magnitude of the contact stiffness. However, it may require additional iterations, especially in cases where the deformed mesh becomes too distorted.

4.6.4 Contact stiffness and allowable penetration

For the augmented Lagrangian method, normal and tangential contact stiffness are required. The amount of penetration between the bodies in contact depends on the normal stiffness while the amount of slip depends on the tangential stiffness. Higher stiffness values decrease the amount of penetration or slip but can lead to ill-conditioning of the global stiffness and to convergence difficulties. On the other hand lower stiffness values can lead to a certain amount of penetration or slip and produce an inaccurate solution. Ideally, the stiffness should be high enough that the penetration and slip are acceptably small but low enough that the model will behave well in terms of convergence.

In Ansys, default values for the contact stiffness are defined and during the analysis these values are updated based on the contact pressure and the allowable penetration and slip. In this analysis, the default values of Ansys were used since the model was behaving well without any convergence issues. This is recommended and should work in most cases.

4.6.5 Friction model

The basic Coulomb friction model is used through the modelling of the contact behaviour between the pile and the boulder. According to this model, the two contacting surfaces can carry shear stresses up to a certain magnitude across their interface before they start sliding relative to each other. An equivalent shear stress is defined based on the friction coefficient and the contact pressure, at which sliding on the surface begins. Once the shear stress is exceeded, the two surfaces will slide relative to each other.

$$\tau_{lim} = \mu P$$

A coefficient of friction equal to 0.3 is used between the pile and the boulder.

5. Dynamic Finite Element Analysis

5.1 FFT on the applied pulse

The major difference between a structural dynamics problem and a wave propagation problem is that in wave propagation analysis a large number of frequencies are excited in the system. A way to analyse a wave propagation problem is to use a sufficiently high cut-off frequency to obtain enough solution accuracy. A preliminary step lies in identifying the cut-off frequency and in establishing a corresponding finite element problem. A way to identify the frequencies contained in the loading is by using a Fourier analysis.

A Fast Fourier Transformation (FFT) was implemented on the pulse, applied at the top of the monopile, in order to investigate the frequency region of the pulse. This is important, since based on the frequency spectrum of the pulse, the appropriate maximum frequency will be defined, according to which the critical wavelength will be computed. The critical wavelength will be the starting point of the mesh size selection since the mesh size will be described by the number of elements that will be used to discretise this wavelength for an effective computational modelling of the wave propagation along the pile.

The FFT analysis was executed using Excel and the Fourier Analysis algorithm of the Analysis Toolpack. As mentioned in previous chapter, the FFT analysis requires a power of two (2^n) samples, so for the representation of the applied pulse 128 samples were used. The applied force at the top of the monopile over time is represented in Figure 5.1.

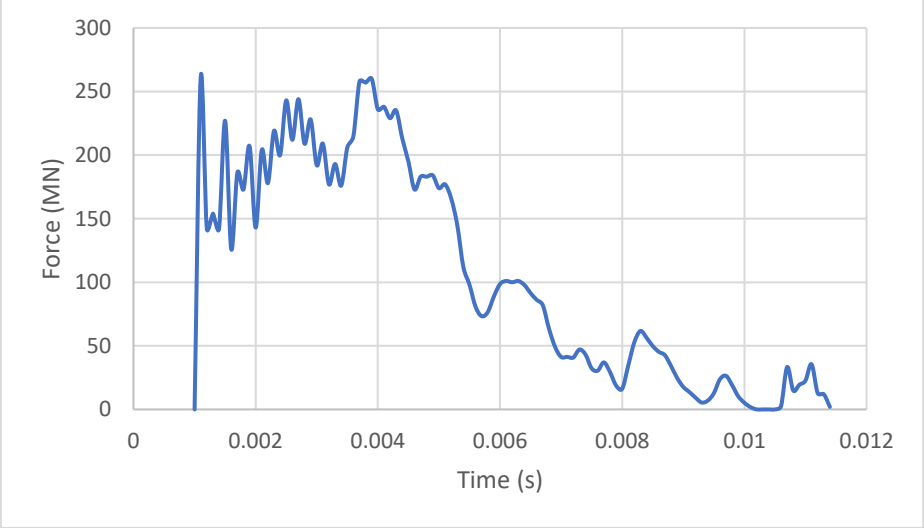

Figure 5.1 *Impact force (Van Oord)*

The frequency of each sample was computed by dividing the sample number with the total analysis time. The sample time increment equals to 0.0001 s which means that the sampling frequency equals to

$$f_s = \frac{1}{dt} = \frac{1}{0.0001s} = 10000\ Hz$$

After performing the FFT analysis, the frequency spectrum in Figure 5.2 was obtained for the applied pulse.

As already mentioned in the Chapter 2 where the theoretical background of the FFT analysis is described, the theoretical maximum frequency that can be determined is half the sampling frequency $(f_s/2)$. This is called the Nyquist limit. After this frequency, the values are mirrored (two side diagram) and there are of no relevance, so they should be neglected. For this reason, the values after the frequency of 5000 Hz are neglected leading to the following one sided diagram of Figure 5.2.

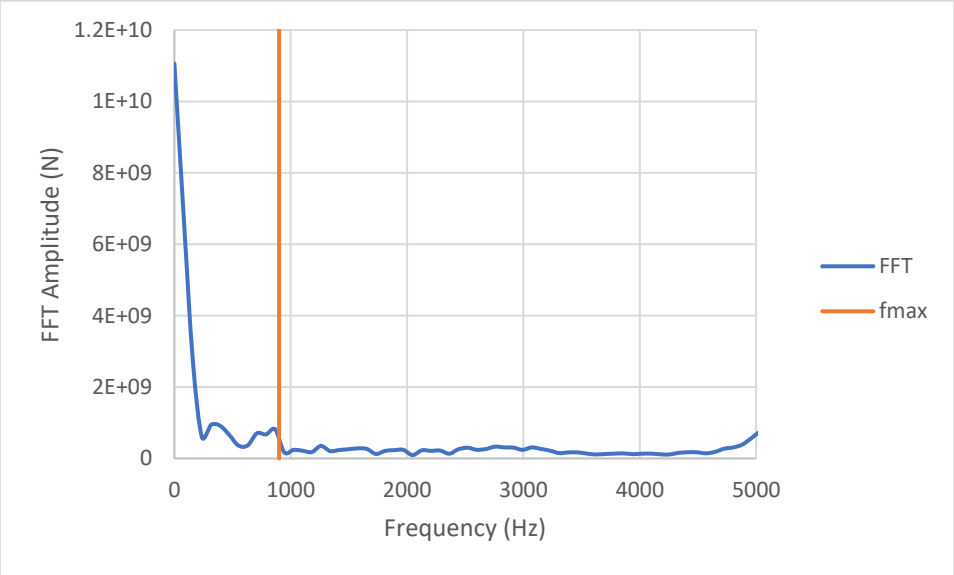

Figure 5.2 *FFT frequency spectrum - one sided*

Based on the information about the frequency region of the loading, extracted from the FFT results, the frequency of 900 Hz was chosen as the maximum frequency that should be taken into account for the accurate representation of the wave propagation. According to this frequency and to the wave speed, the wavelength can be derived which then should be sufficiently discretised to capture the wave propagation along the monopile properly.

5.2 Mesh sensitivity analysis

5.2.1 Introduction

When modelling a large structure, like the monopile, defining an appropriate mesh size for the discretization process is a very challenging and important aspect of the whole analysis. First of all, the mesh size should be selected based on the mechanical aspects of the problem, so that it will be able to accurately catch the physical response of the structure. However, when performing numerical modelling, especially in real scale large structures, computational time also becomes a very critical aspect as it is related to software and project resources. So, in practise, the final mesh size selection is based on the balance between the selected accuracy and the computational effort to achieve it. No absolute regulation exist for the best mesh choice.

Each problem has its own critical aspects. There are just general rules, derived in the context of structural engineering, which in combination with the knowledge and experience of the engineer should lead to the most efficient mesh size.

In the next chapters, the selected mesh size to discretize the monopile will be explained. The critical parameters which determined the final choice, were the wave propagation phenomenon and the local behaviour of the monopile around the contact region with the boulder.

5.2.2 Maximum mesh size selection

To study the wave propagation, it is important to have an element size that can approximate the wave motion of a given wavelength with sufficient accuracy. The discretization requirements are already discussed in Chapter 2 and according to the international literature it can be concluded that the use of six to ten elements along the wavelength is sufficient for the representation of the wave propagation with acceptable accuracy.

The wavelength depends on the wave speed and on the frequency and can be computed according to the following formula

$$\lambda = \frac{c}{f}$$

where c is the speed with which the wave propagates through the medium and f is the wave frequency. During the wave propagation in a three dimensional solid, different kind of waves are created despite the load direction. When a pulse is axially applied at a pile, two are the main kind of created waves namely, the longitudinal and the shear waves. Each of these waves propagate with a different speed for a given frequency. Longitudinal waves propagate in steel with approximately 5200 m/s while shear waves are slower with a velocity of approximately 3250 m/s.

So, with what has been discussed so far, it is clear that during a wave propagation problem, not only there are different exciting frequencies but also for each frequency different kind of waves are excited. In order to achieve an accurate representation of the wave propagation, ideally the shortest wavelength should be taken into account, which corresponds to the largest frequency and the smallest wave speed.

The frequency value that will be used is the cut-off frequency, which was selected previously from the FFT analysis, as the maximum frequency which is significantly contained in the loading. So, the frequency value will be 900 Hz. Regarding the wave speed, since the minimum speed is necessary for the shortest wavelength, the smaller, shear wave velocity of 3250 m/s will be used. However, since the initiation stage of the impact is studied, the shear waves will not be able to reach the pile tip before the considered total analysis time which is the time when the faster longitudinal waves are reaching the bottom of the pile. Also, the longitudinal waves are expected to be critical as they will be those who will produce the largest amplitudes of stresses and strains in the pile. For these reasons, also the wavelengths associated with the longitudinal waves, for the cut-off frequency, will be considered for the final selection of an appropriate mesh size.

The wavelength associated with the shear waves is equal to

$$\lambda_{shear} = \frac{c_{shear}}{f} = \frac{3250\ m/s}{900\ Hz} \approx 3.6\ m$$

The wavelength associated with the longitudinal waves is equal to

$$\lambda_{long} = \frac{c_{long}}{f} = \frac{5172\ m/s}{900\ Hz} \approx 5.8\ m$$

Depending on the above wavelengths and on the selected discretization rule the appropriate mesh size can be computed. In Table 5.1, the resulting mesh size is represented whether the shear or the longitudinal waves are used, for three discretization rules, namely six, eight and ten elements per wavelength.

Table 5.1 *Element size for each discretization criterium*

Elements per wavelength	**Element size (m)**	
	Shear wavelength	Longitudinal wavelength
6	0.60	0.97
8	0.45	0.73
10	0.36	0.58

Depending on the kind of wave under consideration and on the number of elements used to discretise the wavelength, the resulting element size varies from 0.36 m to 0.97 m. The most conservative approach would be to consider the shear waves and ten elements along their wavelength. But this would also lead to the largest computational demand. As described earlier, the longitudinal waves are expected to be critical for studying the initiation stage of the impact between the pile and the boulder. Moreover, the above element sizes would be more relevant to refer to the distance between two nodes. Since, in the herein analysis, high order elements are used, the existence of intermediate nodes along the element is expected to improve the accuracy.

Taking into consideration the above aspects, the element size should probably be selected somewhere in between the resulting values for the shear and longitudinal wave. After a mesh sensitivity analysis, the element size of 0.7 m was selected as an appropriate mesh size to represent the wave propagation along the monopile. This value lies between the resulting element sizes for the eight element discretization rule. This mesh was verified by comparing it with finer mesh sizes and there was no deviation in the resulting quantities. In the next diagrams, the comparison between the 0.7 m and the 0.4 m mesh sizes is represented, regarding the resulting stress at the bottom of a fixed pile and the total reaction force. The results between the mesh sizes are perfectly matching which leads to the conclusion that the 0.7 m size is sufficient for an accurate representation of the wave propagation and no further refinement is needed.

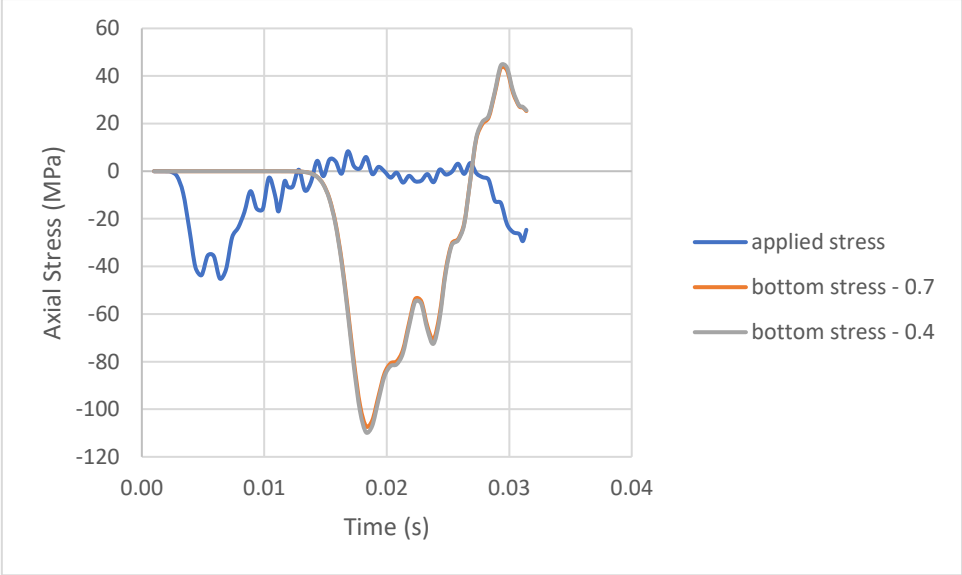

Figure 5.3 *Overall mesh size - Axial stress over time – Fixed pile*

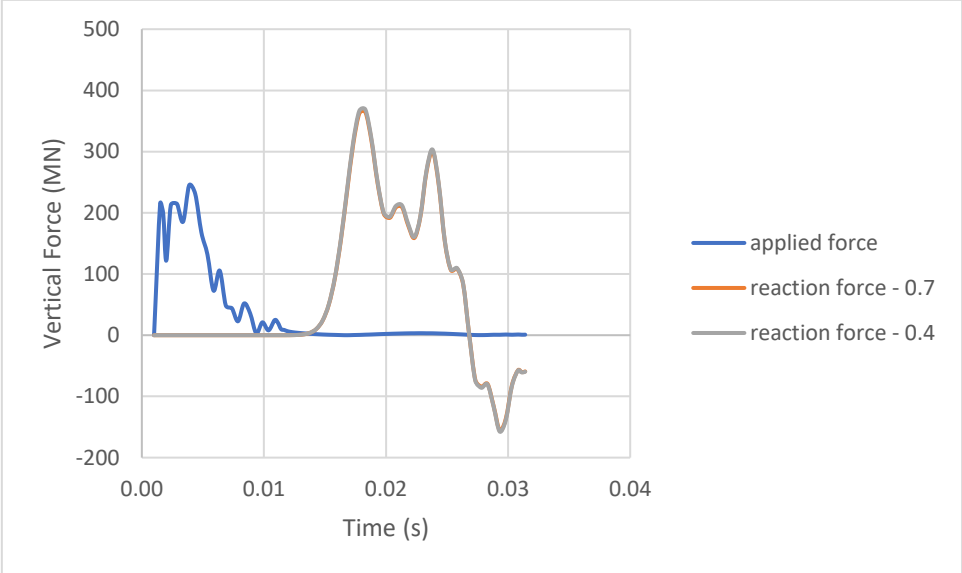

Figure 5.4 *Overall mesh size – Reaction force over time – Fixed pile*

5.2.3 Longitudinal mesh sensitivity analysis

As already mentioned, choosing the mesh size in a finite element analysis of a system of structures is a challenging task on itself. The studied monopile, has a length of 80 m and impacts a boulder with a diameter of 2 m. For such a large and complicated system, choosing a very small mesh size for the whole system is not an option, since it would result to extremely large computational times, making the model unpractical. In addition, the impact of a monopile with a boulder during driving is a very complicated process with a high computational demand which is an additional argument on why an efficient mesh size is more than necessary.

In the previous chapter, the maximum allowable mesh size was selected to be equal to 0.7 m. This size was determined based on the wave frequency of the excited waves on the pile, caused by the applied pulse and it is the maximum size that can be applied to achieve an accurate capture of the wave propagation phenomenon during pile driving. However, in addition to the wave propagation, there is also the impact process which will result in a very local response of the monopile around the contact region. This region is expected to be characterized by large resulting stresses and strains as local buckling and plastic deformation of the monopile will occur. As a result, for capturing the local stress and strain fields and the out of plane deformations of the pile tip, a sufficiently fine mesh is necessary to be applied. Furthermore, the dynamic response of the problem and the nonlinearity included in the impact process provide additional computational demand and make the use of a fine mesh a necessity.

This is the reason why a 3-zone mesh strategy was selected for the pile. Close to the contact region and for a height of 2 m, a very fine mesh was used using hexahedral solid elements. The top 73 m of the pile, was meshed using the selected maximum allowable mesh size of 0.7 m and hexahedral solid elements. In between, a 5 m transition zone is intersected which is responsible for the smooth transition between the bottom, fine and top, coarse mesh size. For this transition zone tetrahedral solid elements were used to be able to match the two different mesh sizes.

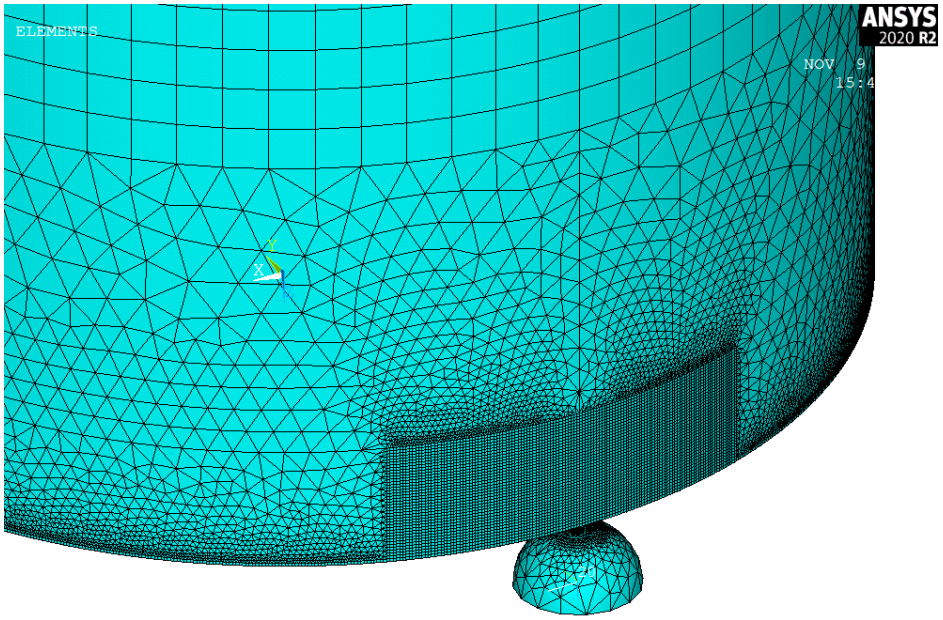

Figure 5.5 *Mesh view – 3-zone strategy*

The boulder mesh was important because it is related to the way Ansys is modelling contact. A contact pair has to be created consisted of a contact and target body. During the impact process and as the contact algorithm is executed, Ansys prevents the contact to penetrate the target body. This prevention is executed by constraining the nodes of the contact body to pass through the target body. So, the mesh size of the target body should be sufficiently fine to be able to constraint the contact body through the whole contact area. For this reason, the mesh size of the target body should be at least equal to that of the contact body. Taking this into

consideration, the boulder was divided into two zones. The top part of the boulder which comes in contact with the pile is having the same, fine mesh size with the bottom of the pile, while the rest of the boulder is meshed with a much more coarse mesh. In this way, except for modelling the contact in the right way, the boulder is also meshed more efficiently, using the fine mesh size only in a small region.

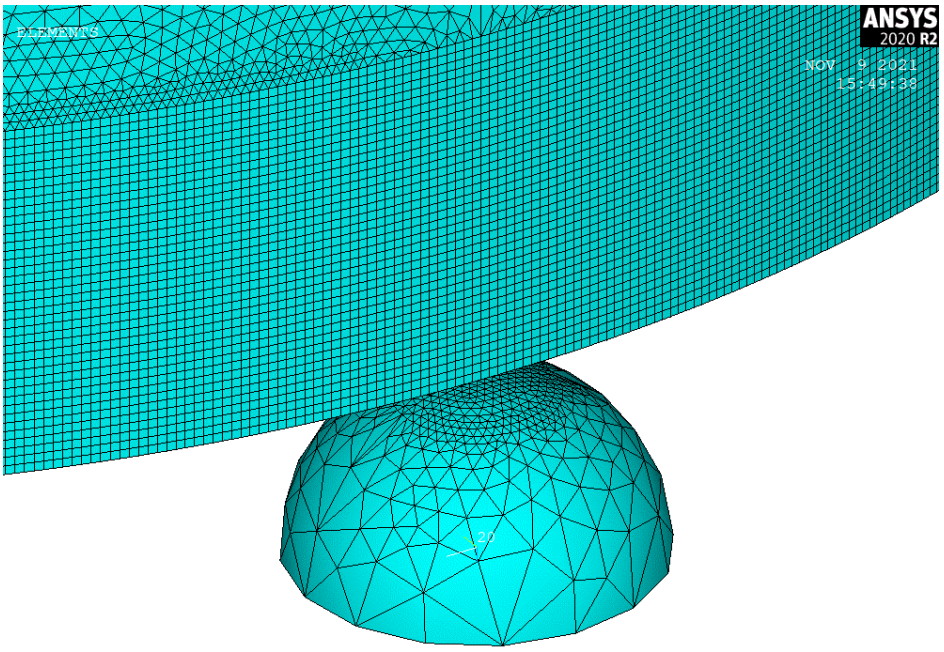

Figure 5.6 *Mesh view – contact region*

In this chapter, the mesh sensitivity analysis that will be presented will refer to the fine, bottom mesh size of the pile close to the contact region. The mesh size of the above part of the pile was examined in the previous section and is kept constant to 0.7 m for the rest of the analyses.

Different mesh sizes were applied at the bottom of the pile, around the contact region, to examine its influence both on the local response of the tip and on the global response of the system. The results that will be presented in this section will refer to the Von Mises stress and strain and to the reaction force at the boulder. The equivalent Von Mises stress was selected as the most appropriate parameter to investigate and draw conclusions regarding the stress intensity at the tip since, during the impact, all the different kind of stress components are induced, namely the axial, radial and tangential stresses. Von Mises stress takes into consideration all of them and gives a good indication of the stress intensity and the possible plasticity extent. The same holds for the Von Mises strain. The total reaction force at the boulder was selected as an appropriate parameter to give an indication about the global response of the system. In addition, it is a very important quantity when studying the impact of monopiles with boulders during driving and it is crucial to obtain it accurately.

The mesh sizes that were tested were equal to 0.4, 0.3, 0.2, 0.1, 0.05, and 0.025 m. In Figure 5.7, the equivalent Von Mises stress is represented over time, for the bottom node of the pile which is in contact with the boulder.

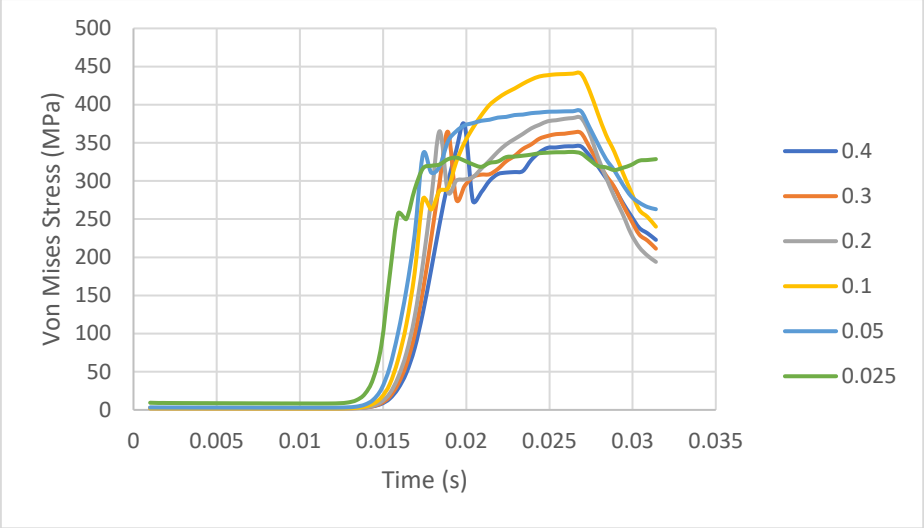

Figure 5.7 *Mesh sensitivity – Von Mises stress – Bottom node of the pile*

It is clear that no conclusion can be made since the resulting stress does not seem to follow a specific pattern or converge as the mesh size decreases. This can be explained if the different stress components are examined. Below, the axial stress component in the bottom node of the pile is represented which is also the first principal stress.

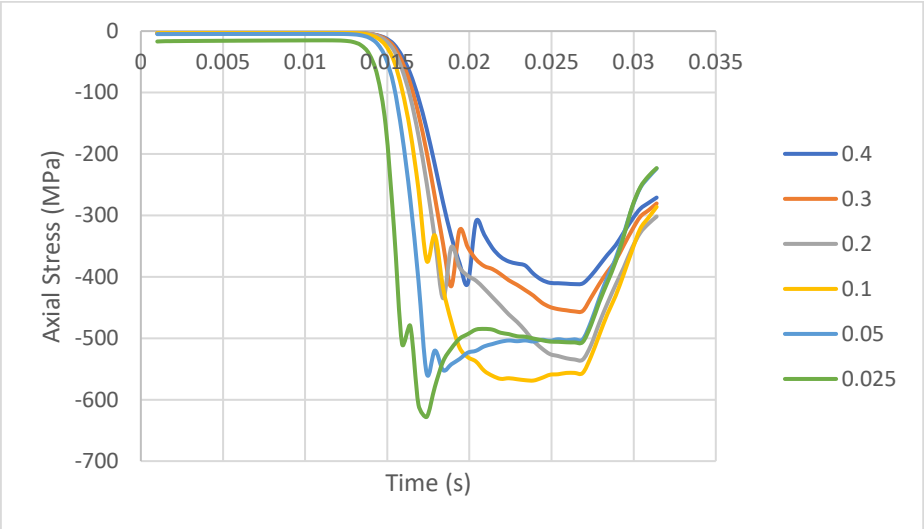

Figure 5.8 *Mesh sensitivity – Axial stress – Bottom node of the pile*

It can be seen, that as the element size decreases, the stress magnitude increases and the response becomes more and more sharp at the time when the wave reaches the bottom of the pile. The same trend is noticed in the other stress components too. This response indicates the existence of a singularity at this point. This is expected since the pile and the boulder will probably contact each other through one point, located at the top of the curved surface of the boulder. In order to avoid this one-point contact, if possible, an extremely fine mesh should be applied to both the pile and the boulder around the contact region, such that it would make the model unfeasible due to the high computational time.

However, a singularity, usually, is not a decisive parameter in finite element modelling since it can be handled based on the necessary engineering principles. A singularity is the mathematical outcome of the theoretical assumption that the contact force is applied in a point. In reality, the force is never applied to a body through just one point. In mathematical terms, the magnitude of the measurement at this point will go to infinity.

The Saint-Venant principle is the main concept under which an engineer can deal with singularities and is more analytically discussed in Chapter 2.9. According to this principle, sufficiently far from the loaded region, there is no influence of the load distribution to the force resultants on the body. In other words, the local effects are vanished over a distance from the applied load. In general, there is no specific rule about the magnitude of this distance since it is a problem-dependent parameter and usually it is defined after some investigation. However, the Saint-Venant principle can work as a guide since it states that this distance should be comparable to the linear dimensions of the loaded region. In shell structures, usually a rule of thumb is applied, according to which the local effects are vanished after a distance equal to the shell thickness.

Additionally to the above considerations, an investigation was conducted on which parameter should be considered for the mesh sensitivity analysis. It turned out that the strains needed to be checked in a larger distance from the contact point in order to converge, compared to the stresses.

Taking into consideration all the above arguments, all the quantities were found to converge at 10 cm above the pile tip, which is approximately equal to the pile thickness. Below, the Von Mises stress, strain and stress-strain relation are represented over time for the different mesh sizes.

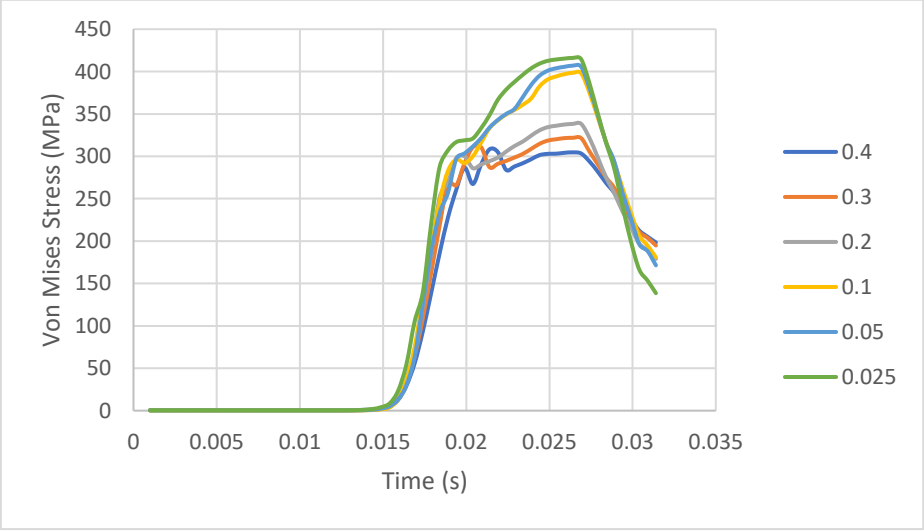

Figure 5.9 *Mesh sensitivity – Von Mises stress – 10cm above the pile tip*

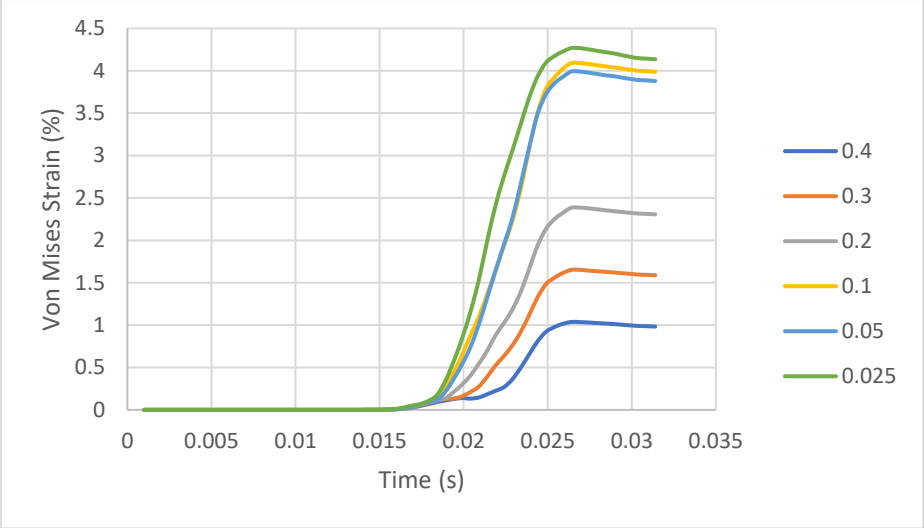

Figure 5.10 *Mesh sensitivity – Von Mises strain – 10cm above the pile tip*

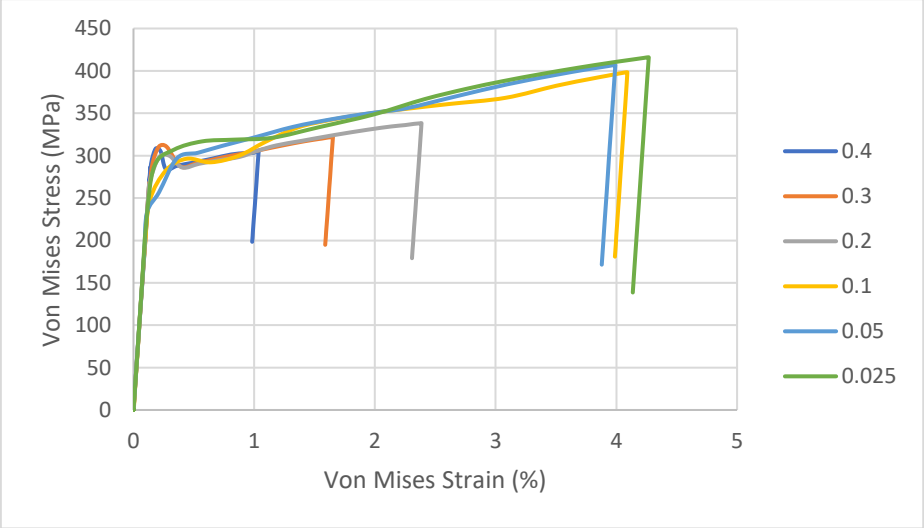

Figure 5.11 *Mesh sensitivity – Von Mises stress-strain relation – 10cm above pile tip*

Both the stresses and the strains clearly seem to converge at 10 cm above the pile tip. The convergence pattern is similar for both of them. The difference between the results for the different mesh sizes is much larger for the strains while the stress level is more balanced. The maximum convergence error between the analyses for each mesh size is 17.7% for the stress while for the strain reaches a value of 71.5%. Nevertheless, both stress and strain seem to have a significant small convergence error after the mesh size of 5 cm with a value of approximately 2%. In the Figure 5.12, the evolution of the convergence error is represented during the mesh sensitivity analysis.

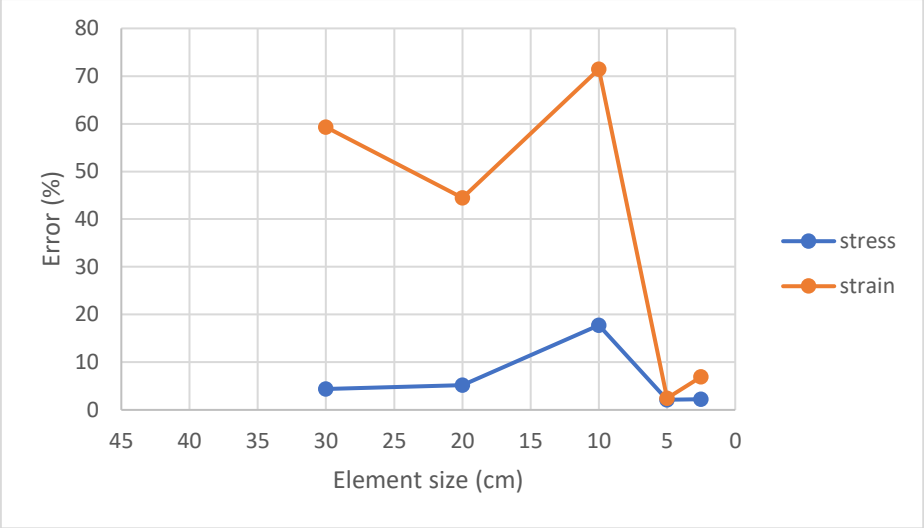

Figure 5.12 *Mesh sensitivity analysis – Convergence error of stress and strain*

So far, the mesh sensitivity analysis was based on checking the convergence of the stress and strain fields. This is a general approach and its results are credible. However, there are two disadvantages, in this case, related with this approach. The first one is related to the Saint-Venant principle and the local behaviour of the model. The impact of the pile with the boulder induces a local response at the pile tip where large stresses and strains are induced. As already discussed, the results should be retrieved in a sufficient distance from the loaded region in order to be reliable. Although, engineering knowledge and experience can be very helpful in defining this distance relatively fast, still, it is dependent on the studied problem and will usually need an additional investigation for its proper definition. Moreover, the implementation of plasticity, makes the aspects of the mesh sensitivity analysis even more complicated. In the contact region, the induced stress values will reach way beyond the yield limit of steel, resulting in an extended material plasticity. In such cases, checking the stress becomes almost irrelevant as it will anyway reach the applied limit and no solid conclusions can be extracted from the structure behaviour.

For the above reasons, it becomes clear that in problems like the impact of a pile, where a lot of influential parameters are present and their effect, given the non-linear nature of the problem, cannot be readily assessed, the definition of a more solid parameter, independent of too many uncertainties, would be very useful for extracting quick and reliable results. In this context, the extent of the plasticity zone of the pile tip was selected as an appropriate parameter, not only for the mesh sensitivity analysis, but also in general when studying the response of the pile. The measure of the plasticity extent will be the distance from the impact point up to the point where plastic strains are observed. The advantage when using the plasticity zone is that it can provide results directly and no prior study of the distance in which the local effects are vanished is needed. In Figure 5.13, the convergence process of the height of the plastic zone is presented, as the mesh size is decreasing.

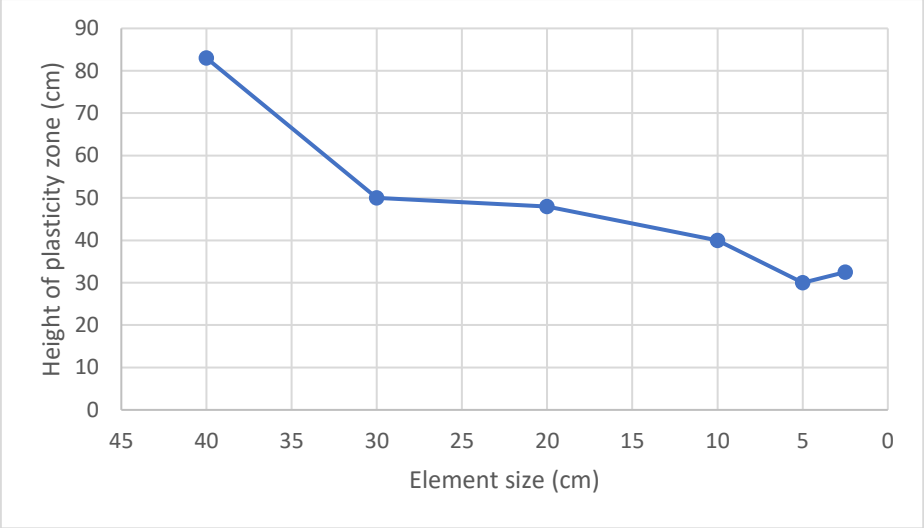

Figure 5.13 *Mesh sensitivity analysis – Height of the plasticity zone*

From the above results, it is clear that the height of the plastic zone converges after the 5 cm element size, same as the stress and strain. The relative convergence errors are a bit higher, but one should notice that in this case the results are not extracted for the same node, since the node positions are not the same for different mesh sizes. So, an additional error already exists just from the different element size. For this reason, the allowable convergence errors should be higher without having an impact on the reliability of the analysis.

After an extensive mesh sensitivity analysis, the 5 cm element size was selected as the most efficient for modelling the pile tip and was used for the rest of the analyses. In Figure 5.14, the total analysis time for each bottom mesh size is represented. For the selected mesh size of 5 cm the analysis time is approximately 2 hours.

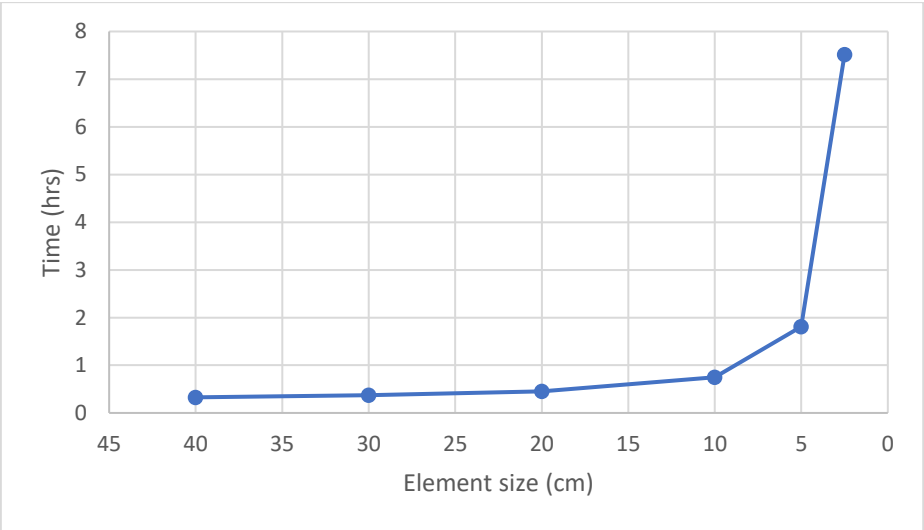

Figure 5.14 *Analysis time for different bottom mesh sizes*

5.2.4 Number of elements along the pile thickness

Except for the discretization in the longitudinal direction, an additional investigation was conducted in order to conclude about the influence of the discretization in the transverse direction (through the pile thickness) to the overall behaviour of the model. The discretization through the pile thickness should be able to adequately capture not only the wave propagation but also the local distortion of the pile tip due to the impact with the boulder. For this reason, a sensitivity analysis was done where the influence of the number of elements through the pile thickness was investigated.

Greenspon (1960), investigated vibrations of an elastic cylinder by implementing and comparing different approximate shell theories with the exact theory. Shell theories are focused on the displacements of the middle surface of the shell, while the complete three-dimensional theory considers the most general displacement distribution which satisfies the equations of motion and the surface conditions. When the frequencies get so high that the displacement distributions are no longer linear, then the shell theories may become inaccurate, since the displacement distribution can no longer be described by the middle surface and the slope. Nevertheless, the author concluded that for thin shells with a ratio of outer diameter to thickness larger than 100 and in a specific range of wavelengths, the results between the shell theories and the exact three-dimensional theory are practically the same. This leads to the conclusion, that the pile behaviour under wave propagation phenomena, in general, should not be influenced by the discretization along the pile thickness. Shell theories are based on the assumption that quantities vary linearly along the shell thickness. So, even the use of one or more 3-d elements along the thickness should not lead to considerable changes and should be close to the shell theory solution.

Three different analysis were run, using 2, 4 and 6 elements through the pile thickness for a pile which comes in contact with a boulder after a transient load is applied to the pile. In the next diagrams, the resulting axial stress at the bottom of the pile, the resulting stress-strain relation at the bottom of the pile and the resulting vertical reaction force at the boulder are represented for each of the three analysis.

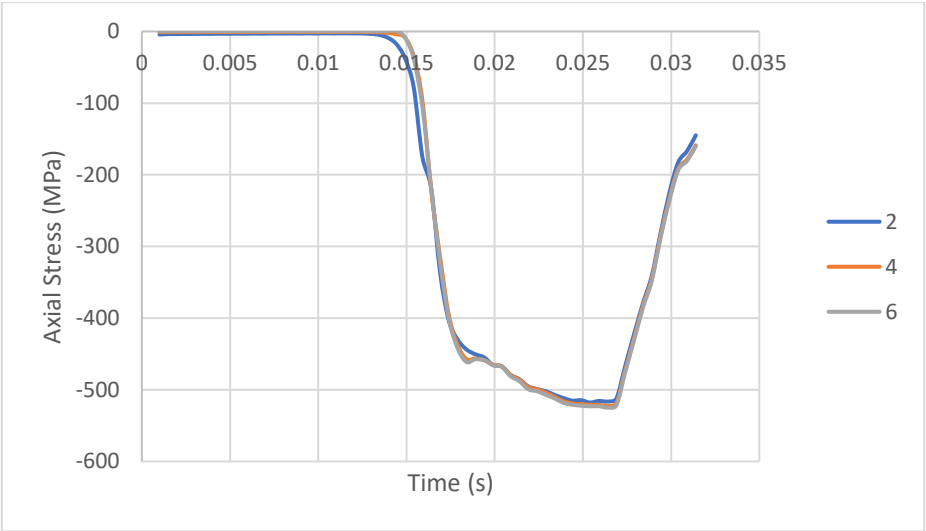

Figure 5.15 *Axial Stress at the bottom of the pile for 2,4 and 6 elements through the thickness*

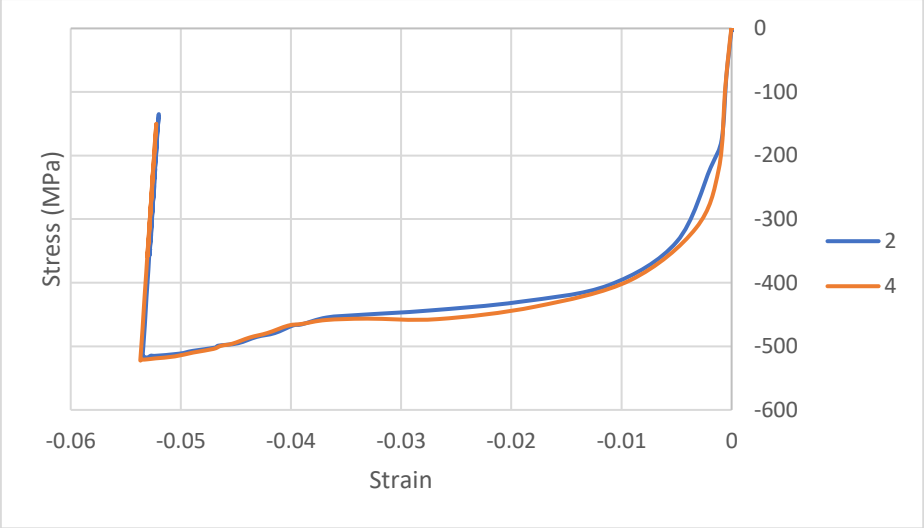

Figure 5.16 *Axial stress-Axial strain relation at the bottom of the pile for 2 and 4 elements through the thickness*

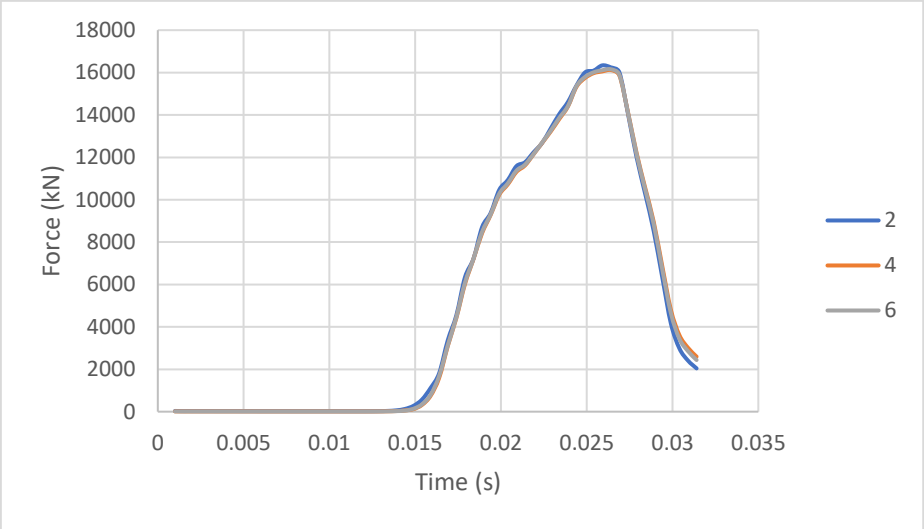

Figure 5.17 *Vertical reaction force at the boulder for 2, 4 and 6 elements through the thickness*

From the above results, it is clear that there is no influence to the resulting quantities due to the number of elements used through the pile thickness. This conclusion comes to an agreement with Greenspon's conclusions as discussed earlier.

Although, no influence due to the number of elements through the thickness is noticed on the overall behaviour of the pile, it is suspected that this parameter should have an effect on the accurate representation of the local buckling phenomenon at the pile tip around the contact region. In this region, the pile wall is subjected to significant stress magnitudes and out of plane deformations. For this reason, 4 elements through the pile thickness was selected to be used close to the contact region and the rest of the pile is modelled with one element over the thickness. In this way, a more accurate description of the local behaviour of the pile tip, due to the contact with the boulder, will be achieved and with insignificant additional computational demand.

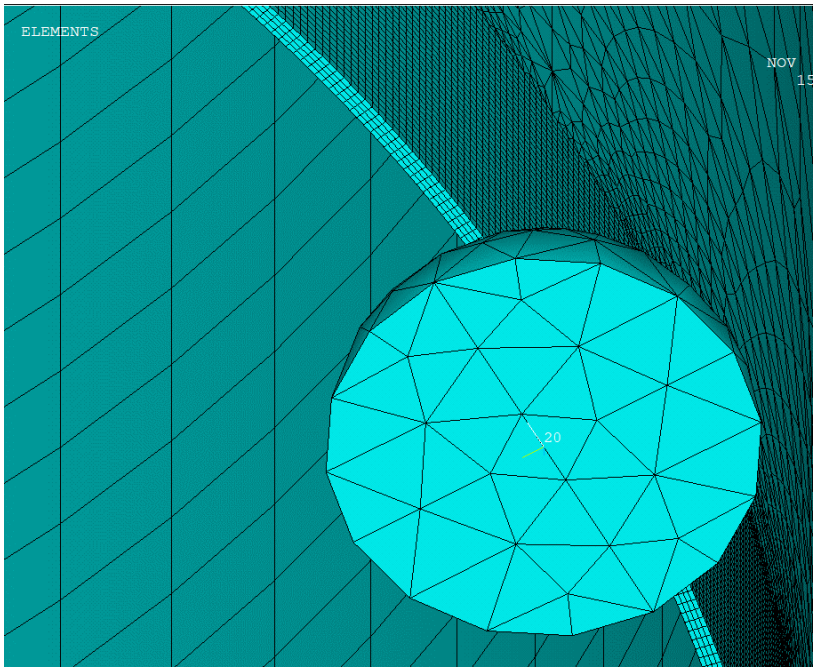

Figure 5.18 *Mesh view – 4 elements along through the pile thickness*

In Figure 5.19, a comparison of the contact pressure is represented between the nodal and the element solution, at the time when the pressure reaches its maximum value. In nodal solution the resulting nodal stress is the average of all the elements' stresses next to this node while in element solution it is not and in one node there are different stress values. Hence, the more the two solutions are matched, the more adequate the discretization is. From the figures below, it can be seen that with 4 elements along the pile thickness, the stress distribution is represented quite accurately confirming the contact region discretization choice.

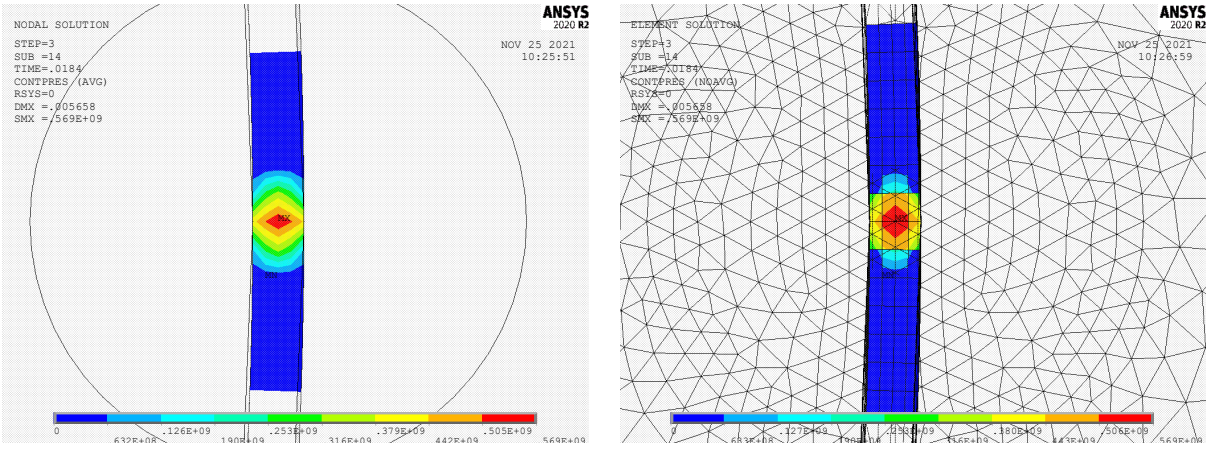

Figure 5.19 *Maximum contact pressure – Nodal (left) and element (right) solution – Central impact*

5.3 Boulder position analysis

5.3.1 Introduction

In a driving scenario, the way the monopile would impact with the boulder is not fixed. The contact could happen at any point along the surface of the boulder and in any orientation. Each boulder position is expected to have a different effect to the damage of the monopile tip and perhaps with significant differences among them. For this reason, investigating the influence of the different contact points between the monopile and the boulder is a necessary step in the process of understanding pile tip damage and deriving credible results on the pile tip damage during driving.

An analysis was conducted in order to extract information regarding the influence of the impact process to the monopile tip, for different contact points along the boulder's surface. The analysis was based on the definition of the boulder position. During the analysis, the pile position was kept constant and the position of the boulder was varying. The starting point was the central impact, where the contact point was the middle, top point of the boulder and then the boulder was moved right and left resulting in an eccentric impact. In this way, the impact process was modelled for different contact points along the boulder's surface and for both the cases of the boulder being inside or outside the pile wall.

The boulder's position was defined by the difference between the position of the center of the spherical boulder and that of the center of the pile wall. For the central impact this difference would be zero and the center of the pile wall would match the center of the boulder. For positive values of the difference, the boulder's center would be right or outside the pile's diameter and for negative values the boulder would move left or inside the pile's diameter. Except from the central impact, three different boulder's positions for each side of the pile wall were taken into account, equal to 0.2, 0.4 and 0.6 m. In Figure 5.19, the central and the 0.4 m positions of the boulder are represented.

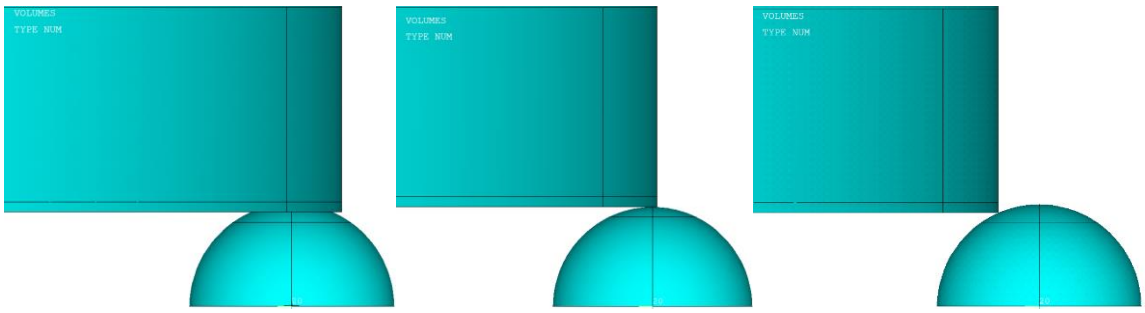

Figure 5.20 *Boulder positions: -0.4 m (left), 0 m-central (centre), +0.4 m (right)*

The impact process is characterized by a very local response of the pile around the contact point with high non-linear material behaviour. For this reason, processing the results becomes challenging since it is unclear which is the most appropriate measure to use, for a credible comparison between each case. In this chapter, the different results for each boulder position will be studied, with the purpose to understand the behaviour of the monopile through the impact process and try to make a valid comparison between each case. In accordance with the

mesh sensitivity analysis, as demonstrated in previous chapter, all the results will be extracted for the node that is 10 cm above the contact point, to get rid of any local effects and obtain an accurate representation of the pile tip behaviour. Due to similarity between the different cases, the results will be represented for selected representative cases that suffice for extracting the response trend. For more detailed information, one could refer to Appendix C.

5.3.2 Stress investigation

Depending on the contact orientation, the different stress and strain components are activated in a different manner, resulting in different response of the pile tip. A first measure to indicate the pile tip response, during impact with a boulder, was the Von Mises stress in which all the stress components are taken into account and provides an estimate of the material stress intensity. In the following figures, the Von Mises stress through the pile tip thickness is represented for the central impact and for the case where the centre of the boulder is 0.4 m outside the pile wall (+0.4 m).

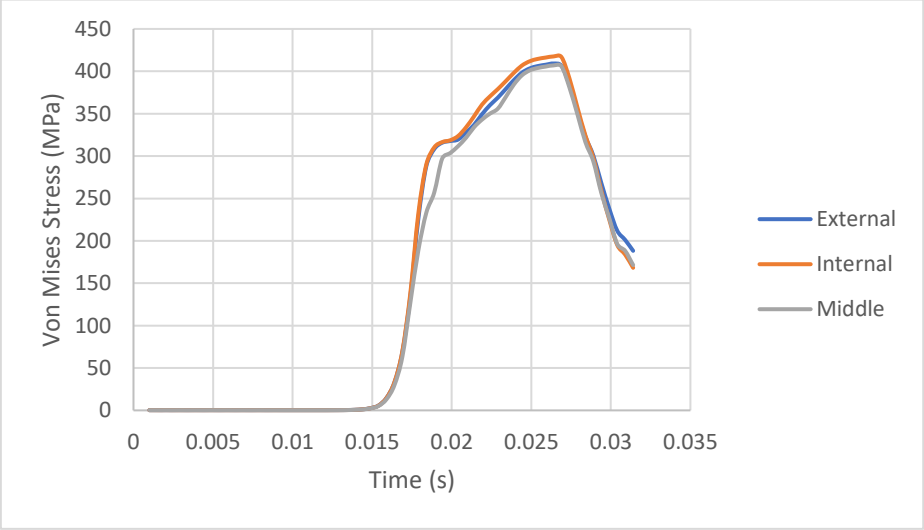

Figure 5.21 *Von Mises stress through the pile tip thickness, 0 m (Central impact)*

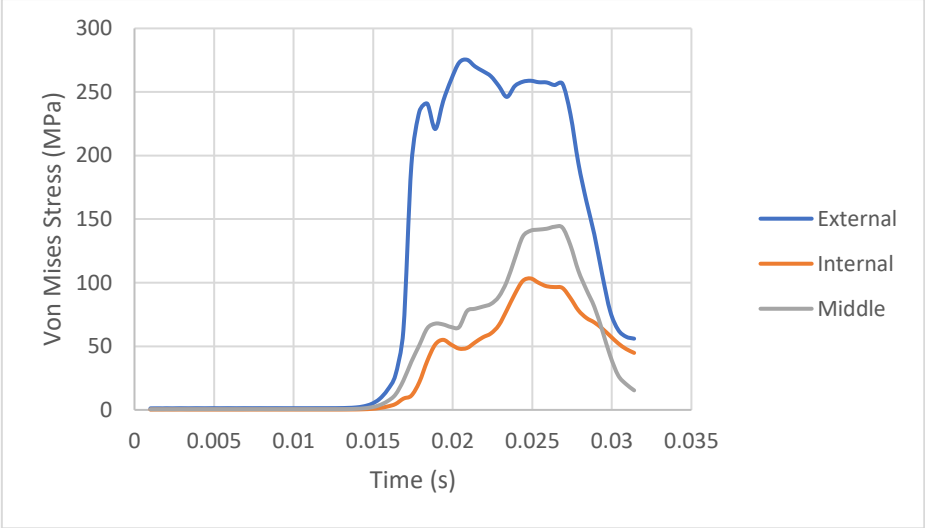

Figure 5.22 *Von Mises stress through the pile tip thickness, +0.4 m (Eccentric impact)*

The Von Mises stress is represented for 3 points along the pile thickness, the external, the internal and the middle node of the pile wall. In case of the central impact, the stress reaches higher values, way above the yield stress of 316.7 MPa, approaching the ultimate stress ($\approx 450\ MPa$) as defined in DNVGL for the S355 steel. Hence, locally, the pile tip appears to be plastically deformed in a large extent. In the case of the eccentric impact, the stress remains in lower levels, even below the yield stress. This is expected since in case the pile does not impacts with the boulder centrally, it is less constrained, sliding along the boulder, resulting in smaller reaction forces. In addition, it is noticed that in central impact the stress distributes better through the pile wall while in eccentric impact, the stress is larger close to the contact point. In Figure 5.22, the evolution of the Von Mises stress, at the pile tip, over time is represented for the case of central impact and the case when the boulder centre is +0.4 m outside the pile wall. Again, it is clear that as the impact point moves sideways, the stress intensity at the pile tip is significantly reduced.

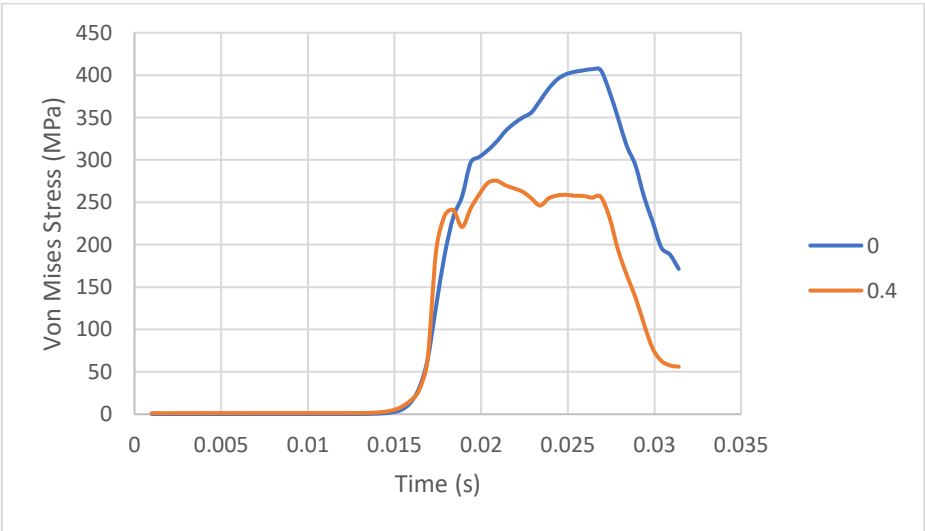

Figure 5.23 *Von Mises stress over time – Central (0 m) and eccentric (+0.4 m) impact*

Although the Von Mises stress gives a useful indication of the stress intensity, a better understanding of the impact process would be achieved by investigating each stress component that contributes to the total stress state around the pile tip. For this reason, a separate closer look is followed, to the stress components in the axial, radial and tangential direction. In the following figures, the evolution of each stress component over time is represented for the same cases of central (0 m) and eccentric (+0.4 m) impact.

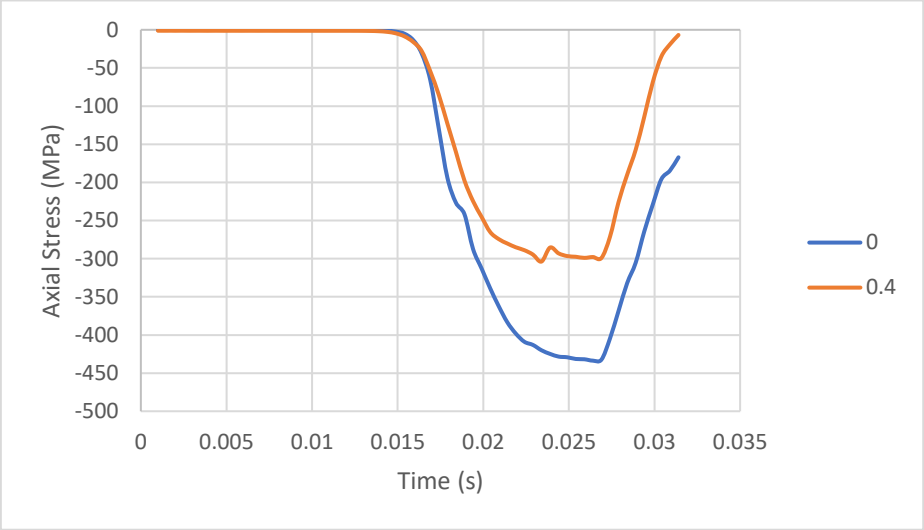

Figure 5.24 *Axial stress over time – Central (0 m) and eccentric (+0.4 m) impact*

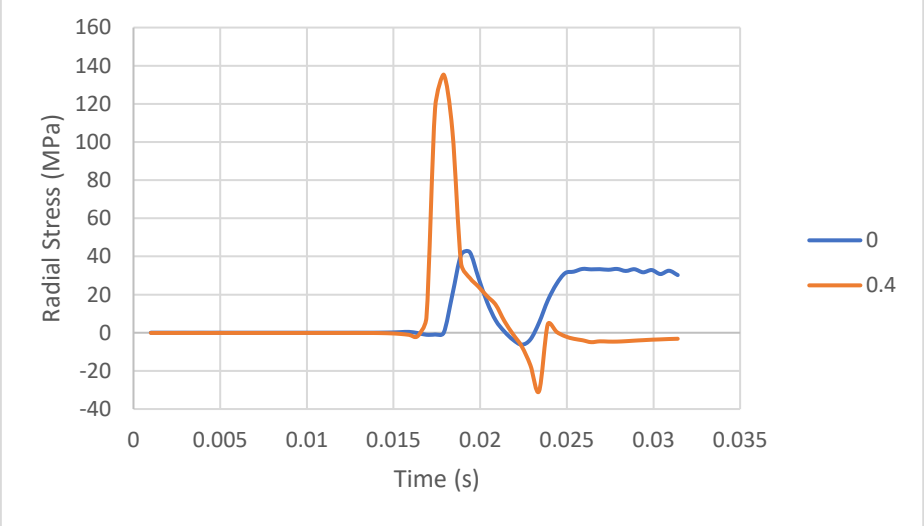

Figure 5.25 *Radial stress over time - Central (0 m) and eccentric (+0.4 m) impact*

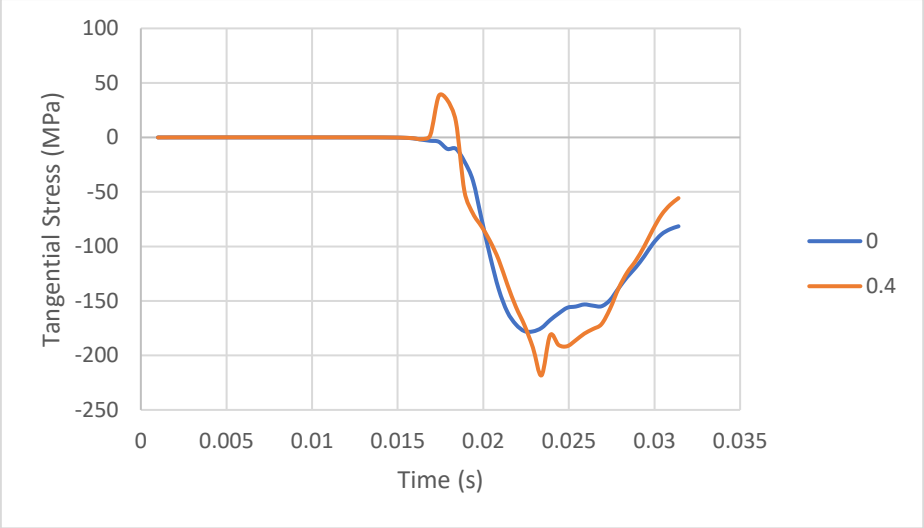

Figure 5.26 *Tangential stress - Central (0 m) and eccentric (+0.4 m) impact*

By inspecting the above diagrams, useful information can be extracted. First of all, it is clear that for the central impact the axial stress reaches its highest value and as the boulder moves sideways it is significantly reduced for about 30% of the induced stress due to the central impact. However, for the eccentric impact, the radial stress at the pile tip increases more than 220% compared to the central impact. The tangential stress seems to be influenced less with an increase for the eccentric position of the boulder for about 20%. Based on the above results, it is clear that in case the pile impacts the boulder centrally, the axial stress component seems to be the critical one as it reaches very high values leading to yield of the material. However, as the impact becomes eccentric, the axial stress is significantly reduced and the critical stress component is likely to be the radial stress, leading to out of plane deformation of the pile tip.

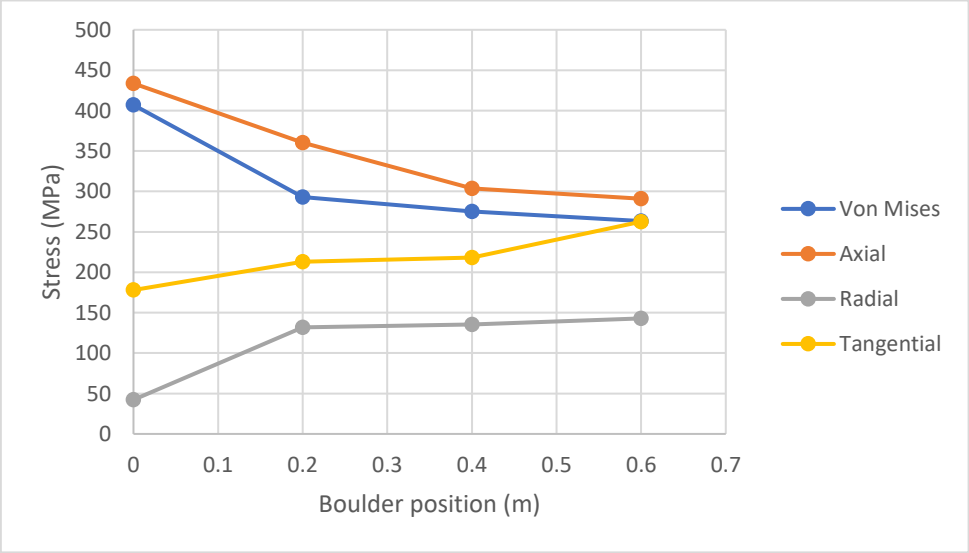

Figure 5.27 *Maximum stress values – Central (0 m) and eccentric (0.2, 0.4, 0.6 m) impact*

In Figure 5.26, the maximum values of the Von Mises stress and of each stress component are represented, as the impact becomes from central to more eccentric. As the centre of the boulder moves further away from the pile wall, the stress intensity at the pile tip, which can be described by the Von Mises stress, is reduced. However, considering only the Von Mises stress will not provide a clear view on the highly distorted pile tip which is observed even for the eccentric impacts. Although, the axial stress component reduces as the impact becomes more eccentric, the radial and tangential stress components increase. This is expected, as in the eccentric impact, the horizontal component of the reaction force at the tip becomes larger. On the other hand, in the central impact, it is expected that the horizontal reaction force will be close to zero and the vertical component will obtain its highest value. The tangential stress component seems to increase as the impact becomes more eccentric. This increase is expected to be linked to the increase of the radial stress. As the radial stress increases, it is anticipated that also the resistance stress in the circumferential direction will increase. The radial and tangential stress components are related to the out of plane radial deformations and can explain the resulting deformed shape of the pile tip, which is studied on a next subchapter.

5.3.3 Boulder reaction force

An important parameter, when studying the impact of a pile with a boulder during driving, is the reaction force that is applied on the boulder, from the surrounding soil, as the impact takes place. The magnitude of this force might be used to predict whether the boulder will move through the soil, will be damaged locally or will split. Although the scope of this thesis is on the pile tip behaviour and not on the geotechnical aspects, the generated reaction force on the boundary of the fixed boulder was investigated as it is considered a fundamental parameter in understanding the impact process. Modelling the boulder as fixed can be considered as the most conservative scenario which will generate the highest possible stresses at the pile tip. However, such an approach might be realistic in very stiff and dense soils or in case of large boulders and this is also represented by Holeyman (2015). In Figure 3.13, the results of Holeyman's research are represented and it can be seen that for large boulders the resulting contact force is less than the penetrating resistance of the considered soil type. This means that under certain circumstances, during contact the boulder is likely to remain in place resulting in a combination of pile and boulder damage. In addition, this force could be used in future studies, when the implementation of soil and rock mechanics will take place, as an indication of the expected generating force during impact.

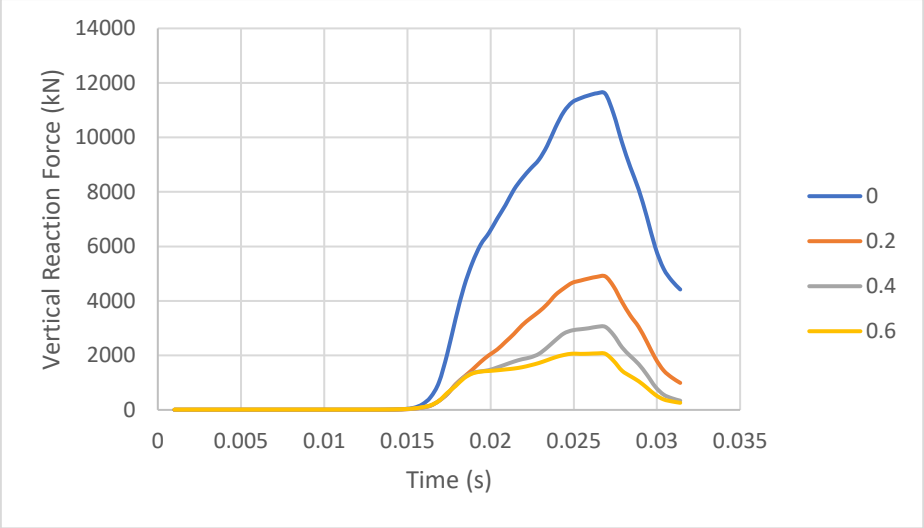

Figure 5.28 *Vertical reaction force at the boulder for different impact orientations*

In Figure 5.28, the vertical reaction force on the boulder is represented, for the different boulder positions. The central impact generates the largest vertical force while, as the impact becomes more and more eccentric the vertical force is significantly reduced. This is an expected trend since in the central impact the pile is kept more constrained at the contact point and a larger amount of load is able to be transferred. As the impact becomes eccentric, the pile is sliding along the boulder's surface and less vertical load is transferred through the contact to the boulder.

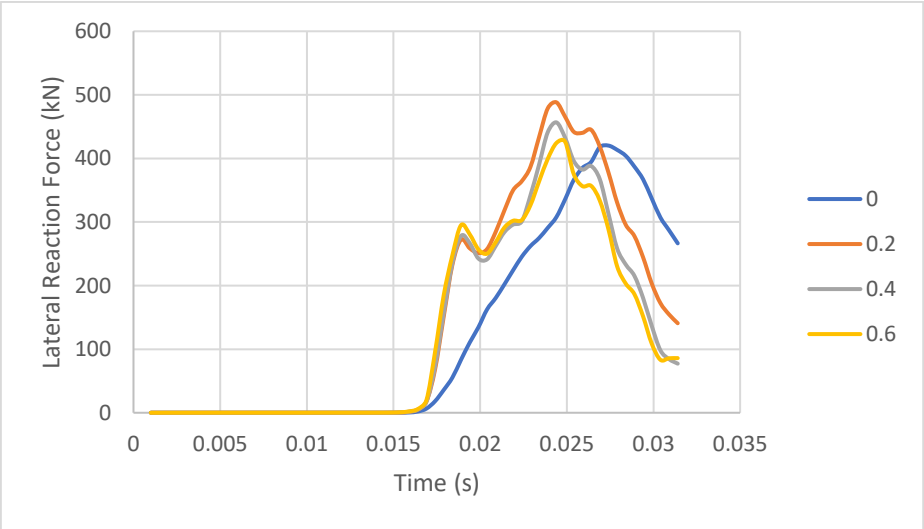

Figure 5.29 *Lateral reaction force at the boulder for different impact orientations*

Figure 5.29 compares the resulting lateral reaction force on the boulder for different boulder positions. In contrast with the vertical reaction force, the lateral force seems not be influenced by the different impact orientations, as it is kept almost the same regardless the boulder position. This result can be attributed to the fact that the shell structure of the pile does not have the strength and stiffness to transfer out of plane loads. Hence, once a lateral load is applied,

the pile tip is radially deformed. This will be more clear in the next subchapter where the distorted pile tip will be studied in terms of the radial deformation.

In Figure 5.30, the comparison between the vertical and the lateral reaction force is illustrated for the case where the boulder centre is located 0.4 m outside the pile wall. This illustration helps in representing the extreme difference between the vertical and the lateral force. Although the small lateral force could be taken as irrelevant to the driving and impact process, still it is very important since it indicates the incapability of the pile to resist concentrated lateral loads and how prone it is to out of plane deformations.

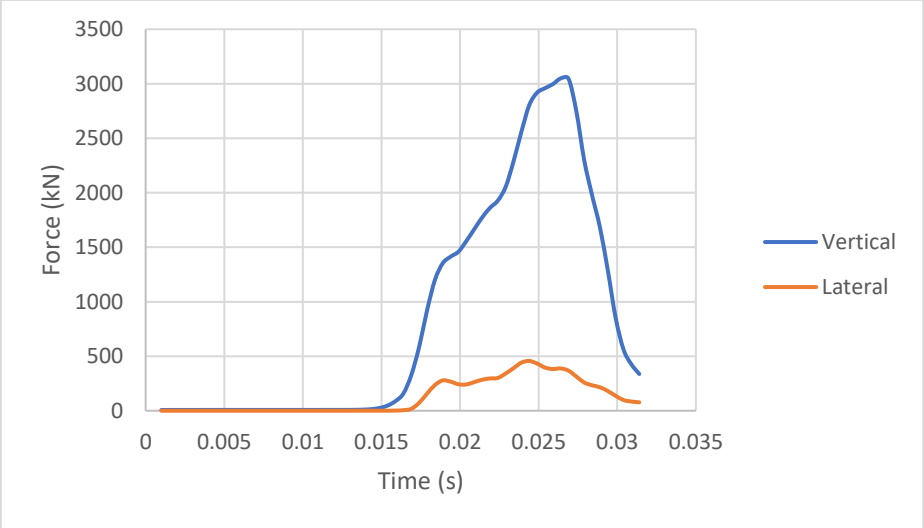

Figure 5.30 *Vertical and lateral reaction force on the boulder – eccentric (+0.4 m) impact*

Finally, Figure 5.31 illustrates the amount of load transferred through contact in comparison with the total applied force at the top of the pile, in case of the central impact. Only a small fraction of the applied force is transferred to the boulder which is less than 1/20. However, the fact that the force is concentrated at the contact region can induce significant damage to the pile tip with possible consequences in the driving process.

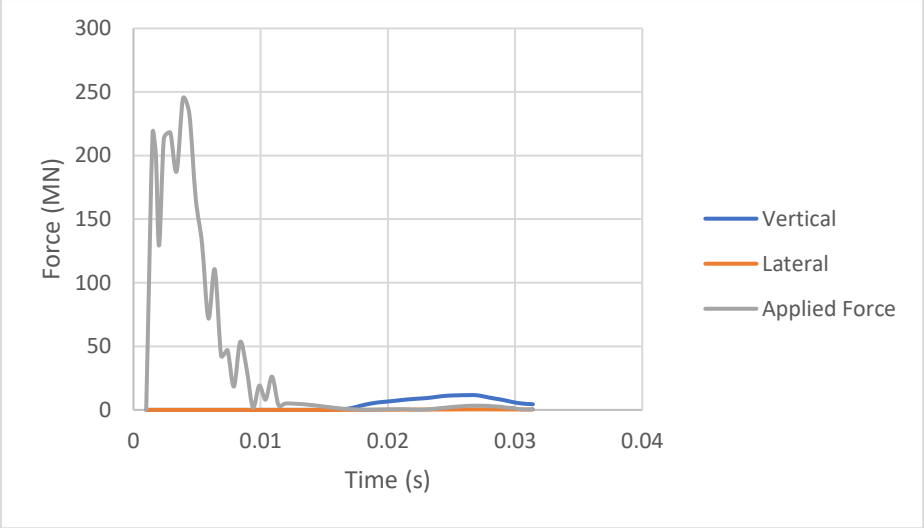

Figure 5.31 *Applied force, vertical and lateral reaction force – central (0 m) impact*

5.3.4 Radial deformation and plasticity of the pile tip

The induced radial deformations of the pile tip, after the contact with the boulder is taking place, is probably the most important parameter that needs to be investigated. The radial deformations will define the final distorted pile tip after the impact. As already discussed, driving refusal can result from the extended distortion of the pile tip which is caused by the continuous impacts with hard objects and it gradually propagates. In the guidelines that are used in practise, no guidance exists regarding the limitation of the radial deformations of the pile tip caused by impact. It is generally accepted that once an initial distortion is developed, it is much easier to propagate and magnified. In absence of existing experimental or numerical data, investigating the initial distortion of the pile tip is crucial in order to have a clue about when the distortion starts and to what extent.

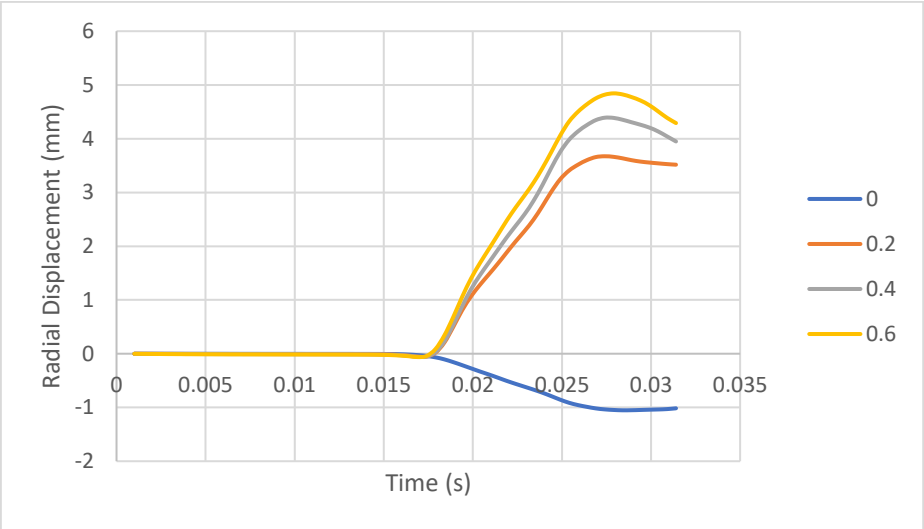

Figure 5.32 *Radial displacement at the pile tip*

In Figure 5.32, the radial deformation of the pile tip is represented, for each boulder position. In case of the central impact, the radial deformations are kept limited to around 1 mm after the first impact. This is caused due to the fact that in central impact the pile tip is more constrained at the contact point, leading to a more stiff behaviour of the tip. As the impact becomes eccentric, the radial deformations are increasing, reaching a value of about 5 mm for the most eccentric boulder position considered. This is in accordance with the radial stress results as illustrated before and it is a direct indication of the initial damage that would occur in the pile tip after the impact with a boulder. The highest difference is observed between the central impact and when a slight eccentricity is introduced. But between all the eccentric boulder positions the difference in the radial deformation is more limited.

During the mesh sensitivity analysis, the height of the plasticity zone in the contact region was selected as a convenient parameter to study mesh convergence. This choice was made by considering that the extent of the plasticity zone would also provide a good indication of the extent of the pile tip damage. Hence, the same parameter was investigated for the different impact configurations. The resulting height of the plasticity zone is represented in Figure 5.33 for each boulder position.

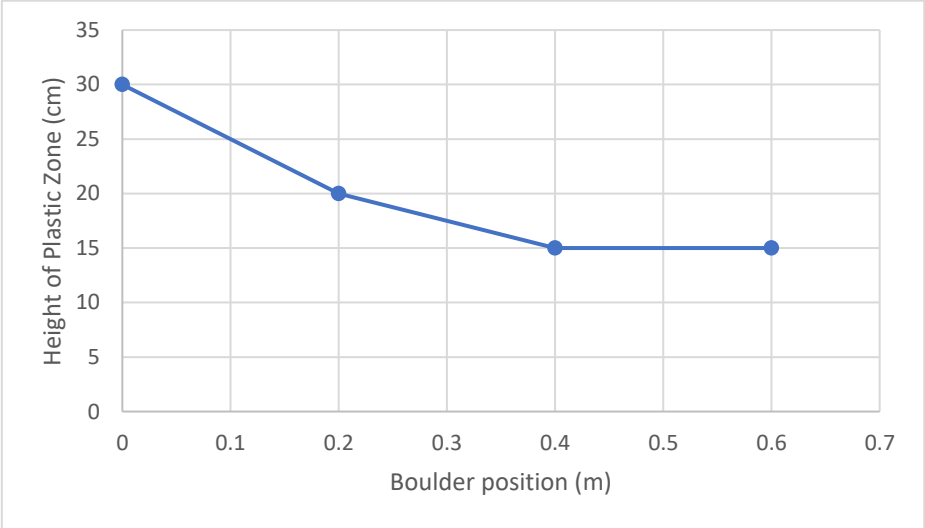

Figure 5.33 *Plastic zone height for each boulder position*

It is noticed that as the impact becomes more eccentric the height of the plasticity zone above the contact point is reducing. As the boulder moves sideways, the response of the pile during the impact becomes more local and the material yields to a lesser extent, closer to the contact point. This is opposite to the trend of the tip radial deformations. Although the radial deformations are increasing, as the impact becomes more eccentric, the extent to which the steel yields is decreasing. Hence, studying the plastic zone of steel around the contact region seem to be less relevant to the extent of the initial damage at the pile tip. The radial deformation is a more appropriate measure of the initial distortion of the pile tip.

5.3.5 Damage: pattern & extent

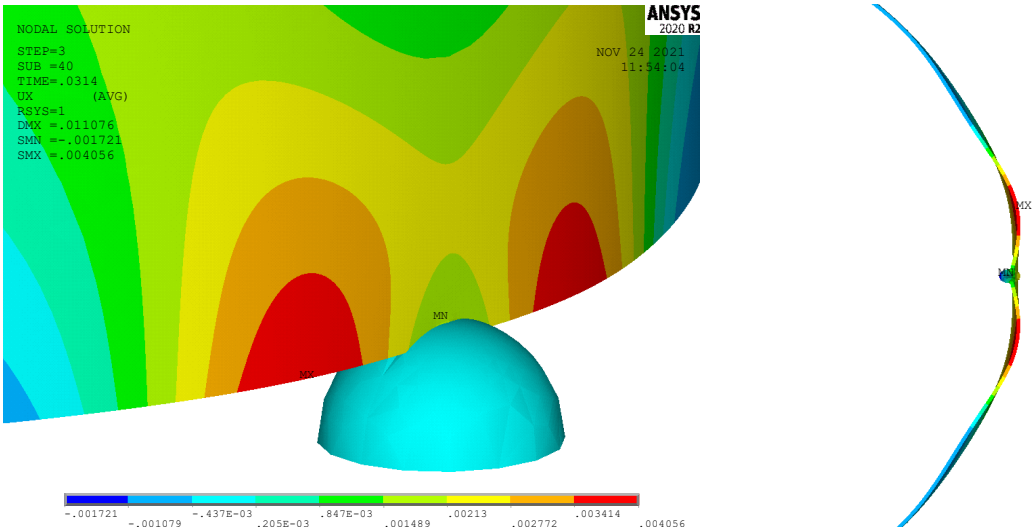

Figure 5.34 *Radial deformation - 3D side view (left, scaled by 20) and bottom view (right, scaled by 100) – Boulder position: 0 (central impact)*

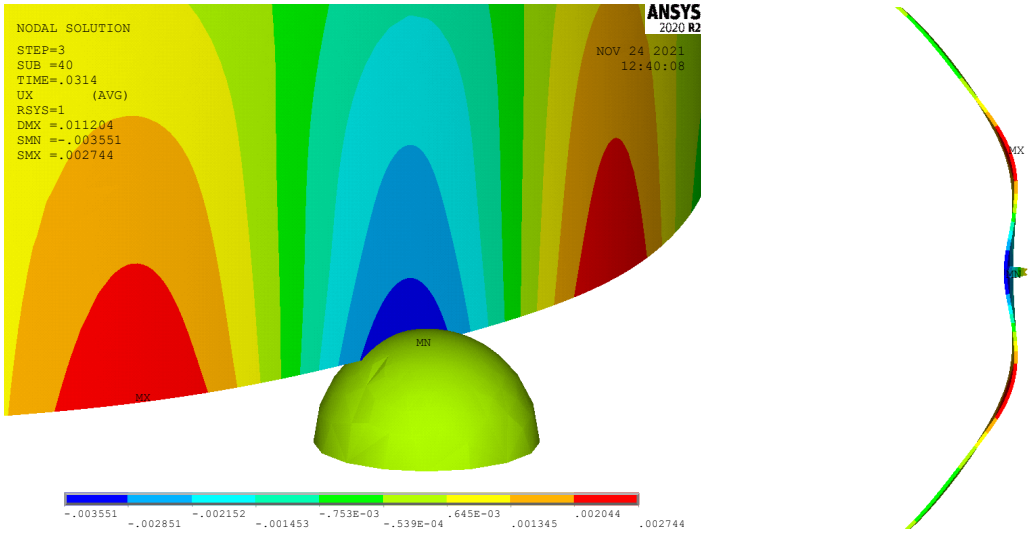

Figure 5.35 *Radial deformation - 3D side view (left, scaled by 20) and bottom view (right, scaled by 100) – Boulder position: +0.2*

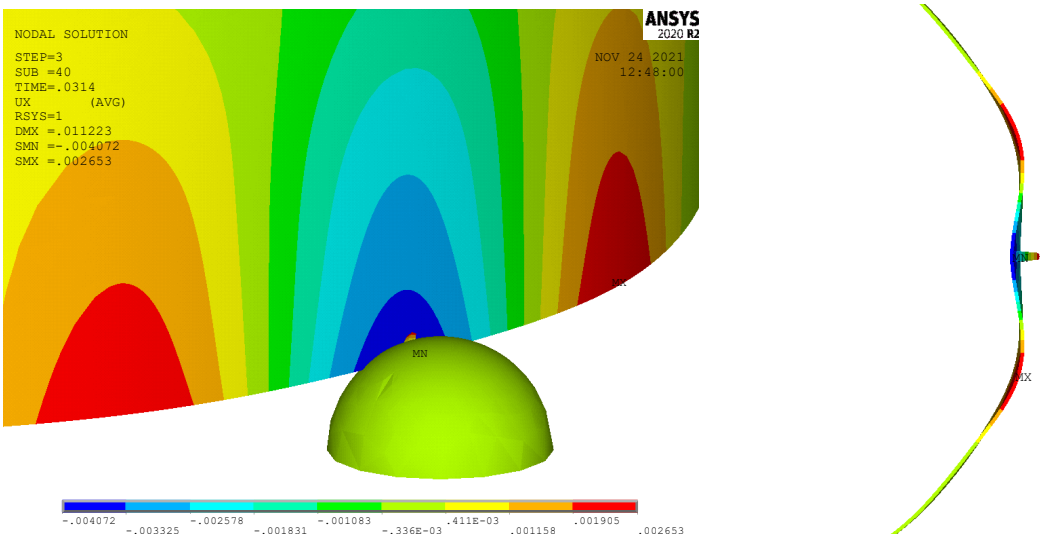

Figure 5.36 *Radial deformation - 3D side view (left, scaled by 20) and bottom view (right, scaled by 100) – Boulder position: +0.4*

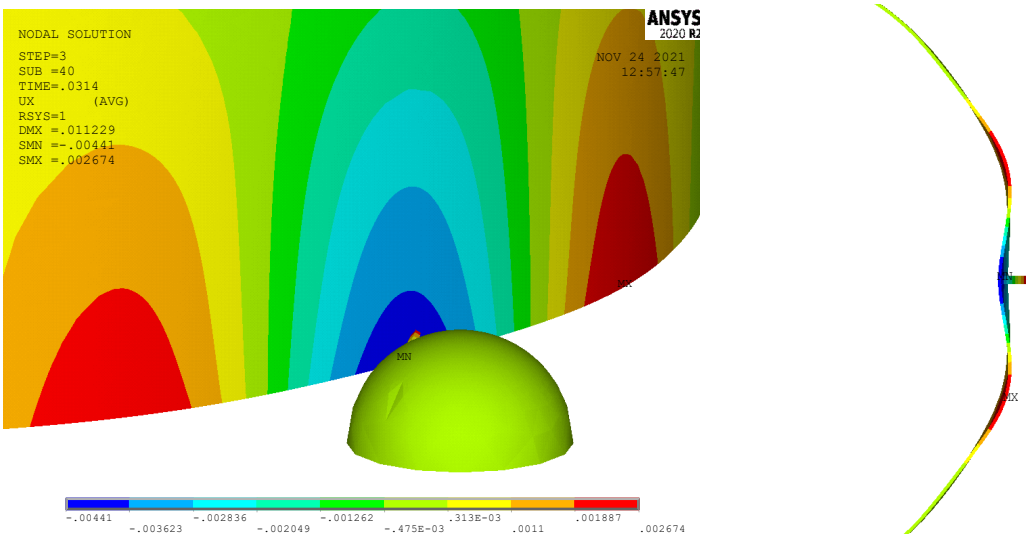

Figure 5.37 *Radial deformation - 3D side view (left, scaled by 20) and bottom view (right, scaled by 100) – Boulder position: +0.6*

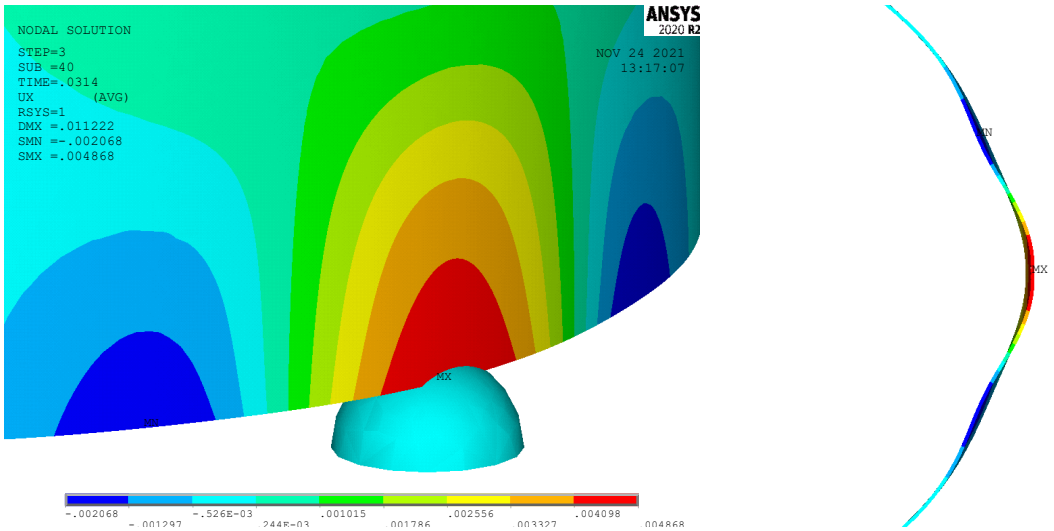

Figure 5.38 *Radial deformation - 3D side view (left, scaled by 20) and bottom view (right, scaled by 100) – Boulder position: -0.2*

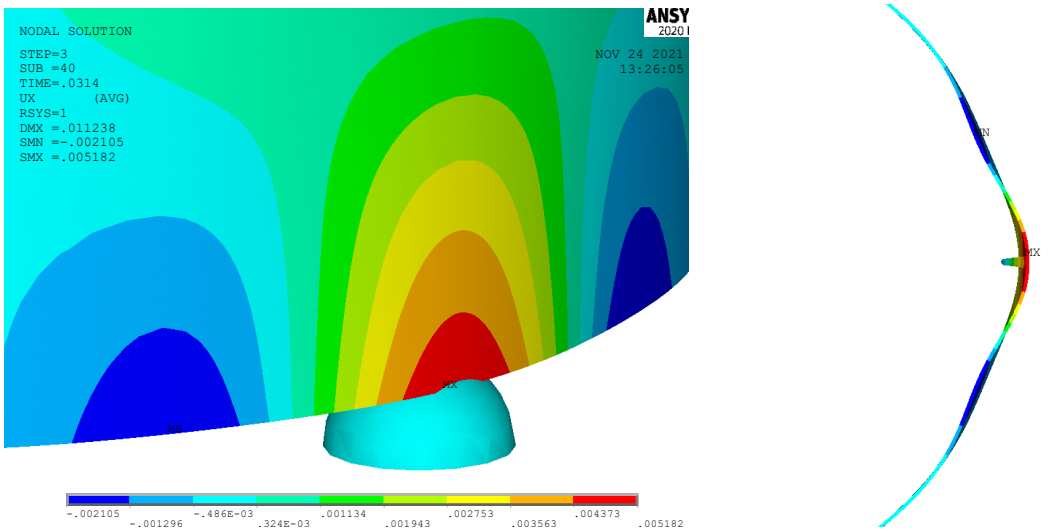

Figure 5.39 *Radial deformation - 3D side view (left, scaled by 20) and bottom view (right, scaled by 100) – Boulder position: -0.4*

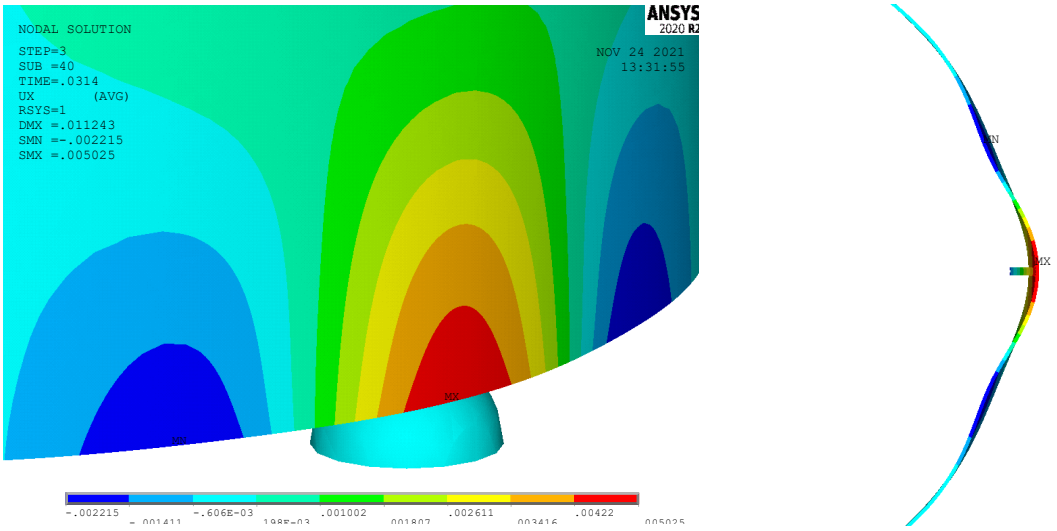

Figure 5.40 *Radial deformation - 3D side view (left, scaled by 20) and bottom view (right, scaled by 100) – Boulder position: -0.6*

In Figures 5.34 to 5.40, the pile radial deformations in the contact region are represented for the final time step of the analysis, which is after the pulse has reached the tip and reflected back. So basically, these are the permanent deformations of the pile tip due to contact with a boulder, after the first pulse is applied to the pile. It can be noticed that as the impact takes place, the radial deformation of the pile is not restricted only close to the contact point. Instead, the pile is radially deformed in a region which extends symmetrically in both sides of the contact point. Depending on the boulder position, it is straight forward how the pile will deform above the contact point. The side regions will deform in the opposite direction resulting in a wavy deformed shape around the contact region. This is clearly illustrated in the above figures, where the red and blue colours represent the peaks in outward and inward radial deflection respectively.

It is expected that the larger radial deformation should occur above the contact point. However, this is not always the case and when it is, still, the deformations that occur further are not negligible. In the case of central impact, it was already discussed that the radial deformations are limited above the contact point, as the pile is better constrained due to the larger contact area. However, the radial deflection a bit further reaches values of about 4 mm. This magnitude of deflection is similar to the deflection above the contact point for the case where the centre of the boulder was 0.4 m outside the pile wall. For all the other cases of eccentric impact, the radial deflection in the side regions is smaller than that above the contact point. The magnitude of the side regions' radial deflection seems to be larger when the contact point is on the outer side of the pile wall and the sides' regions are deflected outwards. Additionally, the more eccentric the impact the larger the induced radial deflection, in the side region, is. The magnitude of these deflections varies between 40%, for the -0.4 m boulder position and 77%, for the +0.2 m boulder position, of the radial deflection above the contact point. This indicates the fact that significant deformation in the pile tip is induced not only above the contact point but also sideways for all impact orientations.

Finally, a remark can be made regarding the extent of the damage caused due to impact. From the obtained results, it seems that as the impact becomes more eccentric, the radially deformed

region around the contact area becomes larger. This is represented in Figure 5.41, where a comparison of the deformed regions is made, between the central impact and the case where the centre of the boulder is 0.6 m out of the pile wall. The black frame around the contact region represents a part of the pile circumference that corresponds to a 40º angle. It can be seen, that in the case of central impact the deformed region is inside this frame, while for the eccentric impact the deformed region expands further from the frame. For the eccentric impact, the extent of the radially deformed region is almost double that of the central impact. Hence, impact with a boulder, can induce pile tip deformations in a pretty extended area around the contact point, especially in the case of eccentric contact.

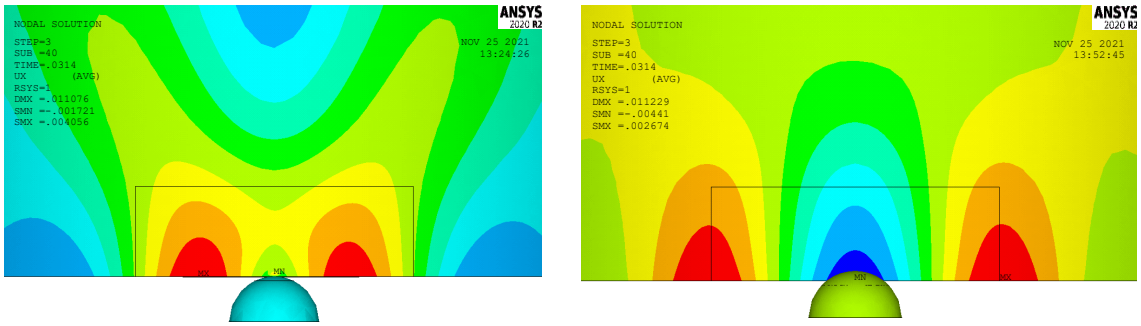

Figure 5.41 *Extent of radial deformations: central impact (left) and eccentric for +0.6 m boulder position (right), the black frame represents the pile circumference which corresponds to a 40º angle*

5.4 D/t ratio investigation

Technological advancement and experience increase within the offshore wind industry pushed for the installation of monopiles in deeper waters and for the use of larger turbines. The more harsh conditions in which the monopiles have to operate, require increased diameters in order to withstand the increased applied loads. However, increased slenderness is necessary, for the respective diameters, in order to maintain the monopiles as an economical efficient foundation system. For this reason, nowadays, the slenderness of the constructed monopiles can reach values of up to 160, exceeding by far the recommendations of the applied guidelines.

The above described trend, is expected to have a significant effect on pile tip buckling during the driving process. As already mentioned in Chapter 3, current guidelines do not cover the case of local buckling at the pile tip, when the pile impacts with a boulder. Increasing the pile slenderness makes the uncertainty around the local buckling phenomenon even larger. In case of larger D/t ratios, the pile's stiffness decreases which should lead to increased tip deformations, making impact with an object even more critical.

Three different D/t ratios were investigated, namely 100, 125 and 150. The monopile outer diameter was kept constant and the pile wall thickness was modified according to the D/t ratio. In Table 5.2, the pile thickness is represented for the different D/t ratios under consideration.

Table 5.2 *Monopile wall thickness for the different D/t ratios*

D/t	Pile Wall Thickness (cm)
100	9.0
125	7.2
150	6.0

In Figure 5.42, the radial displacement at the pile tip over time is represented. It is noticed that as the D/t ratio increases, the radial displacement at the tip is as well significantly increased. In particular, for D/t equal to 100, the maximum radial displacement reaches a value of approximately 4.5 mm. For D/t equal to 125, the radial displacement is increased by 75% reaching a value of 7.7 mm while in the case of D/t equal to 150, it is increased by approximately 170% reaching a radial displacement of about 12 mm. These results confirm that as the pile becomes more slender, the pile tip deformation, caused by impact with an object, is significantly increasing.

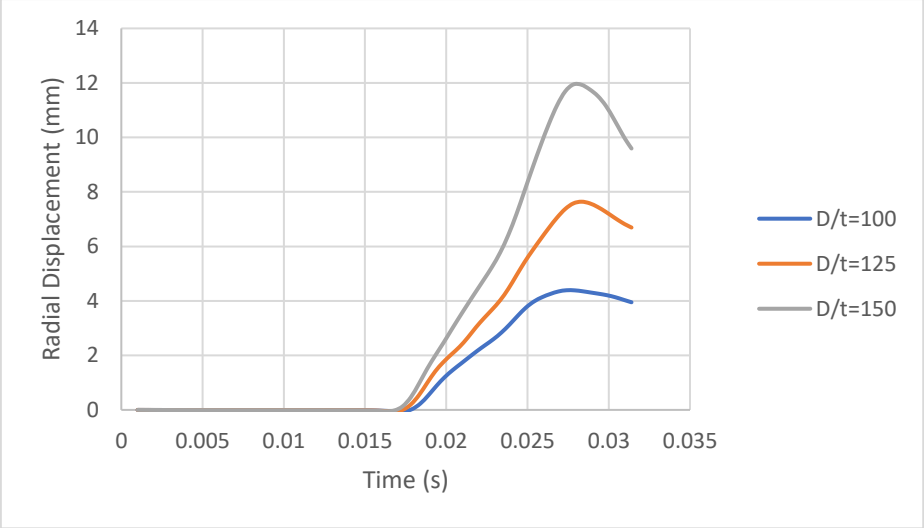

Figure 5.42 *D/t ratio investigation – Radial displacement at the pile tip*

Figure 5.43 represents the lateral reaction force induced during impact, at the pile tip, for the different D/t ratios under consideration. It is observed that the force is almost the same regardless the D/t ratio. This trend confirms the observation, which already noticed in the previous chapter, that the pile is not capable of transferring large lateral loads. The monopile slenderness will result in radial deformations when a lateral load is applied at the tip.

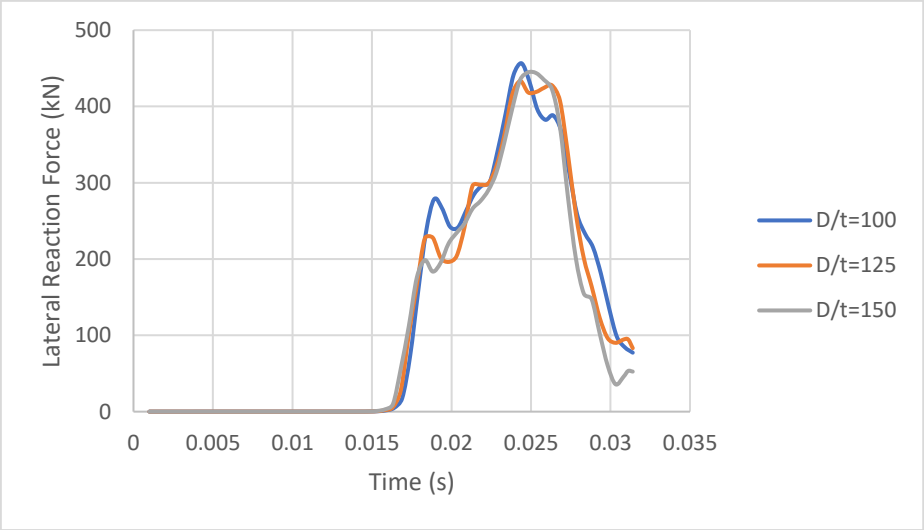

Figure 5.43 *D/t ratio investigation – Lateral reaction force at the pile tip*

5.5 Alpha and Beta damping – Rayleigh damping

Damping can be introduced as a material property to account for dissipative mechanisms in dynamic analyses. In this chapter the influence of damping to the response of the monopile when impacts with a boulder will be investigated.

Damping was applied to the model through the introduction of the material Rayleigh damping. Rayleigh damping is widely used to provide an energy dissipation mechanism when analyzing complex engineering structures responding to dynamic loads. Material damping is implemented into the system through the definition of the mass-proportional Rayleigh damping (Alpha damping) and the stiffness-proportional Rayleigh damping (Beta damping).

Alpha and Beta damping are used to define Rayleigh damping constants α and β. These constants are not generally known directly but are calculated from the modal damping ratios ξ_i which is the ratio of actual damping to critical damping for a particular mode of vibration i. If ω_i is the natural frequency of mode i, then α and β satisfy the relation

$$\xi_i = \frac{\alpha}{2\omega_i} + \frac{\beta\omega_i}{2}$$

where

$$\omega_i = 2\pi f_i$$

In order to specify α and β for a given damping ratio ξ, it is commonly assumed that the sum of the α and β damping terms, as represented above, is almost constant over a range of frequencies.

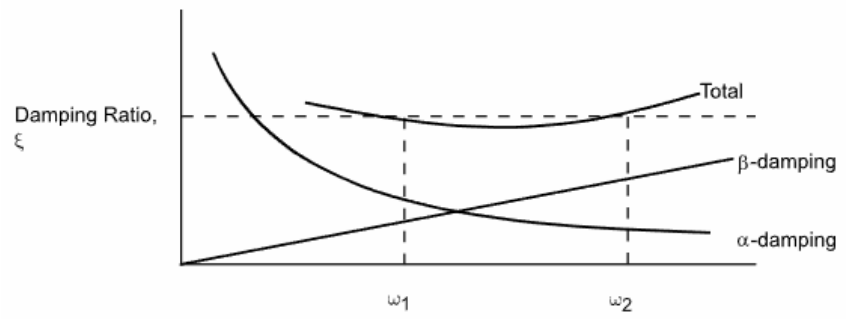

Figure 5.44 *Rayleigh damping*

Therefore, given ξ and a frequency range ω_1 to ω_2, a system of two equations can be solved for α and β, giving the following relations

$$\alpha = \left[\xi_1 - \left(\frac{\omega_1}{\omega_2}\right)\xi_2\right] / \left(\frac{1}{2\omega_1} - \frac{\omega_1}{2\omega_2}\right)$$

$$\beta = \left(\xi_2 - \frac{1}{2\omega_2}\alpha\right)\frac{2}{\omega_2}$$

It is clear, that in order to compute the α and β Rayleigh damping constants, two eigenmodes and the damping ratio are necessary. The damping ratio of steel was taken equal to 0.24%. The modes were chosen such as, to be representatives of the response frequency range of the monopiles. After investigation, the frequency values of 70 Hz and 90 Hz were selected. In Figure 5.45, the eigenmode for the frequency of 70 Hz is represented, as it was computed from a modal analysis of the monopile.

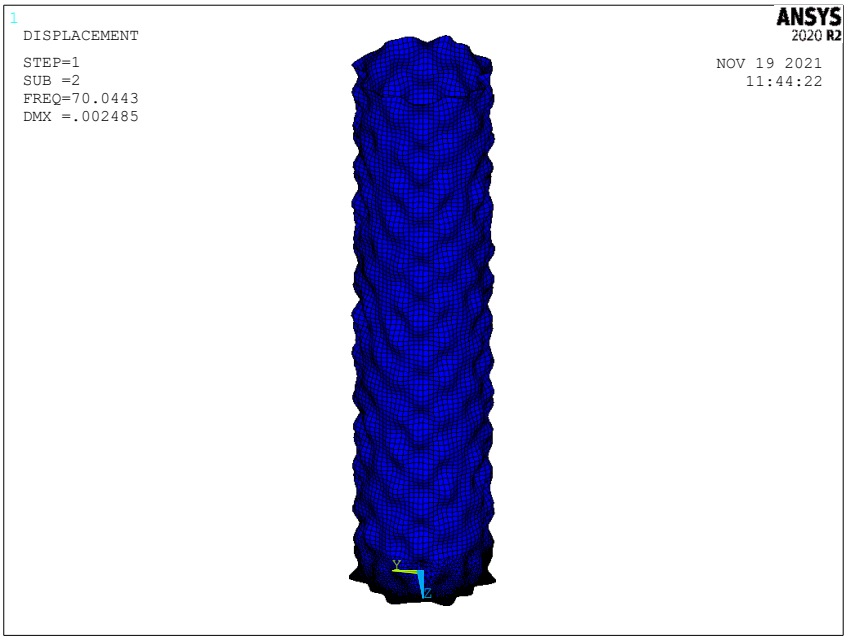

Figure 5.45 *Eigenmode for the 70 Hz frequency*

Finally, after substitution of the selected values, the resulting Rayleigh α and β damping constants were found to be equal to

$$\alpha \approx 1.188$$

$$\beta \approx 4.8 * 10^{-6}$$

Figure 5.46 represents the α and β damping terms as well as the total damping, for the selected range of monopile frequencies.

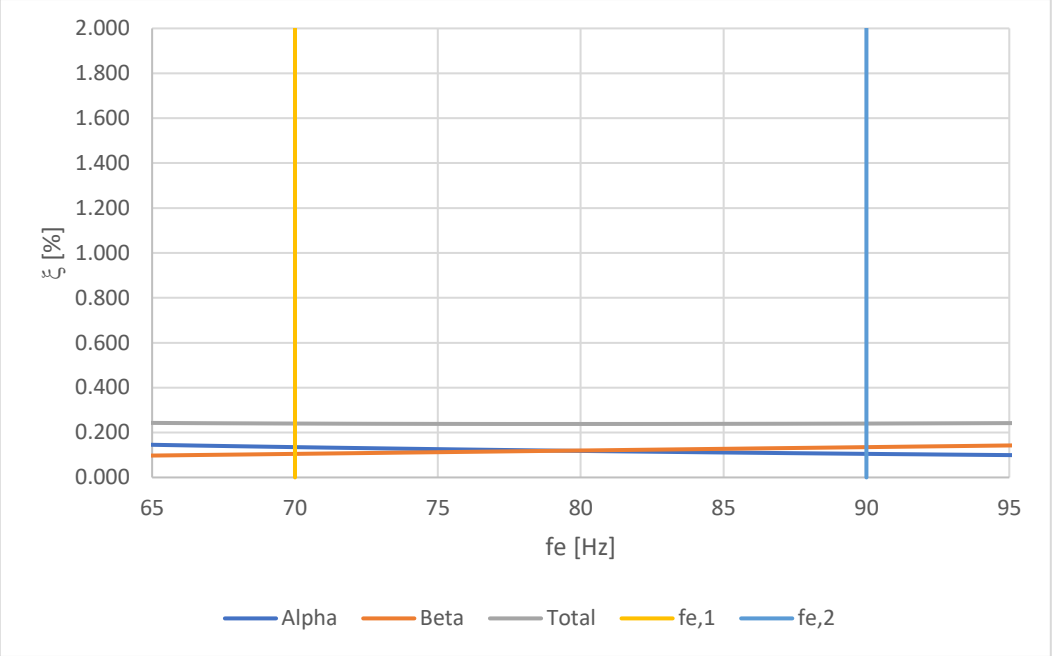

Figure 5.46 *Computed Raleigh damping for the selected range of monopile frequencies*

The Rayleigh damping coefficients, as they calculated before, were implemented in a model, in order to inspect their influence in the response of the monopile during the impact with a boulder. In Figures 5.47 and 5.48, the axial stress at the pile tip and the vertical reaction force on the boulder over time are represented for both the cases where damping is and not taken into account.

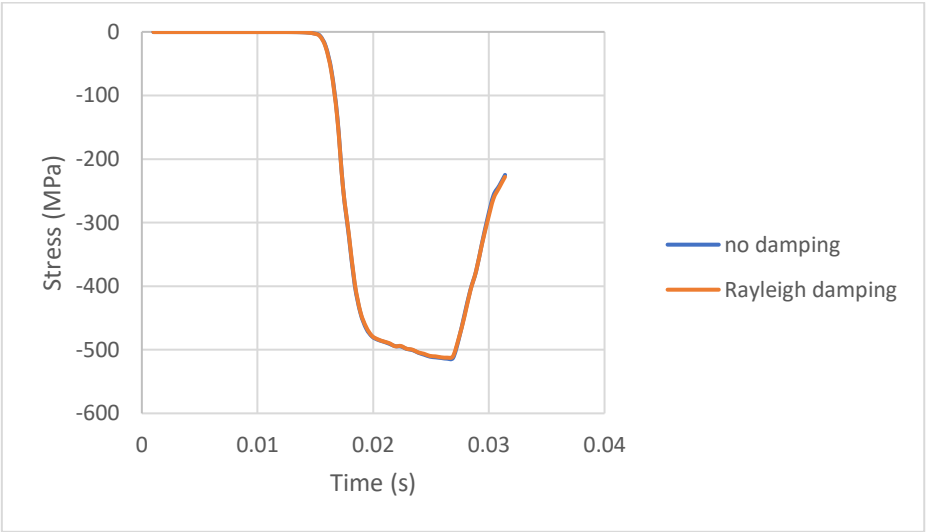

Figure 5.47 *Damping investigation - Axial stress at the pile tip over time*

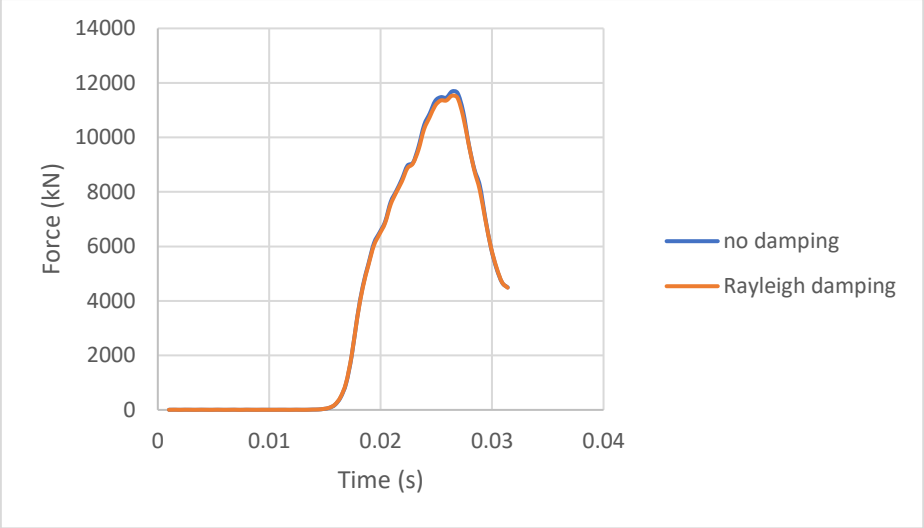

Figure 5.48 *Damping investigation – Vertical reaction force at the boulder*

It is clear that the use of damping has no influence on the response of the system. The axial stress at the tip is not reduced at all and the total reaction force remains the same whether there is damping in the system or not. Two remarks have to made though. First, the analysis done here regards the initial impact, up to the point where the first stress wave reaches the pile tip and reflects back. It is expected that damping will have a contribution in dissipating the stress intensity over time and after the wave travels up and down more times. Secondly, it has to noted that Rayleigh damping is greatly frequency dependent. This might work well when analysing structural dynamics problems, like the response of structures under earthquake, where only a few modes are excited. In stress propagation problems, where the range of the excited frequencies is very large, Rayleigh damping is not the most appropriate way to consider the energy dissipation. Nevertheless, the above conclusion about the influence of the Rayleigh damping is considered valid and implementing damping in the analysis is not considered relevant to the herein analysis.

5.6 Results breakdown

From the results presented so far some useful remarks can be made by considering the literature findings presented in Chapter 3.

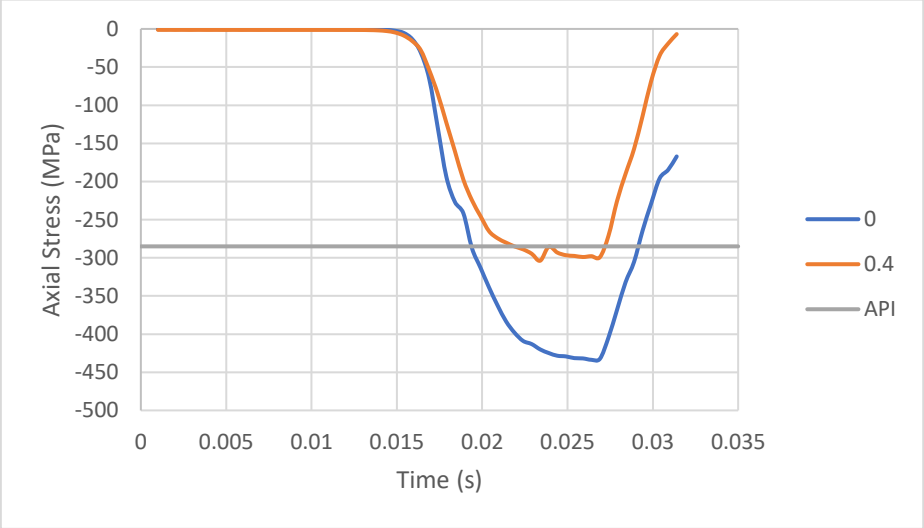

Figure 5.49 *Axial stress for central (0 m) and eccentric (+0.4 m) impact and API driving stress limit.*

In Figure 5.48 the resulting axial stress in case of central and eccentric impact is compared with the recommended API stress limit during driving. It is obvious that the axial stress at the tip exceeds the API limit (90% of the yield stress) in both cases of central and eccentric impact. If the lower limits of up to 50% of the yield stress, that are documented in the literature, are considered then the gap becomes even larger. This is indicative of how critical impact with a boulder could be for the pile integrity and the driving process.

Regarding the resulting vertical reaction force at the boulder, in the case of central impact the order of magnitude is confirmed by Holeyman's research where similar contact forces were computed. Holeyman performed a 1-D analysis including the surrounding soil and it was illustrated that with the right combination of hammer, boulder and soil properties the resulting contact force can reach high values regardless of the soil dissipating action. Moreover, in Figure 3.13 where Holeyman's results are represented, it can be seen that for large boulders the resulting contact force could be smaller than the soil penetration resistance. In such a case, the boulder would remain in place resulting in either pile damage or boulder splitting. Hence, considering the boulder fixed, as it is done in the herein research, seems to be a realistic scenario under certain circumstances and by extension the resulting contact forces close to reality.

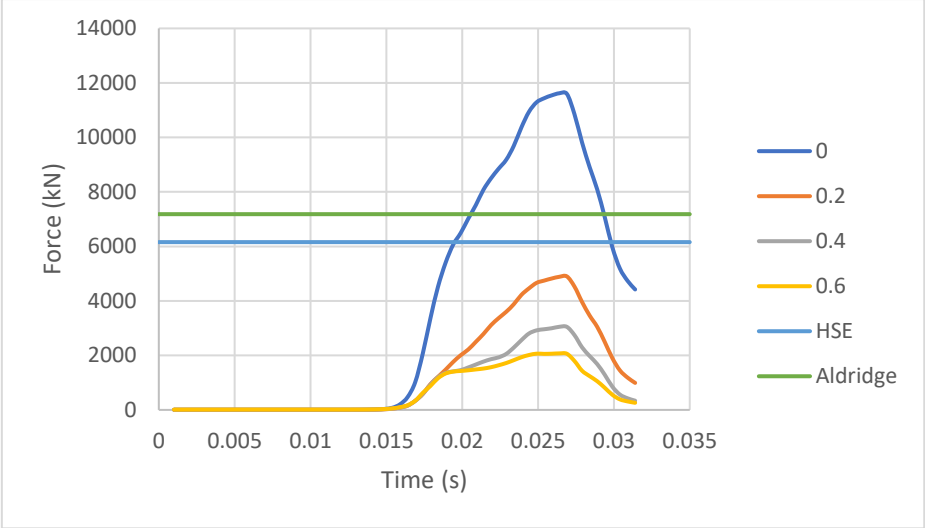

Figure 5.50 *Vertical reaction force at the boulder for different impact orientations and literature force limits*

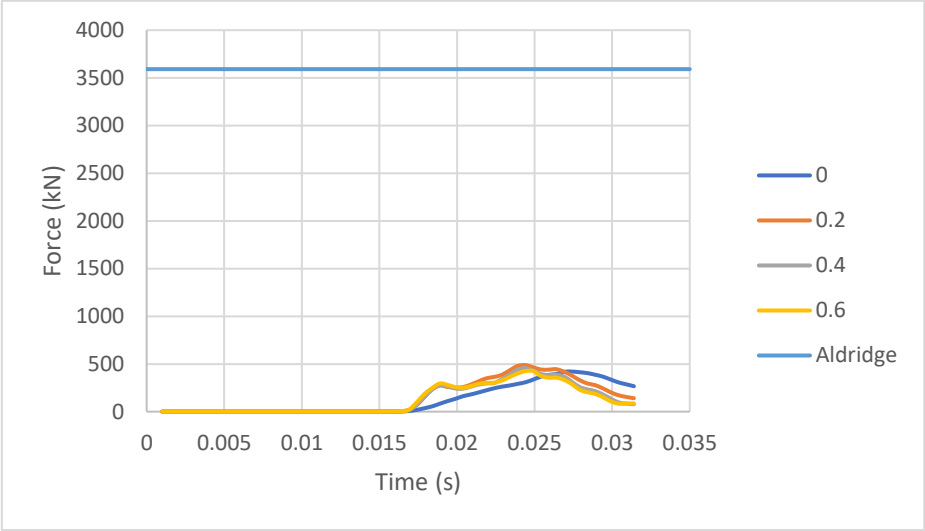

Figure 5.51 *Lateral reaction force at the boulder for different impact orientations and Aldridge's force limit*

In Chapter 3, the force limitation to avoid pile damage according to HSE and Aldridge et al. was presented. Figure 5.49, illustrates the resulting vertical contact forces for the different impact orientations and the respective limits. The vertical force limit for the pile considered in this research is 6156.6 kN and 7182.8 kN according to HSE and Aldridge et al., respectively. It can be seen that in case of central impact the resulting vertical force exceeds by far both limits and confirms that locally the pile will yield and distortion will be induced as was illustrated in the previous chapters. However, these limitations seem to consider only central impact and yielding but not distortion of the pile. In case of eccentric impacts it was illustrated that the pile tip is distorted radially without yielding. The fact that the resulting vertical force in case of eccentric impacts does not exceed the limits defined by HSE and Aldridge et al. shows that although these formulas can provide an indication of when yielding occurs, they are not adequate for defining the integrity of the pile.

Finally, in Figure 5.50, the resulting lateral force at the pile tip is compared with the limit proposed by Aldridge et al. to avoid the formation of a local dent. It is clear that, according to the herein research, in absence of soil the lateral load to cause a local dent is much smaller compared to Aldridge et al. However, the lateral load is expected to be influenced by the surrounding soil and an extensive geotechnical investigation is needed to produce credible results.

6. Discussion & conclusions

6.1 Summary

The scope of the thesis was the investigation of the response of a monopile tip, when an object, such as a boulder, is encountered during the driving process. For this reason, Finite Element Modelling was used as a tool to provide insight into the studied phenomenon.

A real case monopile was modelled in contact with a spherical boulder at its toe. The main monopile geometry that was used had a length of 80 m and an outer diameter of 9 m with a D/t ratio equal to 100, which is a moderate size for the monopiles constructed nowadays, leading to a pile wall thickness of 9 cm. The boulder that was positioned at the boundary had a diameter equal to 2 m and it was fixed at its bottom from moving in the vertical or lateral direction. The scope of the thesis was to study the dynamic response of the monopile tip during impact. For this reason, a real pulse, provided by Van Oord, was applied to the top of the pile. Through this research, a number of parameters were investigated and their influence on the tip response was documented.

6.2 Assumptions

Modelling the impact of a monopile with an object that could be encountered during driving, is a complicated and demanding process. Accurate modelling of contact between two bodies is a complex phenomenon by itself and results in a computationally demanding problem with a number of nonlinearities included and issues to be dealt with. Moreover, the number of parameters involved in the introduction and propagation of damage at the pile tip is large and since limited knowledge and data around this phenomenon is available, an approach aiming to limit the existent variables is necessary. Moreover, the whole process should be decomposed and information should be extracted part by part.

A number of assumptions and simplifications were applied, necessary to limit the scope of this research to some important aspects that influence the pile tip response during impact. First of all, the focus of this thesis was on the initiation of damage caused by impact. This decision was made based on a number of reasons. It is expected that due to the slender structure of a monopile, once an object is encountered during driving, at least a slight damage will be induced at the pile tip. Until now, there are no available data about the kind or extent of damage that such an impact would cause and therefore knowing the response of the monopile tip is very important on its own. But the main motivation in studying the initial stage of the impact process was the important role that the initial damage could have in the propagation of damage as the driving continues. Once a distortion at the pile tip is initiated, the effect of the applied stresses will exacerbate and the damage will more easily extend or propagate as in the case of extrusion buckling. Hence, this study was limited in catching the response of the tip after one pulse reaches the tip and reflects back.

Another simplification that was considered was the conditions of the surrounding environment. The soil surrounding the monopile and the boulder was not taken into account. This decision, on one hand made the model more simple and on the other hand helped in focusing purely on

the effect that the impact has on the pile tip without considering the soil dissipating mechanisms. This assumption is not considered, at this stage, as important as the other studied parameters. It is expected that even if the soil effect will be appreciable, it will be probably favourable for the tip damage by dissipating the pulse energy and providing more uniform boundary conditions at the tip, instead of a very localized contact with the boulder as simulated in this work.

Finally, two assumptions were made regarding the boulder properties. First, the boulder was fixed and not able to move vertically or laterally. This is also a consequence of not considering the surrounding soil. In this way, a conservative scenario is studied where the monopile impacts in solid, immovable rock or is being driven in very hard soils. In such a scenario, the damage at the pile tip and the consequences on the driving process are expected to be very critical. Hence, studying such a scenario would be useful for future definitions of margins regarding the pile damage during driving. Nevertheless, during the research it was shown that a fixed boulder could be close to some real case scenarios. In addition, the boulder was considered to be granite, as an upper limit to the possible boulder stiffness that could be encountered. Since the scope of the this thesis was the pile behaviour during impact, the boulder material was considered as linear elastic and no additional investigation was conducted regarding the boulder properties or failure mode.

6.3 Conclusions

After transforming the applied pulse to the frequency domain, the cut-off frequency was selected as the maximum frequency that is significantly contained to the applied load. Based on this frequency and on the wave speed of the different kind of waves that are generated, the critical wavelength was computed, based on which the structure should be adequately discretised. After considering the longitudinal waves as more critical for the initiation stage of the impact process, it was found that 8 high-order elements over the wavelength is more than enough to capture the wave propagation and its effect on the global response of the monopile. Such a discretization, corresponded to an element length equal to 0.7 m.

Although the 0.7 m mesh size was adequate to capture the wave propagation through the pile, it was not capable of capturing the local response of the pile tip around the contact region. Due to the large resulting stresses and deformations in the contact region, a finer mesh was needed to be applied locally. A mesh sensitivity analysis was conducted to define the mesh size that should be applied in the contact region. Moreover, in order to avoid assessing the results close to the singularity which was observed at the contact point, it was found that the force resultants should be checked 10 cm above the pile tip. This distance is about equal to the pile thickness and could be used as a rule of thumb for such investigations. Eventually, it was found that a mesh size of 5 cm around the contact region is sufficient to achieve convergence. Between stresses and strains, strains were more difficult to converge. Additionally, the height of the plasticity zone was proposed as another parameter which could be used for the mesh sensitivity analysis. Except for being a useful parameter in defining the extent of damage at the pile tip, with this method there is no need for an additional investigation on the distance at which any local effects are vanished.

Additionally to the mesh size in the longitudinal direction of the pile, an investigation was necessary regarding the discretization through the pile thickness. It was found that the number of elements through the thickness have no influence on capturing the wave propagation accurately and one element is sufficient. However, when it comes to the local pile behaviour in the contact region more elements should be used in order to capture the induced out of plane deformations. It was shown that the use of 4 elements through the pile thickness, in the contact region, are enough for an adequate description of the pile tip response.

After building the model, the focus was oriented to retrieving information about the pile behaviour under different scenarios. One of the main parameters on which this research was focused, was the impact orientation. During driving, impact of the pile with a boulder could happen at any point along the boulder surface. Besides the central impact, another 3 different impact points were investigated representing cases of eccentric impacts. These points were considered for both the cases where the impact point is on the inner or the outer side of the pile wall.

The highest stress values are reached for the central impact, with the Von Mises stress exceeding by far the yield limit (316.7 MPa) and approaching the ultimate stress (450 MPa), as they are defined in DNVGL for the S355 steel. Hence, during central impact the pile tip is plastically deformed to a large extent. In case of eccentric impact, the stress remains in lower levels, even below the yield stress. This is attributed to the fact that in case of eccentric impact, the pile is less constrained and it slides along the boulder surface, resulting in smaller reaction forces. So, the stress intensity at the pile tip is much lower in case of eccentric impact. However, after inspecting each stress component, it was found that although the axial stress is reducing as the impact becomes more eccentric, the radial and tangential stresses are significantly increased. In any case, the driving stress limits recommended by relative guidelines (API) or by the international literature will most likely be exceeded in case of impact.

In a similar trend, the vertical reaction force at the boulder achieves its highest value in case of central impact and is significantly reduced as the contact becomes eccentric. The vertical reaction force is only a small fraction of the applied force (maximum 1/20). Although, it could be seen as irrelevant to the driving process, the fact that the force is concentrated on a very small portion of the tip could result in serious damage. The existing limit recommendations for the vertical force seem to be able to capture the initiation of yielding in central impact but refinement is needed in case of eccentric impacts. Nevertheless, they are not suitable for defining the distortion of the pile tip. The lateral reaction force at the tip, caused by the eccentric impact, seemed to be much lower compared to the vertical force and irrelevant of how much eccentric the impact was. This result confirmed the inability of the pile itself, without the soil contribution, to sustain lateral loads and even small portions result to out of plane deformations. The need for investigating the soil contribution to the lateral deformation capacity of the pile tip was highlighted to accurately define a limit on the lateral force caused during impact.

During the literature research it was concluded that once an initial damage is induced at the tip, then it will be much easier to propagate and that there is no available information on the extent of deformation at the tip after impact with an object. On this context, the radial deformation at the tip, caused after impact, was investigated, after one pulse was applied at the top of the pile. The radial deformation above the contact point was limited for the central impact. As the impact

became more eccentric, the radial deformation above the contact point was increasing reaching values of approximately 5 mm for the most eccentric boulder position considered. This is in accordance with the results extracted for the radial and tangential stress and becomes evident that the more eccentric the contact the more critical it is for the tip deformation.

However, the opposite trend was observed for the height of the plastic zone. The more eccentric the impact, the less extended the plastic zone above the contact point was. So, although the radial deformations are increasing, as the impact becomes more eccentric, the extent to which the steel yields is decreasing. Hence, studying the plastic zone of steel around the contact region seems to be less relevant to the extent of the initial damage at the pile tip. The radial deformation is a more appropriate measure of the distortion of the pile tip.

In addition, it was shown that, after the impact, the induced radial deformations are not limited just above the contact point but they are extending sideways in a significantly large area. The side regions are deforming in the opposite direction compared to the contact point resulting in a wavy deformed shape around the contact point. The radial deformations of the side regions are not negligible since they varied between 40% and 77% of the radial deformation above the contact point. Moreover, they seemed to be relatively extended as they occupied a part of the pile circumference which corresponded to up to a 40º angle. The above conclusions indicate the extent of the pile tip damage that can be induced from just one pulse and highlights the need to be considered in the monopile design to avoid propagation of damage and its influence on the driving process. However, the soil contribution to the out of plane deformation capacity of the pile tip should be investigated as it is expected to be beneficial and hence, it is necessary before concluding on the lateral capacity of the tip during impact.

6.4 Future research

Due to the complexity of the problem, a number of assumptions and simplifications were applied through this research. Pile tip damage caused by impact during driving is a process influenced by a lot of parameters and many aspects of engineering are getting involved. Further research is necessary to understand better the whole process and contribute to the development of the Offshore Wind sector. During this research several open issues were recognised and proposals can be made for future research projects.

A critical parameter, which was not taken into account in this research, is the implementation of the surrounding soil. In this thesis, the only boundary to the pile movement was the boulder at the tip. In addition, the boulder was considered as fixed at its base. In reality, both the pile and the boulder are surrounded by soil which contributes with its stiffness and damping. The determination of the soil stiffness and especially damping is a very complex process with a lot of relative ongoing research. In practice, the soil is implemented through the use of springs and dampers or solid elements. Implementing the soil into the model is expected to have a significant influence on the system response. Based on the system properties, the most significant influence of the soil is expected to be concentrated on the boulder movement and on the reduction of the tip lateral deformation. In the herein research the boulder was fixed, representing a conservative scenario of immovable rock leading to large induced stresses during impact. By allowing the boulder to move through the soil the impact force is expected to be smaller leading to less and more realistic tip deformations, at least for the central impact.

For eccentric impacts, it is not clear how different the results should be. In addition, the degree to which the tip deformations will be influenced by the surrounding soil is not clear. For this reason, an extensive geotechnical sensitivity analysis is necessary to figure out the best way to implement the soil and the extent of its influence.

Another parameter which should be investigated is the boulder failure. In this research the boulder was considered as linear elastic. In reality, the impact force could lead to splitting or local failure of the boulder. More detailed aspects of rock mechanics may render the analysis significantly more complex due to the inhomogeneity and the complex crack patterns. Nevertheless, some simplified models for the boulder failure could be created for the more realistic representation of the impact process and to know whether the boulder fails prior to excessive pile tip damage.

An important parameter which could influence the pile tip damage is the hammer energy. An investigation is needed regarding the degree to which the applied energy influences the tip damage by studying a wide range of hammer energies and their impact on the induced tip damage due to contact with an object.

Finally, the context of the herein research was built under the conclusion that the initiation of damage is fundamental for the possible propagation. For this reason and to limit the scope, only the tip response which corresponds to one pulse was investigated. Future research could use larger analysis times and more pulses could applied, representing a real driving scenario and investigating how the distortion propagates over time.

Bibliography

AASHTO (2010), LRFD Bridge Design Specifications, Technical report. American Association of State Highway and Transportation Officials, 5th edition, Washington DC.

Aldridge, T.R., Carrington, T.M. & Kee, N.R. (2005). Propagation of pile tip damage during installation. 1st International Symposium on Frontiers in Offshore Geotechnics, 19–21 September 2005, Perth, 823–827.

Alm, T., Snell, R.O., Hampson, K.M. and Olaussen, A. 2004. Design and installation of the Valhall piggyback structures, Proc. Annual Offshore Tech. Conf., Houston, Paper OTC 16294.

American Petroleum Institute (2000). Recommended practice for planning, designing and constructing fixed offshore platforms–working stress design. Technical report, API Recommended Practice 2A-WSD (RP 2AWSD), 21st Edition.

American Petroleum Institute (2011). Geotechnical and foundation design considerations, Technical report, ANSI/API Recommended Practice 2GEO.

ANSYS inc. (2017), 'ANSYS Help Viewer', Release 18.1.

Barbour, R.J. and Erbrich C.T. (1994). Analysis of in-situ reformation of flattened large diameter foundation piles using ABAQUS. Proc. UK ABAQUS Users Conf., Oxford.

Bathe K.J. (2014) Finite Element Procedures (2nd ed.). USA.

Broos, E., Sibbes, R. and de Gijt, J. (2017). Widening a harbour basin, demolition of a deep see quay wall in Rotterdam. Proc. Of COME2017: Decommissioning of Offshore Geotechnical Structures, Hamburg, Germany, 251-262.

Cathie Associates (2017). Geological and geotechnical causes of pile tip buckling. Future Offshore foundations.

Cerna M., Harvey A.F. (2000) The Fundamentals of FFT-Based Signal Analysis and Measurement. National Instruments, Application Note 041.

Det Norske Veritas AS, Germanischer Lloyd SE (2016). Determination of structural capacity by non-linear finite element analysis methods, Technical report, DNVGL-RP-C208.

Elkadi A. (2019). Simulation of Monopile installation – JIP SIMON.

Greenspon J. (1960). Vibrations of a Thick-Walled Cylindrical Shell-Comparison of the Exact Theory with Appropriate Theories. The Journal of the Acoustical Society of America, 32(5), 571-578.

Holeyman, A., Peralta, P. and Charue, N. (2015). Boulder-soil-pile dynamic interaction. Frontiers in Offshore Geotechnics III-Meyer, 563-568.

HSE (2001). A Study of Pile Fatigue During Driving and In-Service and of Pile Tip Integrity. Offshore Technology Report 2001/018, Health and Safety Executive, UK, published by Her Majesty's Stationery Office, Norwich.

Hussein M., Rausche F. Determination of Driving Induced Pile Damage. Goble Rausche Likins and Associates, Inc., USA.

Jerry A.J. (1977). The Shannon sampling theorem – its various extensions and applications: A tutorial review. Proceedings of the IEEE 65,1565–1596.

Jorna, M. M. (2018). Pile tip deformation caused by obstacles. MSc thesis.

Langer P., Maeder M., Guist C., Krause M., Marburg S. (2017) More Than Six Elements Per Wavelength: The Practical Use of Structural Finite Element Models and Their Accuracy in Comparison with Experimental Results. Journal of Computational Acoustics, 25(4), 1750025, 1-23.

Likins G., Rausche F. Pile Damage Prevention and Assessment Using Dynamic Monitoring and the Beta Method. From Soil Behavior Fundamentals to Innovations in Geotechnical Engineering, 428-442.

Marburg S. (2002). Six boundary elements per wavelength: Is that enough?. Journal of Computational Acoustics, 10(01), 25-51.

Metrikine, A.V., Vrouwenvelder, A.C.W.M. (2017), 'Dynamics of structures – ct4140, part 2 - wave dynamics', TU Delft.

Mostafa Y. E. (2011) Onshore and Offshore Pile Installation in Dense Soils. Journal of American Sciences, 7(7), 549-563.

Papadakis N., Stavroulakis G. (2018) Effect of Mesh Size for Modelling Impulse Responses of acoustic spaces via Finite Element Method in the Time Domain. Euronoise 2018, Crete, 323-330.

Randolph, M., Cassidy, M. Gouvernec, S. and Erbrich, C. (2005). Challenges of offshore geotechnical engineering. International Society for Soil Mechanics and Geotechnical Engineering.

Randolph, M. (2018). Potential damage to steel pipe piles during installation. IPA News Letter, Volume 3, Issue 1, 3-10.

Schmiechen P. (1997). Travelling wave speed coincidence. PhD Thesis, Imperial College of Science, Technology and Medicine, University of London.

The European Union (2006), Eurocode 3: Design of steel structures - part 1-5: General rules - plated structural elements, Technical report, EN 1993-1-5.

Thompson L., Pinsky P. (1994). Complex wavenumber Fourier analysis of the p-version finite element method. Computational Mechanics, 13(4), 255-275.

The European Union (2007), Eurocode 3: Design of steel structures - part 1-6: Strength and stability of shell structures, Technical report, EN 1993-1-6.

The Leanwind Project Final Publication (2017). Driving Cost Reductions in Offshore Wind.

Varma S. J., Gopalakrishman N., Sathish K., Sakaria P. E. (2013) Structural Integrity Evaluation of Pile Foundations by Pile Integrity Testing. International Journal of Structural and Civil Engineering Research, 2(3), 133-140.

Wind Europe (2020). Key trends and statistics 2020, Offshore Wind in Europe.

Appendix A

Data for Figures 3.8 and 3.10 (Mostafa, 2011)

Table 7. Summary information of damaged steel pipe piles during construction

Pile No.	d (mm)	t (mm)	d/t	L (m)	Soil conditions at pile toe	Hammer Type	Estimated Impact driving stresses (MPa)		Failure Location	Source/Location
							Pile Head	Pile Toe		
1	1219	12.7	96	10	Very dense sand with occasional Cobbles/boulders	Diesel D60-62 & Diesel D30-32	175-220	135-150	Head & Toe	Case History 1 (this paper)
2	508	15.8	32	10	Very dense sand with occasional Cobbles/boulders	Diesel D30-32	220	220	Toe	Case History 2 (this paper)
3	610	12.7	48	20	Very dense sand with occasional Cobbles	44.5 kN drop hammer	170-180	110-170	Head & Toe	Case History 3 (this paper)
4	219	6.4	34	20	Compact to dense sand	22.25 kN drop hammer	175-240	50-125	Head	Building, BC, Canada
5	219	6.7	33	20	Compact to dense sand	22.25 kN drop hammer	175-240	50-125	Head	Building, BC, Canada
6	2600	45.0	58	N/A	Calcareous sand	N/A	N/A	N/A	Toe	Goodwyn Platform, Australia
7	1219	15.0	81	N/A	Till-like	N/A	N/A	N/A	Toe	A Dock, BC, Canada
8	1016	12.7	80	N/A	Cobbles/boulders	N/A	N/A	N/A	Toe	A Dock, BC, Canada
9	1829	19.1	96	N/A	Cobbles/boulders	N/A	N/A	N/A	Toe	A Bridge, BC, Canada
10	2134	19.1	112	N/A	Cobbles/boulders	N/A	N/A	N/A	Toe	A Bridge, BC, Canada
11	324	9.5	34	41	Dense sand	Vulcan 80C	138	N/A	Splice	Hussien and Rausche (1991)

Table 8. Summary information of steel pipe piles driven in very dense soils without obvious damage

Pile No.	d (mm)	t (mm)	d/t	L (m)	Soil conditions at pile toe	Impact driving stresses at pile head (MPa)	Source/Location
1	406	12.7	32.0	30	Gravel	N/A	A Bridge over a river, BC, Canada
2	610	12.7	48.0	30	Gravel	N/A	A Bridge over a river, BC, Canada
3	1300	50	26.0	70	Concretions	N/A	North Rankin Offshore Platform, Australia
4	1219	50.8	24.0	N/A	Occasional Cobbles/Boulders	N/A	A Dock, BC, Canada
5	610	12.7	48.0	N/A	Occasional Cobbles/Boulders	N/A	A Dock, BC, Canada
6	914	19.1	48.0	N/A	Occasional Cobbles/Boulders	N/A	A Building, BC, Canada
7	610	12.7	48.0	10	Occasional Cobbles/Boulders	N/A	A Highway Bridge, BC, Canada
8	610	19.1	32.0	10	Cobbles/Boulders	N/A	A Highway Bridge, BC, Canada
9	219	12.7	17.2	25	Dense sand	N/A	A Pedestrian Overpass, BC, Canada
10	324	8.4	38.6	19	Sandy silt till-N=50-100	251	Thompson, C. and Thompson, D.(1979)
11	324	9.5	34.1	19	Sandy silt till-N=50-100	192.0	Thompson, C. and Thompson, D. (1979)
12	324	6.9	47.0	15	Sandy silt till-N=50-100	154.0	Thompson, C. and Thompson, D. (1979)
13	324	9.4	34.5	24	Silt till/gravel-N=80 to >100	203.0	Thompson, C. and Thompson, D. (1979)
14	324	7.1	45.6	24	Silt till/gravel-N=80 to >100	175.0	Thompson, C. and Thompson, D. (1979)
15	324	6.4	50.6	25	Silt till/gravel-N=80 to >100	261.0	Thompson, C. and Thompson, D. (1979)
16	178	7.9	22.5	15	shale bedrock, weathered	188.0	Thompson, C. and Thompson, D. (1979)
17	610	12.7	48.0	35	shale bedrock, weathered	216.0	Thompson, C. and Thompson, D. (1979)
18	1067	51	21	47 - 60	Gypsum rock	225	Sites C, D, Offshore platforms (Webster et al., 2008)
19	1067	44	24	88	Very dense calcareous sand	N/A	Site B, Offshore platform (Webster et al., 2008)
20	1067	38	28	100	Dense Sand/Very stiff clay	224	Offshore pile (Rausche et.al., 2009)
21	1067	44	24	100	Dense Sand/Very stiff clay	224	Offshore pile (Rausche et.al., 2009)

Appendix B

Stress-strain curve according to DNVGL-RP-C208, September 2016

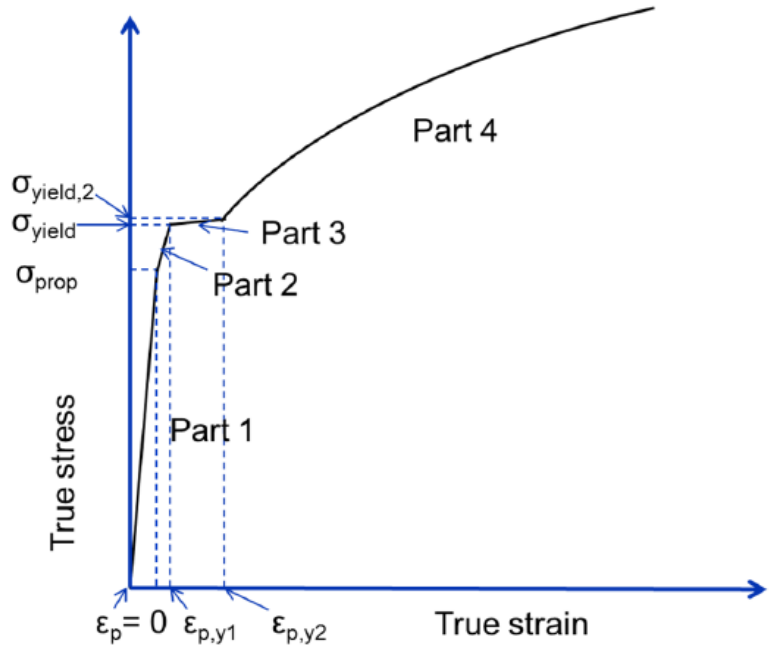

$$\sigma = K\left(\varepsilon_p + \left(\frac{\sigma_{yield\,2}}{K}\right)^{\frac{1}{n}} - \varepsilon_{p\_y2}\right)^{n} \quad for \quad \varepsilon_p > \varepsilon_{p\_y2}$$

Figure B.1 *Stress-strain curve according to DNVGL-RP-C208*

Table B.1 *Steel S355 properties according to DNVGL-RP-C208*

Thickness [mm]	t≤ 16	16< t ≤ 40	40< t ≤ 63	63< t ≤ 100
E [N/mm^2]	210000	210000	210000	210000
σ_{prop} [N/mm^2]	320	311	301.9	284
σ_{yield} [N/mm^2]	357	346.9	336.9	316.7
σ_{yield2} [N/mm^2]	366.1	355.9	345.7	323.8
ε_{p_y1}	0.004	0.004	0.004	0.004
ε_{p_y2}	0.015	0.015	0.015	0.015
K [N/mm^2]	740	740	725	725
n	0.166	0.166	0.166	0.166

Appendix C

Additional figures

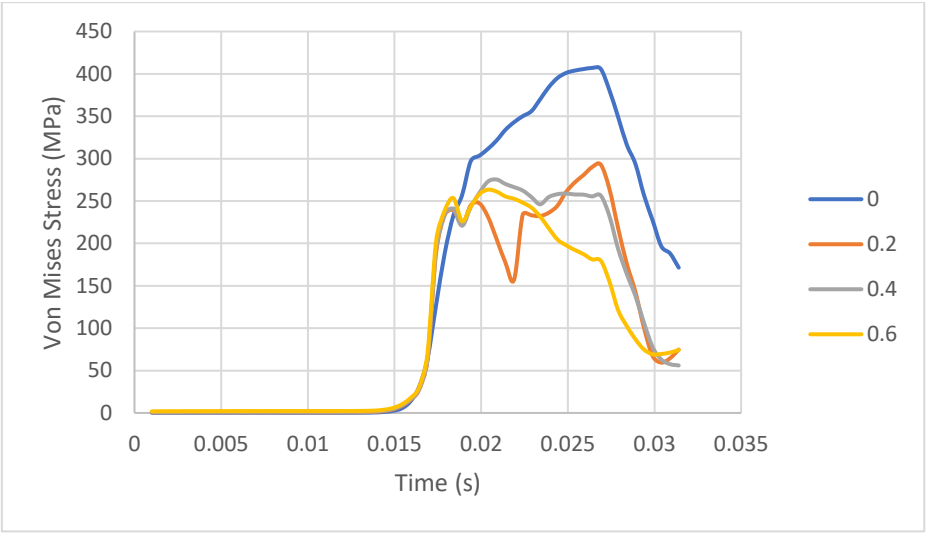

Figure C.1 *Von Mises stress over time at pile tip for central and eccentric (outside the pile wall) boulder positions*

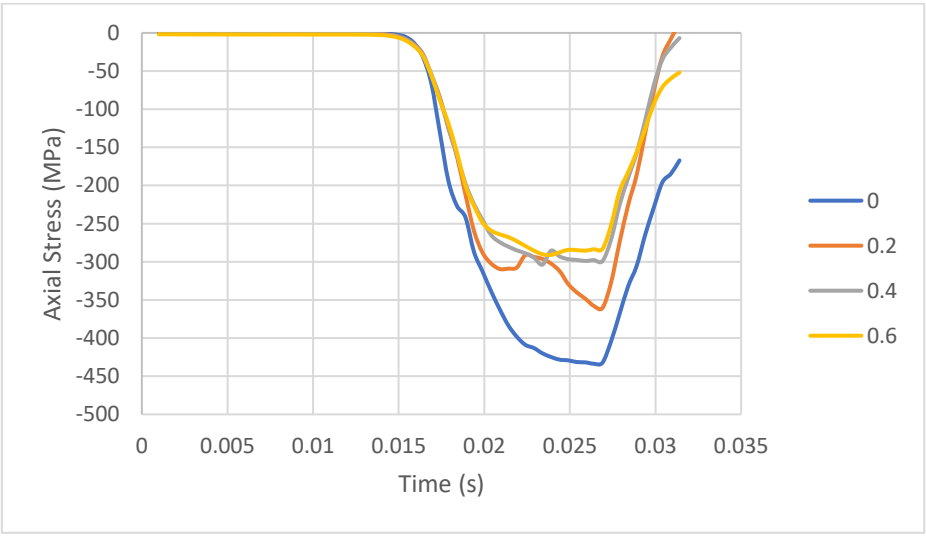

Figure C.2 *Axial stress over time at pile tip for central and eccentric (outside the pile wall) boulder positions*

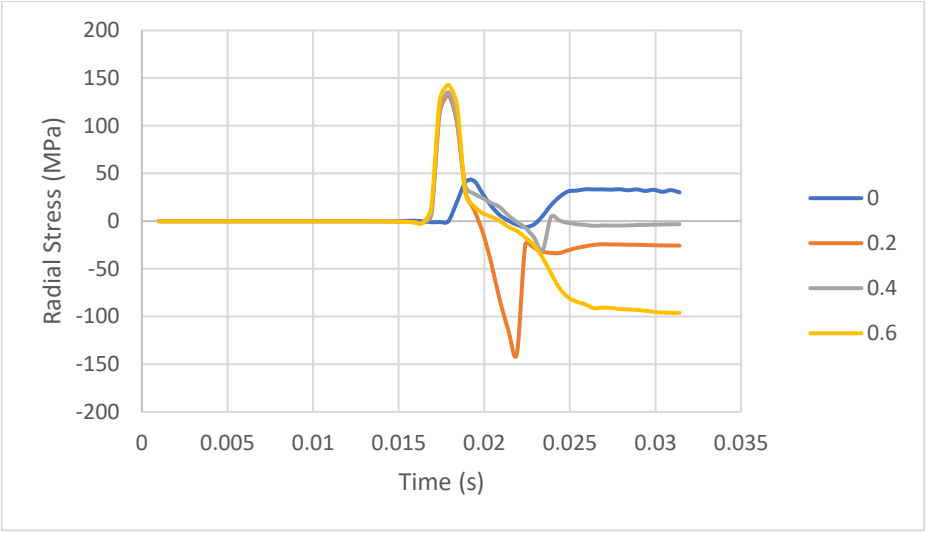

Figure C.3 *Radial stress over time at pile tip for central and eccentric (outside the pile wall) boulder positions*

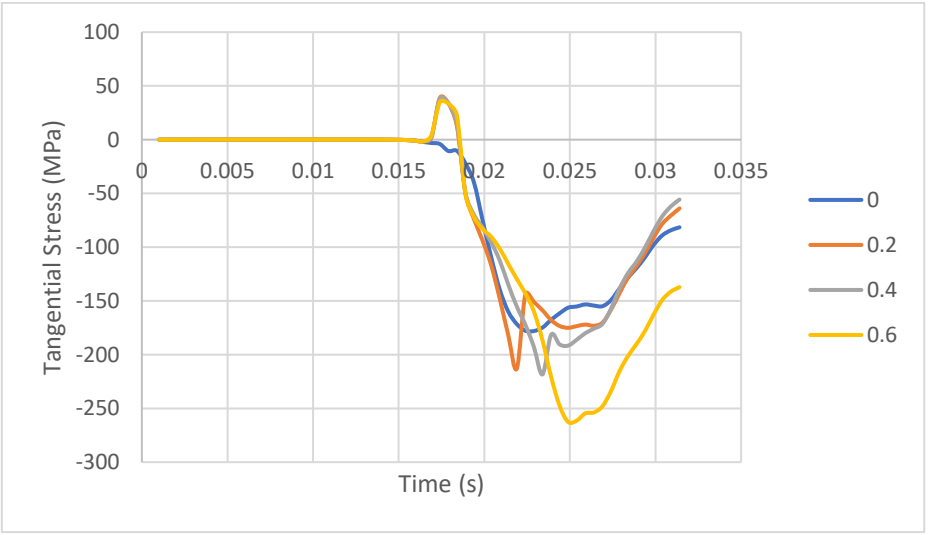

Figure C.4 *Tangential stress over time at pile for central and eccentric (outside the pile wall) boulder positions*

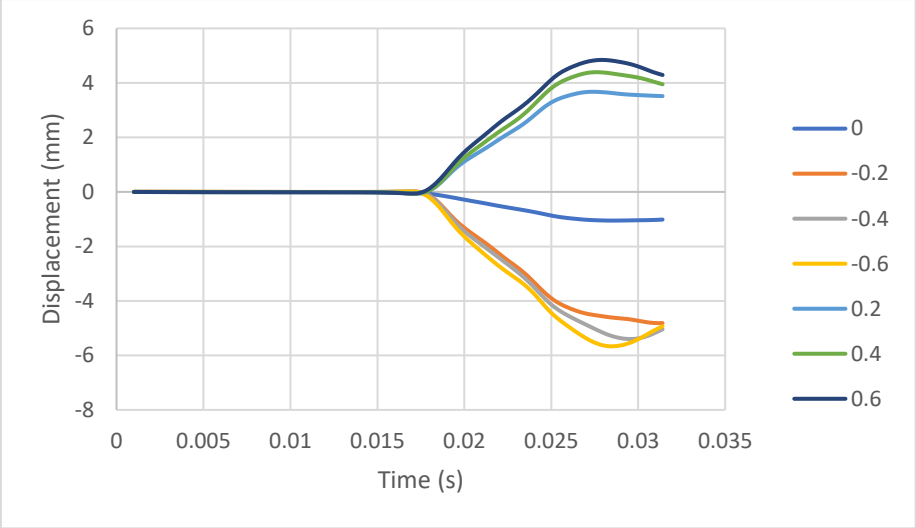

Figure C.5 *Pile tip radial displacement for central and eccentric (inside and outside the pile wall) boulder positions*